

# A Fully-Identified Sample of AEGIS20 Microjansky Radio Sources

S. P. Willner,<sup>1</sup> M. L. N. Ashby,<sup>1</sup> P. Barmby,<sup>2</sup> S. C. Chapman,<sup>3</sup> A. L. Coil,<sup>4</sup> M. C. Cooper,<sup>5</sup>  
J.-S. Huang,<sup>1</sup> R. Ivison,<sup>6,7</sup> and D. C. Koo,<sup>8</sup>

## ABSTRACT

Infrared 3.6 to 8  $\mu\text{m}$  images of the Extended Groth Strip yield plausible counterpart identifications for all but one of 510 radio sources in the AEGIS20  $S(1.4\text{ GHz}) > 50\ \mu\text{Jy}$  sample. This is the first such deep sample that has been effectively 100% identified. Achieving the same identification rate at  $R$ -band would require observations reaching  $R_{AB} > 27$ . Spectroscopic redshifts are available for 46% of the sample and photometric redshifts for an additional 47%. Almost all of the sources with 3.6  $\mu\text{m}$  AB magnitudes brighter than 19 have spectroscopic redshifts  $z < 1.1$ , while fainter objects predominantly have photometric redshifts with  $1 \lesssim z \lesssim 3$ . Unlike more powerful radio sources that are hosted by galaxies having large stellar masses within a relatively narrow range, the AEGIS20 counterparts have stellar masses spanning more than a factor of 10 at  $z \sim 1$ . The sources are roughly 10–15% starbursts at  $z \lesssim 0.5$  and 20–25% AGNs mostly at  $z > 1$  with the remainder of uncertain nature.

*Subject headings:* Galaxies: active, Galaxies: high-redshift, Galaxies: photometry, Infrared: galaxies, Radio continuum: galaxies

---

<sup>1</sup>Harvard-Smithsonian Center for Astrophysics, 60 Garden Street, Cambridge, MA 02138

<sup>2</sup>University of Western Ontario, Dept. of Physics & Astronomy, London, ON, Canada N6A 3K7

<sup>3</sup>Institute of Astronomy, University of Cambridge, Madingley Road, Cambridge, UK CB3 0HA

<sup>4</sup>Department of Physics, University of California at San Diego, 9500 Gilman Dr., La Jolla, CA 92093

<sup>5</sup>University of California, Irvine, Dept. of Physics & Astronomy, 4129 Reines Hall, Irvine, CA 92697

<sup>6</sup>Astronomy Technology Centre, Royal Observatory, Blackford Hill, Edinburgh EH9 3HJ UK

<sup>7</sup>Institute for Astronomy, University of Edinburgh, Blackford Hill, Edinburgh EH9 3HJ UK

<sup>8</sup>UCO/Lick Observatory, Dept. of Astronomy & Astrophysics, Univ. of California, Santa Cruz, CA 95064

## 1. Introduction

Radio observations are an excellent way to identify star-forming galaxies and active galactic nuclei (AGNs). Radio surveys are not subject to selection effects of obscuration or spectral line contamination, which affect visible-light surveys. Even very distant objects can have large radio flux densities. However, radio surveys alone are not sufficient to understand the populations, and followup observations are often more difficult than the initial radio survey. The problem is that redshift  $z > 1$  sources are faint in visible light and require very deep followup studies in order to achieve identifications.

Despite the difficulties of counterpart identification, there are now several radio samples with identification rates of  $\gtrsim 90\%$ . Waddington et al. (2000) found optical counterparts for 96% of the sources in a  $S(1.4 \text{ GHz}) > 1 \text{ mJy}$  sample with images reaching  $R = 26$ . Ciliegi et al. (2003) found counterparts for 92% of  $S(6 \text{ cm}) > 50 \mu\text{Jy}$  sources with  $I_{\text{AB}} = 25$  images. Afonso et al. (2006) were able to identify only 89% of an  $S(1.4 \text{ GHz}) > 61 \mu\text{Jy}$  radio sample even with *HST*/ACS observations reaching magnitude  $z_{850} = 28$ . Simpson et al. (2006) identified  $>90\%$  of a  $100 \mu\text{Jy}$  radio sample using *BRiz'* images reaching AB magnitude 27. Mainieri et al. (2008), using data over a wide wavelength range including the infrared, chose counterparts for 95% of a  $42\text{--}125 \mu\text{Jy}$  radio sample but with an estimated 3% rate of spurious identifications. In other recent work, Bardelli et al. (2010) reported an 82% identification rate in a  $\sim 50 \mu\text{Jy}$  radio sample in the COSMOS field, and Afonso et al. (2011) achieved 83% identification of a sample of ultra-steep-spectrum radio sources with  $S(610 \text{ MHz}) > 100 \mu\text{Jy}$  in the Lockman Hole. Huynh, Jackson, Norris, & Fernandez-Soto (2008) identified 79% of a much fainter ( $S(1.4 \text{ GHz}) > 10 \mu\text{Jy}$ ) radio sample using deep HST images ( $I_{\text{AB}} < 26$ ) albeit with a relatively large matching radius (up to  $1''.96$ ).

Even when counterparts are detected, observed visible light corresponds to rest-frame ultraviolet for high redshift galaxies. While this can give a measure of star formation *rate*, it gives little indication of stellar *mass* and thus little indication of the type of galaxy hosting the radio source. Radio-quiet AGNs and star-forming galaxies both contribute to the faint radio population, but lack of complete identifications and limited wavelength coverage make the proportions uncertain (e.g., Huynh, Jackson, Norris, & Fernandez-Soto 2008).

The All-wavelength Extended Groth strip International Survey (AEGIS) (Davis et al. 2007) offers an unprecedented combination of deep, multiwavelength data over a large area, the Extended Groth Strip (EGS). The data include a radio survey at 20 cm, AEGIS20 (Ivison et al. 2007), which reaches a sensitivity limit of  $50 \mu\text{Jy beam}^{-1}$ . Willner et al. (2006) showed that infrared observations of radio sources can produce very high identification rates for radio source counterparts albeit at much higher flux densities ( $55 \text{ mJy beam}^{-1}$ ) than AEGIS20 and at 6 cm rather than 20 cm. Park et al. (2008) claimed to find all the AEGIS20

radio sources that are also  $24\ \mu\text{m}$  sources on the IRAC images but used a  $2''.5$  matching radius. IRAC data at 20 minute depth contributed to the Afonso et al. (2011) identifications in the Lockman Hole. Infrared data should give high identification rates because the SED of typical stellar populations peaks near  $1.6\ \mu\text{m}$ . For a distant source, this peak will be redshifted to longer wavelength, and the IRAC 3.6 and  $4.5\ \mu\text{m}$  flux densities will not decrease as rapidly as might be expected. Passive evolution also increases the observed flux densities in these band: a stellar population of a given mass was brighter in the past when it was younger. (See Fig. 1 of Eisenhardt et al. 2008.) Thus counterparts should be visible in IRAC observations unless they are either extremely distant, have very low mass, or are heavily obscured by dust, neither of the latter two being likely for a powerful radio galaxy.

This paper reports the matching of AEGIS20 radio sources primarily to IRAC 3.6 to  $8.0\ \mu\text{m}$  data. Barmby et al. (2008) have provided images and catalogs of IRAC data in the EGS. The typical exposure time is 2.5 hours (9 ks), and the 80% completeness limits for the catalog are  $\sim 5\ \mu\text{Jy}$  at 3.6 and  $4.5\ \mu\text{m}$  and  $\sim 10\ \mu\text{Jy}$  at 5.8 and  $8.0\ \mu\text{m}$ . However, fainter objects with known positions can be identified on the images. Additional IRAC data for the EGS exist (Ashby et al., in preparation, 2012) but were not used for this work. In practice, the Barmby et al. data suffice to identify counterparts for all or nearly all of the radio sources. The radio sample is defined and source matching is described in Section 2, counterpart properties including photometry and redshifts are given in Section 3, and results are discussed in Section 4 and summarized in Section 5. Throughout this paper, magnitudes are in the AB system, and the notation  $[w]$  means the AB magnitude at wavelength  $w$  in  $\mu\text{m}$ .<sup>1</sup> Source distances are based on standard  $\Lambda\text{CDM}$  cosmology with  $H_0 = 71\ \text{km s}^{-1}\ \text{Mpc}$  and  $\Omega_M = 0.27$ . Practical calculation of luminosity distances was based on the program ANGSIZ (Kayser, Helbig, & Schramm 1997).

## 2. Sample Definition and Identifications

### 2.1. Selecting Counterparts with IRAC data

The initial radio catalog (Ivison et al. 2007) contains 1122 sources<sup>2</sup> with  $S(1.4\ \text{GHz}) > 50\ \mu\text{Jy}$ . Of these, 511 are in the area of IRAC coverage, defined by at least five independent images in each of the four IRAC channels. (This amounts to one-tenth the nominal IRAC exposure time, but most sources were observed with the nominal exposure time or close

---

<sup>1</sup>Some other papers use the  $[w]$  notation to mean Vega magnitudes, but here it means AB.

<sup>2</sup>One source in the original catalog is a duplicate.

to it.) These 511 radio positions, within an area of  $\sim 950$  arcmin<sup>2</sup>, are the ones we have attempted to match to IRAC sources.

The simplest radio sources to match were the point sources, those unresolved at the 3".8 FWHM of the radio beam (Ivison et al. 2007). There are 342 such sources in the input list. One is 3".0 from the bright ( $K_S = 8.4$ ) star 2MASS J14230588+5333504. No identification is possible for this one, and it was dropped from further consideration. Of the remaining 341 sources, all but one coincide with an IRAC catalog source consistent with Gaussian position uncertainties having a standard deviation of 0".37 in each coordinate. There is no systematic offset in right ascension, and the offset in declination is 0".08, the IRAC positions being systematically north of the radio positions. Figure 1 shows a histogram of the radial offsets. The one badly discrepant source is 434 (Table 1), which has an offset of 1".6.<sup>3</sup> This is too large to be considered a valid identification, and if the radio source is real, it remains unidentified. The radio flux density is at the catalog limit of 50  $\mu$ Jy, just under a  $5\sigma$  detection. Thus 340 of the 341 point sources possible to match are indeed matched by catalog IRAC sources.

Most of the resolved radio sources are equally simple to match — the sources are small, and there is an obvious IRAC counterpart — but some of the complex, resolved sources present more of a challenge. For seven radio sources, the IRAC data suggest two possible counterparts. Radio images for these seven are elongated and statistically consistent with two point sources separated by a few arcseconds. In four of these cases, detection of the weaker radio source was less than  $3\sigma$  significance. In these cases, the radio source was deemed to be a single point source, and the nearest galaxy to it was adopted as the counterpart. The other galaxy might be a radio source as well, but its flux density is below the sensitivity limit of the AEGIS20 survey. In the other three cases, both radio components were detected at  $>3\sigma$ , and these are treated as separate sources, each radio component having an IRAC counterpart. Radio to IRAC offsets are consistent with the position uncertainties found for the point sources.

Finally, there are 15 radio sources with complex morphologies, shown in Figure 2. All but one have a plausible IRAC counterpart, though in some cases there are multiple candidates, and there is no way to be certain we have chosen the correct one. For source 002, there is a bright IRAC source within 5".5 of the radio peak, but a more plausible explanation is

---

<sup>3</sup>Other sources with large offsets are 033 and 487 with offsets of 1".3. The latter source is near the edge of the IRAC map and has only 1/10 normal coverage; its IRAC position uncertainty is thus expected to be about three times larger than normal. Indeed a systematic shift is seen between the 3.6 and 4.5  $\mu$ m images for this source. Source 33 has full-depth IRAC coverage with no obvious position error, but its offset could be the 3-sigma outlier expected in this sample. It is a  $5.4\sigma$  radio detection, thus unlikely to be spurious.

that source 002 is the tip of a jet emerging from source 003. There is a counterjet in the opposite direction, though it is not bright enough in the radio image to have been detected by the automated search as a separate source. The extended ( $\sim 5''$ ) radio source 236 is  $4''.3$  from our suggested IRAC counterpart (an  $R = 24.4$  galaxy at  $z_{\text{phot}} = 0.69$ ) corresponding to a projected separation of about 30 kpc. Alternative IRAC identifications are a fainter galaxy (shown at the northern tip of the radio ellipse in Fig. 2)  $3''.4$  from the radio centroid<sup>4</sup> or that 236 is a radio lobe of source 233 to the southeast. Source 233 has a radio jet and lobe extending to its southwest, but the radio image shows no evidence of any jet connecting 233 to 236. Source 428 has multiple radio lobes, and the counterpart could be any of many sources visible in the IRAC image. We suggest the most likely counterpart is a  $z = 0.8260$ ,  $R = 22.7$  galaxy bright at  $8 \mu\text{m}$  and located near the inner edge of the northwest radio lobe. At the suggested redshift, the projected  $42''$  maximum extent of the radio lobes corresponds to a length of 320 kpc.

The overall identification rate is remarkably high. At most three of 510 radio sources lack IRAC counterparts, and there is a plausible case that the identification rate is 100%. This would require source 2 to be a jet from 3 (as is likely), source 236 to be related to one of two candidate counterparts or be a jet from 233, and AEGIS20 radio source 434 to be spurious. At the near- $5\sigma$  detection level, even a single spurious source is statistically unlikely, but the absence of an IRAC counterpart is hard to explain. At  $z = 1$ , the IRAC  $3.6 \mu\text{m}$  detection limit  $0.7 \mu\text{Jy}$ <sup>5</sup> corresponds to a stellar luminosity of order  $10^9 L_{\odot}$ , and such low luminosity galaxies are unlikely to harbor powerful radio sources. Even at  $z = 5$ , a galaxy with  $L = 10^{11} L_{\odot}$  should have been detected at  $4.5 \mu\text{m}$ . Nevertheless, Huynh, Norris, Siana, & Middelberg (2010) reported two radio sources in the Extended *Chandra* Deep Field South without apparent IRAC counterparts. If such a population exists, source 434 (and less likely source 236) could be a member. The source density suggested by Huynh, Norris, Siana, & Middelberg predicts  $>4$  such sources in the EGS field, where we find at most two and maybe none. This implies radio sources without IRAC counterparts are rare if they exist at all.

---

<sup>4</sup> $R = 24.5$ ,  $z_{\text{phot}} = 0.6$  according to the Rainbow database.

<sup>5</sup>This limit is for the nominal survey exposure time of 9 ks. The actual exposure time at the position of 434 was 3.4 ks at  $3.6 \mu\text{m}$  and 6.6 ks at  $4.5 \mu\text{m}$ , so the actual limits for this source are correspondingly worse.

## 2.2. Selecting Counterparts with $R$ -band data

Deep Subaru  $R$ -band data exist for almost the entire EGS<sup>6</sup> with  $5\sigma$  depths of 26.5 AB magnitudes over most of the strip and 26.1 in the southwest portion. These images were searched with SExtractor (Bertin & Arnouts 1996), and 405 counterparts were found within  $1''$  of the IRAC position. The number would be 372 if a more stringent (and more reasonable) coincidence criterion  $<0''.7$  were used.<sup>7</sup> This detection rate of  $<80\%$  (or  $<73\%$ ) is typical of visible-light counterpart searches (§1). Moreover, for 10 radio sources, the automated  $R$  search found a neighbor object brighter in  $R$  instead of the object detected by IRAC. We regard the latter as more plausible counterparts because most radio sources originate in massive galaxies, which may be red but will seldom have very blue colors, as would be required if any of these 10  $R$  sources is the correct counterpart. Therefore about 2–3% of the proposed counterparts would be incorrect in the  $1''$  search, though all of these would be eliminated with the  $0''.7$  search. Mainieri et al. (2008) also gave examples of counterparts found in infrared  $K_s$  band or IRAC data but invisible at shorter wavelengths. Figure 3 shows images of some sources that an automated  $R$ -band search might misidentify.

## 3. Counterpart properties

### 3.1. Source photometry

No single method of photometry is adequate for all objects. With deep images, many radio counterparts have nearby sources that can contribute to the photometry in large apertures. Other counterparts are significantly extended, and only large apertures can capture all the flux. There are technical problems in some cases because an automated aperture selection can combine unrelated objects or separate a single object into multiple ones, though the latter doesn't seem to have occurred in the present sample. In practice, we have measured IRAC and  $R$ -band fluxes through four apertures for each object: three circular apertures with radii  $1''.53$ ,  $2''.14$ , and  $3''.06$ <sup>8</sup> and the Kron aperture chosen by SExtractor (MAG\_AUTO).

---

<sup>6</sup> Five counterparts in the northern part of the EGS are outside the coverage of the  $R$  images.

<sup>7</sup>The search was based on IRAC positions because the purpose was to determine whether an apparent  $R$  counterpart was the same object as the IRAC source. A purely visible search for radio source counterparts would, of course, start from VLA positions rather than IRAC positions and would probably find slightly fewer counterparts than the numbers stated.

<sup>8</sup>These aperture sizes were those used in the IRAC catalog (Barmby et al. 2008) and correspond to 2.5, 3.5, and 5.0 IRAC mosaic pixels. The IRAC mosaics have pixels half the size of the actual IRAC pixels.

The default photometry aperture was the smallest circular one because of its rejection of neighboring sources and sky fluctuations, but all galaxies with semimajor axis size  $>1''.22$  (measured by SExtractor in  $R$ ) were examined individually on the images, as were objects with  $m(1''.53) - m(2''.14) > 0.25$  or  $|m(3''.06) - m_{\text{auto}}| > 0.25$ . In each case, the most reasonable magnitude to include the whole galaxy but exclude neighbor objects was chosen. This process was necessarily somewhat subjective, but no alternative reasonable choice would change the magnitude by more than about 0.2 mag. In all, 166 counterparts were examined individually to choose apertures.

SExtractor (Bertin & Arnouts 1996) was used to measure both circular and AUTO magnitudes for the sources it detected; the SExtractor IRAC magnitudes were published by Barmby et al. (2008).<sup>9</sup> For sources not detected by the automated SExtractor search, positions were measured from the images and aperture photometry done at those positions with the IRAF task `apphot`. The  $R$  magnitudes were calibrated from SDSS stars (avoiding those saturated in the Subaru data), for which  $R_{\text{Subaru}} = r_{\text{Sloan}} + 0.17(r - i)_{\text{Sloan}}$  with rms scatter  $\sim 0.05$  mag.<sup>10</sup> The  $R$  magnitudes are given in Table 4, and IRAC magnitudes are given in Table 5, which uses SExtractor magnitudes when they exist and APPHOT magnitudes otherwise. When AUTO magnitudes are used, the Kron apertures were derived separately in the IRAC bands and in  $R$  and may differ, but in both cases they are intended to measure the total magnitude of the object. The uncertainties listed in Tables 4 and 5 are statistical only as derived from the local background fluctuations. Upper limits are  $5\sigma$ .

The  $R$  magnitudes were checked in two ways. The Subaru data came from three adjacent images, which overlap enough to include duplicate images of 26 sources not strongly affected by artifacts or image edges. The rms absolute difference of observations of the same source in the  $1''.53$  aperture is 0.04 mag, and the maximum is 0.10 mag. However, a difference of 0.86 mag was found for one source near an image edge (one image being obviously bad at that location), and a very few sources near image edges or with other problems might have bad magnitudes that have not been noticed. The rms difference between SExtractor and APPHOT  $1''.53$  aperture magnitudes is 0.09 mag, presumably due to differences in aperture centering and background calculations. This is a reasonable lower limit on systematic uncertainty for the fainter sources. However, it seems prudent to recognize that in some cases the source

---

<sup>9</sup>Source 036 is not in the published catalog, but its AUTO magnitudes were measured on the images in the same way as for the catalog. Extended source corrections of 0.062, 0.040, 0.137, and 0.212, based on the latest coefficients from the *Spitzer* Science center, are included in the Table 5 magnitudes. The channel 2 correction differs by 0.016 mag from the one that would have been used in 2008, but 036 is the only radio source counterpart that needs an extended source correction.

<sup>10</sup>The color term is poorly determined because the  $r - i$  color covers only the range 0–2 mag.

measured in  $R$  may be a different object than the one measured by IRAC, and a few large errors are possible.

The new `apphot` IRAC aperture measurements agree with the published ones except when there are nearby, confusing sources. In some of those cases, SExtractor can separate the sources, whereas `apphot` simply adds all the counts in the defined aperture. Otherwise, testing showed that SExtractor and `apphot` magnitudes are consistent with each other. Barmby et al. (2008) discussed the uncertainties in the IRAC data, and the new measurements should have equivalent uncertainties. Figures 4 and 5 show the magnitude distributions of the radio source counterparts in [3.6] and  $R$ , respectively.

### 3.2. Source Redshifts

Spectroscopic redshifts come from a variety of sources. The largest number (125) are from the DEEP2 redshift survey (Davis et al. 2007; Newman et al. 2012). Additional redshift sources are listed in notes to Table 4. All in all, 235 counterparts have spectroscopic redshifts, and agreement is excellent for the 44 sources with more than one spectroscopic measurement.<sup>11</sup>

Barro et al. (2011a) have compiled a database of photometric and spectroscopic data<sup>12</sup> in the EGS and used it to derive photometric redshifts (Barro et al. 2011b). Searching their database using the IRAC positions (Table 3) of the radio source counterparts and eliminating duplicates resulted in 440 matches within  $0''.65$ . We examined images and found 8 additional cases where the Rainbow object appears to be the one we identify as the radio source counterpart; position offsets for these were between  $0''.65$  and  $0''.80$ . No objects with offsets  $>0''.8$  appeared to be valid matches. Of the 448 matched objects, 215 have spectroscopic redshifts, and all but 21 agree with the Barro et al. (2011b) photometric redshifts within  $\Delta z \leq 0.2$ . Another large source of photometric redshifts for the EGS is the CFHT Legacy Survey (CFHTLS, Coupon et al. 2009) with 183 altogether of which 105 are for objects with spectroscopic redshifts. Of these, 94 photometric redshifts are within  $\Delta z \leq 0.2$  of the spectroscopic ones, again giving a success rate near 90%. The next largest source is the NEWFIRM Medium Band Survey (NMBS Whitaker et al. 2011) with 76 redshifts. Of these, 5 of 42 differ from a spectroscopic measurement by  $\Delta z > 0.2$ . Finally, 236 photometric redshifts are from unpublished work (Huang et al. 2012b). These use a neural network technique that is inherently limited to  $z \leq 1.1$  because of insufficient galaxies at larger

---

<sup>11</sup> $\Delta z \leq 0.0015$  except for one source with  $\Delta z = 0.0054$ .

<sup>12</sup> The Rainbow database can be found at [https://rainbowx.fis.ucm.es/Rainbow\\_navigator\\_public/](https://rainbowx.fis.ucm.es/Rainbow_navigator_public/).



redshifts in the training set. Nevertheless, of 71 with spectroscopic measurements, only 11 deviate by more than  $\Delta z = 0.2$ . The overall results suggest a photometric redshift success rate near 90%, but sources lacking spectroscopic redshifts tend on average to be fainter, and the success rate could be lower for them. Table 4 gives the best redshift we could find for each object. We have preferred NMBS if available because the use of medium band filters should give better redshift performance. The least-preferred survey was the one from Huang et al. (2012b) because of its limitation to  $z < 1.1$ , but order of preference among the other surveys was not obvious. Changing the order would not change the results of this paper. All in all, Table 4 has 235 spectroscopic redshifts, 238 photometric redshifts, and 38 objects with no redshift available. Thus about 93% of the radio source counterparts have a redshift of some kind, but at least 24 of the photometric redshifts (5% of the full sample) likely differ from the true redshift by  $\Delta z > 0.2$ .

## 4. Discussion

### 4.1. Identification Rate

The overall identification rate of >99% is unprecedented for a radio sample of this size and depth, and the sensitive infrared data from IRAC were critical. 87 counterparts or 17% of the sample are fainter than the 90% catalog completeness limit of 21.08 mag. If the IRAC images had been shallower, these sources would have been unidentified or incorrectly matched to neighboring sources brighter than the correct counterparts. Indeed, Afonso et al. (2011) achieved only 83% identification with their shallower IRAC data, though their radio sample (consisting solely of ultra-steep-spectrum radio sources) is not identical to ours and may preferentially include higher-redshift objects.

Spurious counterpart identifications from chance coincidence of radio sources with unrelated IRAC sources are unlikely. The IRAC source density (Barmby et al. 2008, Fig. 9) at  $[3.6] < 21$  is about  $0.002 \text{ arcsec}^{-2}$ . Thus we would expect blind position matching of the whole radio sample with radius  $0''.7$  to produce less than one spurious match at this magnitude level. In fact, 417 counterparts have  $[3.6] < 21$  (Fig. 4), and position offsets are mostly  $< 0''.7$  (Fig. 1), consistent with expected position uncertainties. Of the fainter 93 sources, we expect  $\sim 1$  spurious match within  $0''.7$  and  $[3.6] < 23$ , but again the magnitudes are nearly all brighter and the position offsets smaller than these values. The most suspicious source is 033 with  $[3.6] = 22.4$  and a position offset  $1''.3$ . The proposed counterpart has a relatively flat SED (in  $F_\nu$ , Table 5) from 3.6 to  $8.0 \mu\text{m}$ , unusual for a normal galaxy but not for a radio source counterpart. Thus we regard even a single spurious IRAC match for the simple radio sources as unlikely. The areal density of  $R < 26$  sources is about 5

times higher than of  $[3.6] < 23$  sources, and a few spurious matches at  $R$  cannot be ruled out. For the complex sources, the issue is not so much chance coincidences as uncertainty in the expected location of the counterpart relative to the radio emission. As discussed in Section 2.1, alternate counterpart identifications are possible in some cases.

## 4.2. Nature of Sources

Radio emission can arise either from an AGN or from star formation (e.g., Rieke et al. 1980; Yun, Reddy, & Condon 2001; Condon, Cotton, & Broderick 2002; Bell 2003 and especially §2.1 of Padovani et al. 2009 for comprehensive discussion). There are a variety of ways to separate the respective contributions (e.g., Padovani et al. 2009; Morić et al. 2010), but in general detailed followup at wavelengths other than radio and mid-infrared (MIR) is required.

For some objects, the source of emission is obvious. The low-redshift starburst population can be seen in Figure 6, where the  $8\ \mu\text{m}$  PAH emission makes low- $z$  starbursts red in the  $[4.5] - [8.0]$  IRAC color (but does not affect  $[3.6] - [5.8]$ , which remains blue) as long as  $z \lesssim 0.5$ . (See Fig. 8 of Huang et al. 2007. Fig. 2 of Padovani et al. 2011 is the equivalent diagram for their sample.) Figure 7 shows a different color-color plot. In both plots, the low-redshift galaxies are mostly within the starburst region, but a significant minority are in the AGN region. Depending on which color-color plot and the exact criteria one chooses, there are about 50–60  $z \leq 0.5$  galaxies in the low- $z$  starburst category.

Other cases where the emission source is obvious are those with spectra that show strong PAH features. Huang et al. (2009) found 11 sources with  $1.6 \leq z \leq 3.0$  and strong PAH features; seven of them are in the present radio sample. A seventh radio source in the Huang et al. list, not in their original sample but discovered serendipitously, shows no PAH features and is likely to be an AGN at  $z = 2.12$  both from its spectrum and its MIR colors.

Radio power itself can be used as a criterion to separate star formation from active nuclei in local galaxies (e.g., Padovani et al. 2009), but it may not work well at large redshifts. A radio luminosity (measured for convenience at rest frequency 3 GHz)  $L(3\ \text{GHz}) = 10^{23}\ \text{W}\ \text{Hz}^{-1}$  corresponds to  $\text{SFR} = 100\ \text{M}_\odot\ \text{yr}^{-1}$  (Yun, Reddy, & Condon 2001) for typical spectral index 0.7. Most local galaxies have SFR much lower than this.  $\text{SFR} = 200\ \text{M}_\odot\ \text{yr}^{-1}$  would correspond to  $L(\text{FIR}) > 10^{12}\ \text{L}_\odot$  (Kennicutt 1998), i.e., to a ULIRG, which galaxies are very rare locally. However, the ULIRG abundance is much higher at high redshift (e.g., Le Floc’h et al. 2005 Fig. 14; Magnelli et al. 2011 Fig. 9b), and the detection of 8234  $z \leq 1.2$  LIRGs in the COSMOS field (Feruglio et al. 2010) suggests that there could be of order 20 ULIRGs at  $z < 1.2$  in the present sample. Figure 8 shows observed radio luminosities versus

redshift for sample galaxies with known redshifts. At  $z \leq 1.2$ , there are 87 sample galaxies with  $L(3 \text{ GHz}) > 2 \times 10^{23} \text{ W Hz}^{-1}$ . Of these, 14 have  $L(3 \text{ GHz})$  an order of magnitude or more above this limit and are unlikely to be star forming, but the sheer numbers of such luminous galaxies also suggests that most are AGNs. The two objects with highest radio luminosity (at  $z \leq 1.2$ : 017 and 193) are radio doubles, clarifying the presence of an AGN at least in them. Over all redshifts, 27 sources have  $L(3 \text{ GHz}) > 5 \times 10^{24} \text{ W Hz}^{-1}$ , above any known value for star formation (Chapman et al. 2010). The Huang et al. (2009, 2012a) sources should by selection be among the most luminous star formers, and their luminosities are all between 0.8 and  $4 \times 10^{24} \text{ W Hz}^{-1}$ . It is therefore likely but not certain that the radio emission from the most luminous radio sources comes from an AGN, but radio luminosity alone is an uncertain criterion.

The MIR colors themselves can indicate the nature of the sources (Stern et al. 2005; Donley et al. 2012) but not with perfect reliability. Donley et al. found almost 40% of powerful radio galaxies from the SHzRG sample (Seymour et al. 2007) outside their AGN selection region and fully 2/3 of  $z > 1$  3CRR radio galaxies (as distinguished from 3CRR quasars) outside it. Apparently some combination of obscuration of the MIR AGN emission by dust and veiling by the host galaxy can make the overall colors look like a normal or star-forming galaxy, especially if the host galaxy is luminous compared to the AGN. Worse, purely star-forming galaxy SEDs (at least as represented by some templates) can enter the Stern et al. (2005) AGN color-color region at some redshifts and for some values of dust reddening (Donley et al. 2012). The Donley et al. criteria were designed to avoid this contamination but at the price of missing some AGNs. In the present sample, 97 objects (19%) have MIR colors in or very near the Donley et al. AGN box.<sup>13</sup> Park et al. (2010) found 31 of these to be power-law galaxies, which are clearly AGNs. (The Park et al. radio sample was the same one used in this paper.) Radio luminosities for the 83 objects with redshifts and AGN MIR colors range from  $3 \times 10^{20}$  to  $8 \times 10^{25} \text{ W Hz}^{-1}$ , again showing that radio luminosity by itself is a poor criterion for source type.

The galaxies that lack redshifts have MIR colors consistent with AGN emission or high redshift or both. In Figure 7 in particular, almost all the galaxies without redshifts are either in the AGN wedge or just to its left where the  $z > 1.5$  templates (and most of the 3CR radio galaxies) lie. This is confirmed more directly by Figure 9, which shows that the galaxies without redshifts almost all have  $[3.6] - [4.5] > 0.1$ . This color is consistent with  $z \gtrsim 1.1$  or AGN emission or both. The objects without redshifts tend to be the faintest

---

<sup>13</sup>Specifically, the count includes all objects with  $[3.6] - [5.8] > 0.2$  and  $[4.5] - [8.0] > 0.375$ . Given their redshifts as indicated in Fig. 6, the objects meeting these criteria are likely to be AGNs rather than star-forming contaminants.

ones in the sample, as shown in Figure 5. This will make it difficult to obtain redshifts but is consistent with their being obscured AGNs or at  $z \gg 1$ . Higdon et al. (2005) studied a sample of “optically invisible radio sources” (OIRSs) with  $R \gtrsim 26.0$  and  $I \gtrsim 25.6$ . The surface density of such sources (Higdon et al. 2005) predicts more than 25 such objects in the present sample (which is slightly deeper in  $S(1.4 \text{ GHz})$  than the Higdon et al. sample), and in fact there are 46 objects with  $R > 26$ . Higdon et al. suggested that the vast majority (87%) of such sources are AGNs based on the lack of  $24 \mu\text{m}$  detections, and Houck et al. (2005) gave evidence that even some OIRSs with  $24 \mu\text{m}$  detections have spectra consistent with being powered by an AGN. Half of the OIRSs in the present sample have MIR colors outside the AGN boxes in Figures 6 and 7, and it seems likely that many of these are AGN-powered despite their MIR colors.

Even when the source of the radio emission is an AGN, the AGN emission need not dominate the rest-frame near infrared emission. Figure 9 shows that for the majority of the sample,  $[3.6] - [4.5]$  is consistent with a stellar population at the observed redshift. Figures 6 and 7 show many radio source counterparts inside the AGN regions but most outside. Thus a substantial minority of radio source counterparts show AGN emission in the infrared, but most do not. The origin of the radio emission from these sources is unclear, and detailed followup will be needed to determine which galaxies are star forming and which are AGNs.

Authors studying other  $\mu\text{Jy}$  radio samples have disagreed on the origin of the radio emission, although it has always been clear that AGNs and star forming galaxies are both present (Benn et al. 1993). Barger, Cowie, & Wang (2007) used visible spectroscopy and X-ray emission to separate star formers from AGNs and concluded that the majority of the  $z < 1$  sample are star formers while at least 1/3 of the  $L(3 \text{ GHz}) > 2.6 \times 10^{23} \text{ W Hz}^{-1}$  sample (mostly at  $z > 1$ ) have X-ray luminosity characteristic of AGNs. A substantial allowance for X-ray obscured AGNs (e.g., Donley, Rieke, Rigby, & Pérez-González 2005) must be added to the numbers of that last group. Chapman et al. (2010) detected far-infrared emission characteristic of star formation in at least 40 galaxies of a sub-sample of 68 radio sources above the same radio luminosity limit, but the requirement to have a spectroscopic redshift may have biased their sample against AGNs, and Morić et al. (2010) give reason for caution in interpreting FIR fluxes. Padovani et al. (2011) classified 63% of their radio source counterparts as AGNs based on a complex scheme involving a wide variety of data. They also found that the AGN fraction depends strongly on the radio flux density limit and on redshift.

All in all, about 10–15% of the AEGIS20 sample consists of nearby star-forming galaxies, and about 20–25% are AGNs, mostly at  $z > 1$ . The rest are a mix of types, but the exact proportions are still unclear. Because the sample has essentially complete counterpart identification, it should be valuable in determining the origin of the radio emission and the

fraction of obscured AGNs at high redshift. For comparison with other samples, the median redshift of the AEGIS20 sample is 1.03 (assuming the unmeasured redshifts are above this value). This is lower than that of the slightly deeper ( $S_{1.4} > 43 \mu\text{Jy}$ ) Mainieri et al. (2008) sample, which has a median redshift of 1.18 with 92% redshift completeness (Padovani et al. 2011). That degree of redshift completeness is vital; an earlier study (Padovani et al. 2009) of the Mainieri et al. sample with only 70% redshift completeness found a median redshift of 0.67.

### 4.3. The $K$ - $z$ Relation and Stellar Mass

Several studies (e.g., Willott, Rawlings, Jarvis, & Blundell 2003; Rocca-Volmerange et al. 2004; Bryant et al. 2009) have noted a strong correlation between redshift and the observed  $2.2 \mu\text{m}$  flux density. However, these studies have all involved samples with limiting radio flux densities  $\gtrsim 200 \text{ mJy}$ . Figure 10 shows the  $3.6 \mu\text{m}$  magnitude versus redshift for the current sample, for which few  $2.2 \mu\text{m}$  ( $K$ ) magnitudes are available. The wavelength difference between  $K$  and [3.6] will introduce a modest, redshift-dependent offset in the relation, but the basic form should not change because the dominant radiation source in both wavelengths is stars in the host galaxy. Indeed Figure 10 shows that the [3.6]- $z$  data are distributed around the known  $K$ - $z$  relation but with large scatter. The scatter is larger for sources with photometric redshifts but still substantial even for objects with spectroscopic redshifts. Using a synthetic  $K$  magnitude  $K_{\text{synth}} \equiv [3.6] + a([3.6] - [4.5])$ , where  $a$  is a constant of order unity, does not dramatically reduce the scatter. The two objects (233, 480) with [3.6] far brighter than the standard relation are likely to be QSOs, which are normally excluded from the  $K$ - $z$  relation. The scatter is far too large to use the  $3.6 \mu\text{m}$  magnitude as a way to determine redshift for individual objects, but as a group, the objects without measured redshifts have magnitudes consistent with  $z > 1.1$ .

The observed  $3.6 \mu\text{m}$  magnitudes of the radio source counterparts give an indication of the stellar masses. At the redshifts of interest, radiation observed at  $3.6 \mu\text{m}$  was emitted near the stellar radiation peak at  $1.6 \mu\text{m}$ , and this is closely associated with the mass of the stellar population (e.g., Bell & de Jong 2001). Figure 10 shows the magnitudes that would be observed for single stellar populations that form instantaneously at  $z = 6$  and evolve passively thereafter (Bruzual & Charlot 2003). Most of the radio source counterparts fall between the lines for  $10^{11}$  and  $10^{12} M_{\odot}$  but with substantial numbers below the  $10^{11} M_{\odot}$  line. If the populations formed at  $z < 6$ , the actual galaxy masses could be up to a factor of 3–5 smaller than indicated. Using Chabrier instead of Salpeter IMF would lower the masses by a factor of 1.7 (Bundy et al. 2006). Furthermore, some of the  $3.6 \mu\text{m}$  light could come from an AGN rather than a stellar population; this is almost certainly the case for

the extreme galaxies such as 480 and 473. On the other hand, the stellar population models do not include dust extinction, which could cause the masses to be underestimated by an unknown amount. Model-fitting could give better mass estimates for individual galaxies, but the overall picture is that the radio sources live mostly in massive galaxies, but the range of stellar masses represented in the sample is larger than an order of magnitude.

## 5. Conclusions

IRAC images are a powerful means of identifying and classifying radio sources. Images with  $\sim 9$  ks IRAC depth giving  $\sigma \approx 0.1 \mu\text{Jy}$  (Barmby et al. 2008) are sufficient to detect essentially all counterparts of radio sources in a sample with 1.4 GHz brightness limit of  $50 \mu\text{Jy/beam}$ . Radio sources at this depth are roughly 10–15% local ( $z \lesssim 0.5$ ) starbursts and 20–25% AGNs mostly at  $z > 1$  with the remainder of uncertain nature. More than 1/3 of the sample have counterparts with  $R_{\text{AB}} > 24$ , and 15% have  $R_{\text{AB}} > 25.5$ . These sources would be very difficult to identify in  $R$ -band surveys, and if simple position matching were used, many would be incorrectly identified with brighter objects that are nearby on the sky but unrelated to the radio source.

The AEGIS20 sample, now essentially 100% identified, offers a great opportunity for detailed studies of the radio population. X-ray observations and additional spectra should enable a better classification between star-forming and active-nuclei galaxies, and the sample should yield luminosity functions and evolutionary history of the various populations.

The authors thank Jennifer Donley for valuable discussions on interpretation of IRAC color-color plots and Kate Whittaker for drawing our attention to and help with the NMBS survey. We thank Satoshi Miyazaki for providing the Subaru  $R$  images. We also thank Pablo Pérez González for help using the Rainbow Navigator query system and especially for his and Guillermo Barro’s work to create the Rainbow database. This work is based in part on observations made with the Spitzer Space Telescope, which is operated by the Jet Propulsion Laboratory, California Institute of Technology under a contract with NASA. Support for this work was provided by NASA through an award issued by JPL/Caltech. The National Radio Astronomy Observatory is a facility of the National Science Foundation operated under cooperative agreement by Associated Universities, Inc. A.L.C. acknowledges funding from NSF CAREER grant AST-1055081. DEEP spectroscopy is supported by the National Science Foundation grants AST-0071198, AST-0507483, and AST-0808133. This study makes use of data from AEGIS, a multiwavelength sky survey conducted with the Chandra, GALEX, Hubble, Keck, CFHT, MMT, Subaru, Palomar, Spitzer, VLA, and other telescopes and supported in part by the NSF, NASA, and the STFC. This work has made

use of the Rainbow Cosmological Surveys Database, which is operated by the Universidad Complutense de Madrid (UCM). IRAF is distributed by the National Optical Astronomy Observatory, which is operated by the Association of Universities for Research in Astronomy (AURA) under cooperative agreement with the National Science Foundation.

Facilities: Spitzer/IRAC Spitzer/MIPS Keck Subaru VLA

## REFERENCES

- Afonso, J., Mobasher, B., Koekemoer, A., Norris, R. P., & Cram, L. 2006, *AJ*, 131, 1216
- Afonso, J., et al. 2011, arXiv:1108.4037
- Bardelli, S., et al. 2010, *A&A*, 511, A1
- Barger, A. J., Cowie, L. L., & Wang, W.-H. 2007, *ApJ*, 654, 764
- Barmby, P., et al. 2006, *ApJ*, 642, 126
- Barmby, P., Huang, J.-S., Ashby, M. L. N., Eisenhardt, P. R. M., Fazio, G. G., Willner, S. P., & Wright, E. L. 2008, *ApJS*, 177, 431
- Barro, G., et al. 2011, *ApJS*, 193, 13
- Barro, G., et al. 2011, *ApJS*, 193, 30
- Bell, E. F. 2003, *ApJ*, 586, 794
- Bell, E. F., & de Jong, R. S. 2001, *ApJ*, 550, 212
- Benn, C. R., Rowan-Robinson, M., McMahon, R. G., Broadhurst, T. J., & Lawrence, A. 1993, *MNRAS*, 263, 98
- Bertin, E., & Arnouts, S. 1996, *A&AS*, 117, 393
- Bundy, K., et al. 2006, *ApJ*, 651, 120
- Bruzual, G. & Charlot, S. 2003, *MNRAS*, 344, 1000
- Bryant, J. J., Johnston, H. M., Broderick, J. W., Hunstead, R. W., De Breuck, C., & Gaensler, B. M. 2009, *MNRAS*, 395, 1099
- Chapman, S. C., et al. 2010, *MNRAS*, 409, L13
- Ciliegi, P., Zamorani, G., Hasinger, G., Lehmann, I., Szokoly, G., & Wilson, G. 2003, *A&A*, 398, 901
- Coil, A. L., et al. 2009, *ApJ*, 701, 1484
- Condon, J. J., Cotton, W. D., & Broderick, J. J. 2002, *AJ*, 124, 675
- Cooper, M. C., et al. 2011, *ApJS*, 193, 14
- Cooper, M. C., et al. 2012, *MNRAS*, 419, 3018



- Coupon, J., et al. 2009, *A&A*, 500, 981
- Davis, M., et al. 2003, *Proc. SPIE*, 4834, 161
- Davis, M., et al. 2007, *ApJ*, 660, L1
- Donley, J. L., Rieke, G. H., Rigby, J. R., & Pérez-González, P. G. 2005, *ApJ*, 634, 169
- Donley, J. L., et al. 2012, *ApJ*, 748, 142
- Eisenhardt, P. R. M., et al. 2008, *ApJ*, 684, 905
- Feruglio, C., et al. 2010, *ApJ*, 721, 607
- Higdon, J. L., et al. 2005, *ApJ*, 626, 58
- Houck, J. R., et al. 2005, *ApJ*, 622, L105
- Huang, J.-S., et al. 2007, *ApJ*, 664, 840
- Huang, J.-S., et al. 2009, *ApJ*, 700, 183
- Huang, J.-S., et al. 2012, in preparation (IRS paper).
- Huang, J.-S., et al. 2012, in preparation (phot-z paper).
- Huynh, M. T., Jackson, C. A., Norris, R. P., & Fernandez-Soto, A. 2008, *AJ*, 135, 2470
- Huynh, M. T., Norris, R. P., Siana, B., & Middelberg, E. 2010, *ApJ*, 710, 698
- Iverson, R. J., et al. 2007, *ApJ*, 660, L77
- Kayser, R., Helbig, P., & Schramm, T. 1997, *A&A*, 318, 680
- Kennicutt, R. C., Jr. 1998, *ApJ*, 498, 541
- Le Flocc’h, E., et al. 2005, *ApJ*, 632, 169
- Magnelli, B., Elbaz, D., Chary, R. R., Dickinson, M., Le Borgne, D., Frayer, D. T., & Willmer, C. N. A. 2011, *A&A*, 528, A35
- Mainieri, V., et al. 2008, *ApJS*, 179, 95
- Minkowski, R. 1960, *ApJ*, 132, 908
- Morić, I., Smolčić, V., Kimball, A., Riechers, D. A., Ivezić, Ž., & Scoville, N. 2010, *ApJ*, 724, 779

- Newman, J. A. et al. 2012, ApJS, submitted (preprint at <http://lanl.arxiv.org/abs/1203.3192>)
- Padovani, P., Mainieri, V., Tozzi, P., Kellermann, K. I., Fomalont, E. B., Miller, N., Rosati, P., & Shaver, P. 2009, ApJ, 694, 235
- Padovani, P., Miller, N., Kellermann, K. I., Mainieri, V., Rosati, P., & Tozzi, P. 2011, ApJ, 740, 20
- Park, S. Q., et al. 2008, ApJ, 678, 744
- Park, S. Q., et al. 2010, ApJ, 717, 1181
- Rieke, G. H., Lebofsky, M. J., Thompson, R. I., Low, F. J., & Tokunaga, A. T. 1980, ApJ, 238, 24
- Rocca-Volmerange, B., Le Borgne, D., De Breuck, C., Fioc, M., & Moy, E. 2004, A&A, 415, 931
- Seymour, N., et al. 2007, ApJS, 171, 353
- Simpson, C., et al. 2006, MNRAS, 372, 741
- Stern, D., et al. 2005, ApJ, 631, 163
- Waddington, I., Windhorst, R. A., Dunlop, J. S., Koo, D. C., & Peacock, J. A. 2000, MNRAS, 317, 801
- Whitaker, K. E., et al. 2011, ApJ, 735, 86
- Willner, S. P., Coil, A. L., Goss, W. M., Ashby, M. L. N., Barmby, P., Huang, J.-S., Ivison, R., Koo, D. C., Egami, E., & Miyazaki, S. 2006, AJ, in press.
- Willott, C. J., Rawlings, S., Jarvis, M. J., & Blundell, K. M. 2003, MNRAS, 339, 173
- Yun, M. S., Reddy, N. A., & Condon, J. J. 2001, ApJ, 554, 803

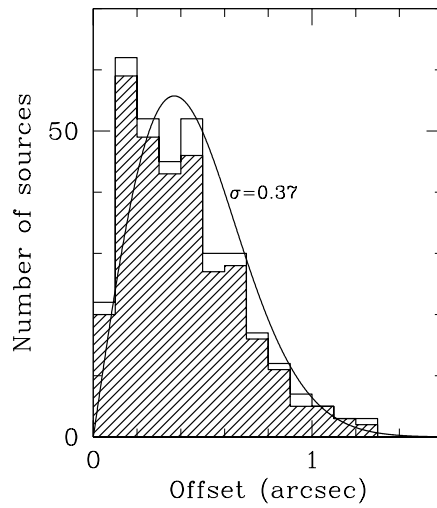
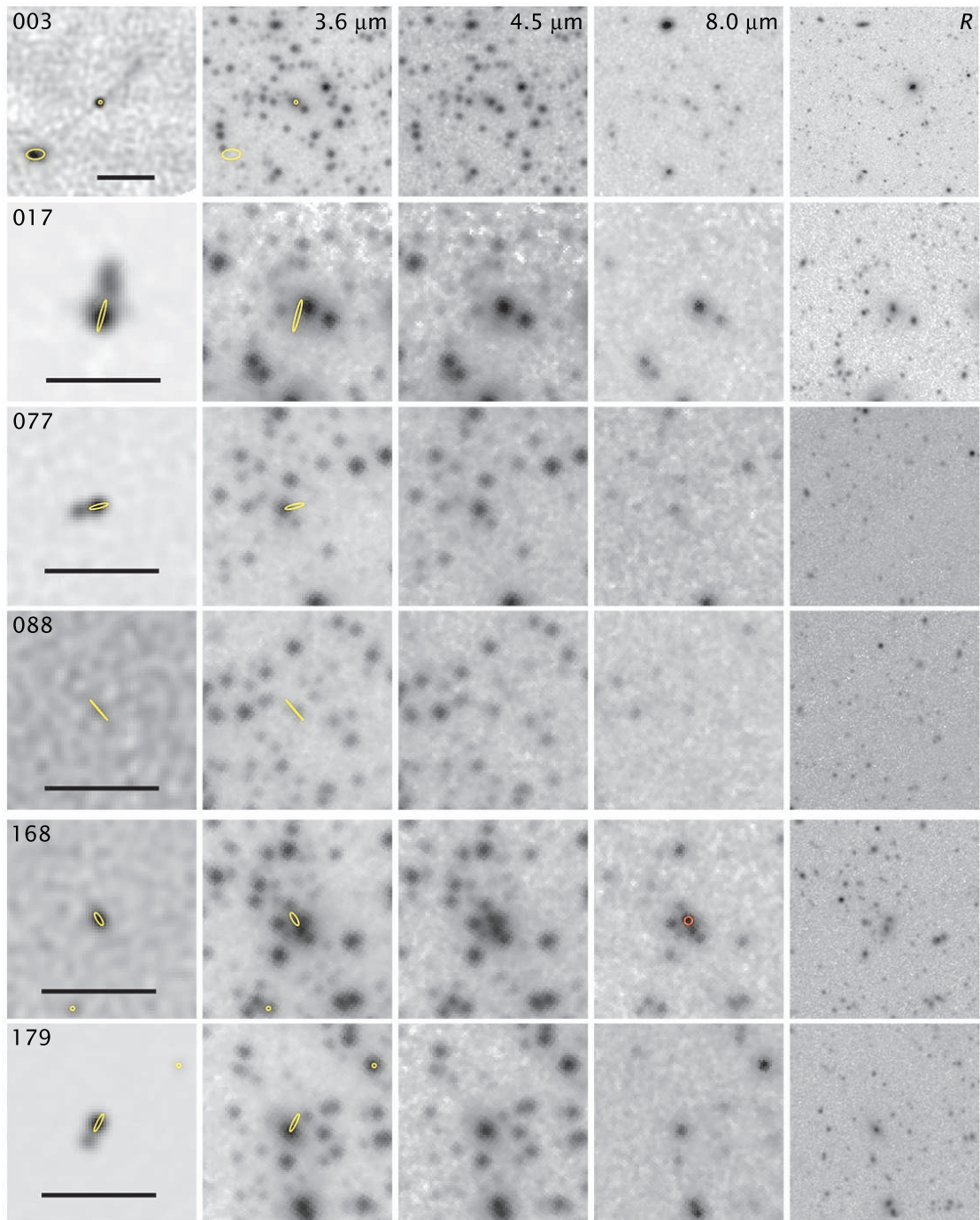


Fig. 1.— Histogram of radial offsets between radio and IRAC positions for 340 radio point sources. The shaded region shows offsets for 314 sources with  $[3.6] < 22$ . The curve shows the expected distribution for Gaussian position errors of  $0''.37$  (Barmby et al. 2008) in each coordinate.





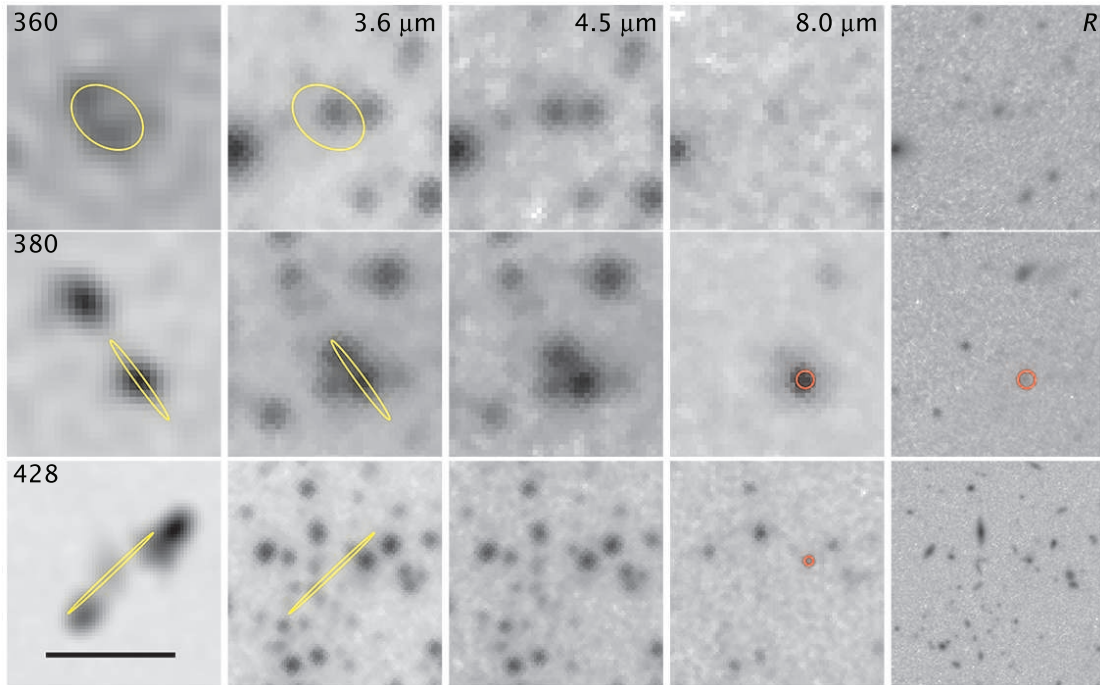
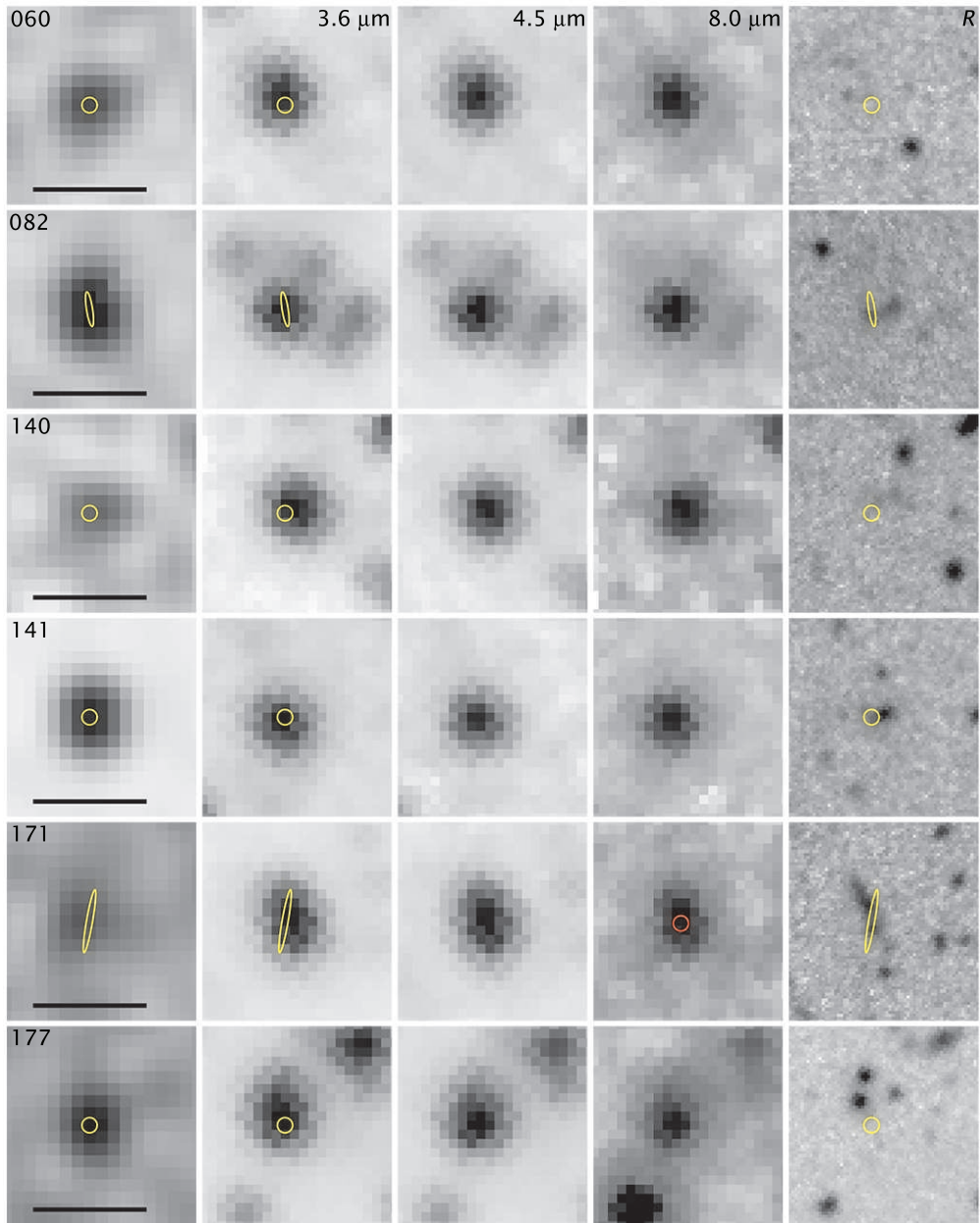


Fig. 2.— Postage stamp images of complex sources. From left to right, each row shows the VLA 20 cm radio, the IRAC 3.6  $\mu\text{m}$ , 4.5  $\mu\text{m}$ , and 8.0  $\mu\text{m}$  images and the Subaru  $R$  image of a source. The source numbers from Table 1 are indicated in the left panels. Scale bars indicate 30''; each stamp image is 100'', 50'', or if no scale bar is shown, 25'' across. North is up and east to the left in all images. Yellow contours show the Gaussian fit (Ivison et al. 2007) to the deconvolved radio source. The fits are generally smaller than the radio images themselves because of the radio beam size. Red circles are 2'' in diameter and show the position of the IRAC counterpart where it might not be obvious.





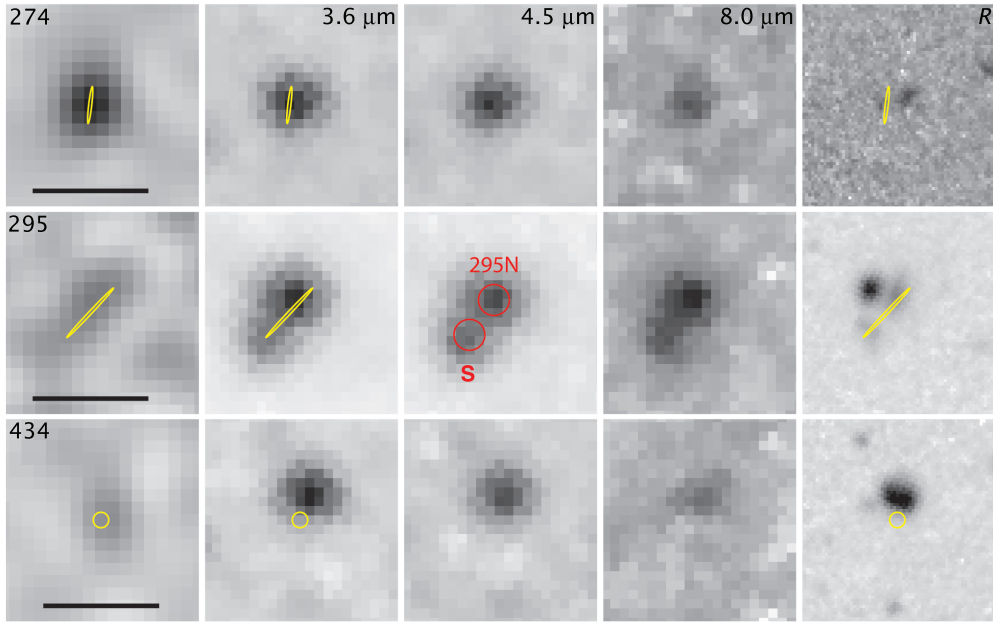


Fig. 3.— Postage stamp images of counterparts that might be misidentified if only  $R$  images were available and one source possibly lacking an IRAC counterpart. Each row shows one source with number (Table 1) indicated in the left panel. Panels from left to right show the 20-cm radio image, IRAC  $3.6 \mu\text{m}$ ,  $4.5 \mu\text{m}$ , and  $8.0 \mu\text{m}$  images, and the Subaru  $R$  image. Scale bars indicate  $7''.5$ ; each stamp image is  $12''.5$  across. North is up and east to the left in all images. Yellow contours show the Gaussian fit (Ivison et al. 2007) to the deconvolved radio source or a  $1''$  diameter circle if the radio source was unresolved. Red circles are  $1''$  in diameter and show the position(s) of the IRAC counterpart(s).



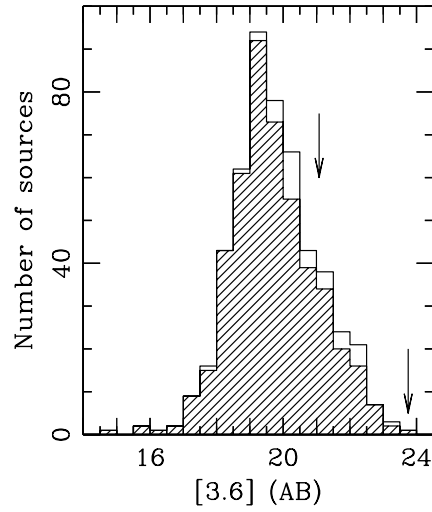


Fig. 4.— Histogram of  $3.6 \mu\text{m}$  magnitudes of radio source counterparts. The hatched histogram shows magnitudes for sources with redshifts. Arrows show the 90% and 50% completeness limits of the Barmby et al. (2008) catalog, but magnitudes can be measured on the images to fainter limits than these. Bins are half a magnitude in width because the distribution of  $3.6 \mu\text{m}$  magnitudes is narrower than the distribution of  $R$  magnitudes (Fig. 5).

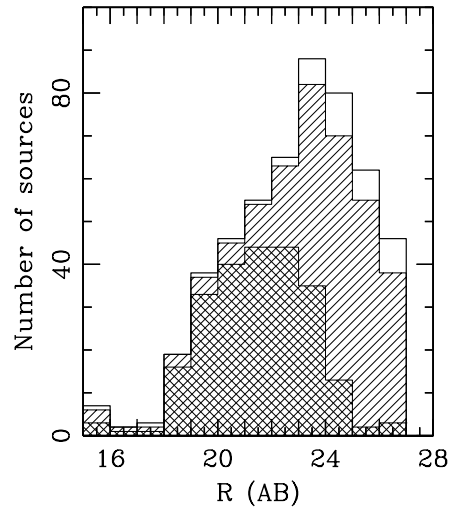


Fig. 5.— Histogram of  $R$  magnitudes of radio source counterparts. The hatched histogram shows magnitudes for sources with redshifts (including photometric ones), and the cross-hatched histogram for sources with spectroscopic redshifts. When no source was detected at  $R$ , its magnitude was placed in the bin corresponding to the upper limit. Some sources are likely much fainter than  $R = 27$ .

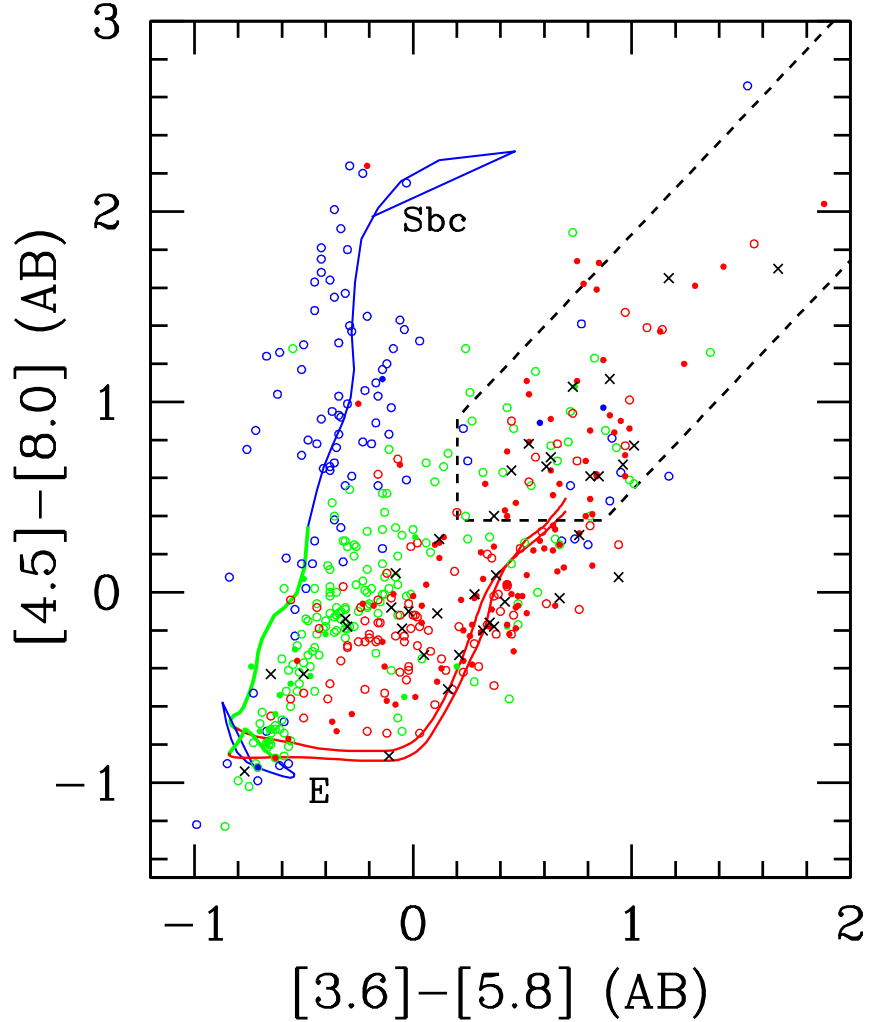


Fig. 6.— Color-color diagram for radio source counterparts showing the AGN selection region proposed by Donley et al. (2012). Circles denote objects with redshifts: blue for  $z \leq 0.5$ , green for  $0.5 < z \leq 1.1$ , and red for  $z > 1.1$ . Circles are filled if the radio luminosity  $L(3 \text{ GHz}) > 10^{23} \text{ W Hz}^{-1}$  at  $z \leq 0.5$  or  $> 10^{23} \text{ W Hz}^{-1}$  at  $z > 0.5$ . Crosses denote objects lacking redshifts. Curves illustrate the colors of two template SEDs, one for an elliptical galaxy (E) and the other for an Sbc galaxy, as redshift increases. The curves are color coded by redshift in the same way as the points and labeled near their respective  $z = 0$  locations.

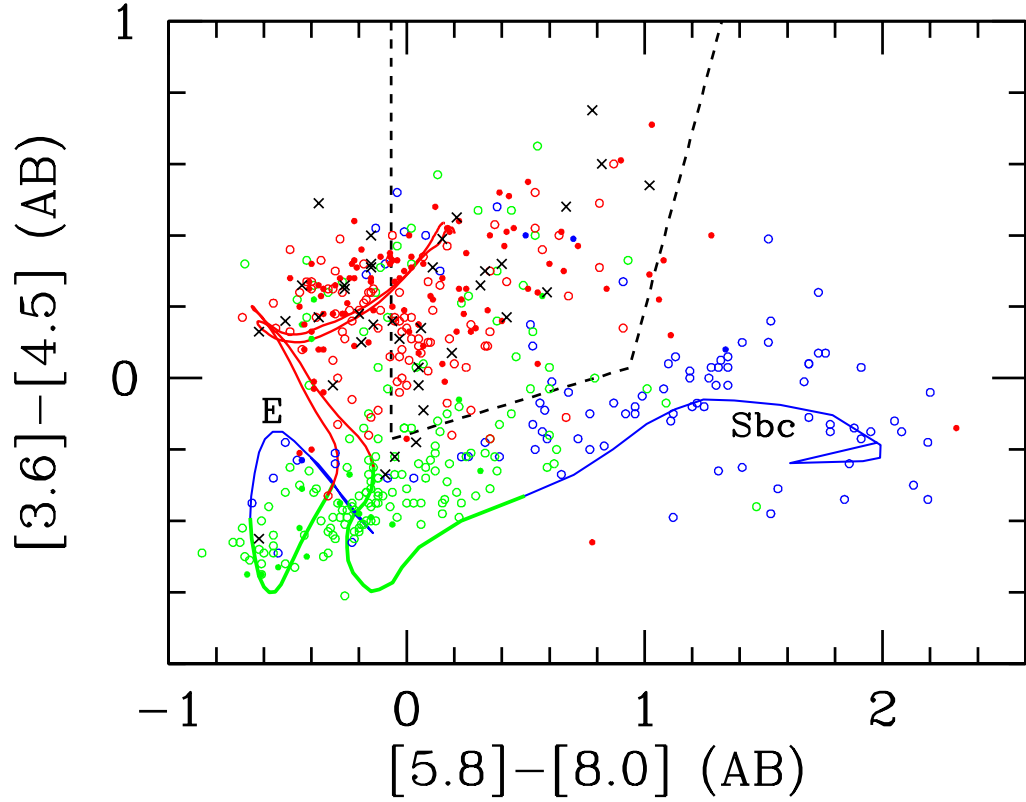


Fig. 7.— Color-color diagram for radio source counterparts showing the AGN selection wedge proposed by Stern et al. (2005). Circles denote objects with redshifts: blue for  $z \leq 0.5$ , green for  $0.5 < z \leq 1.1$ , and red for  $z > 1.1$ . Circles are filled if the radio luminosity  $L(3 \text{ GHz}) > 10^{23} \text{ W Hz}^{-1}$  at  $z \leq 0.5$  or  $> 10^{23} \text{ W Hz}^{-1}$  at  $z > 0.5$ . Crosses denote objects lacking redshifts. Curves illustrate the colors of two template SEDs, one for an elliptical galaxy (E) and the other for an Sbc galaxy, as redshift increases. The curves are color coded by redshift in the same way as the points.

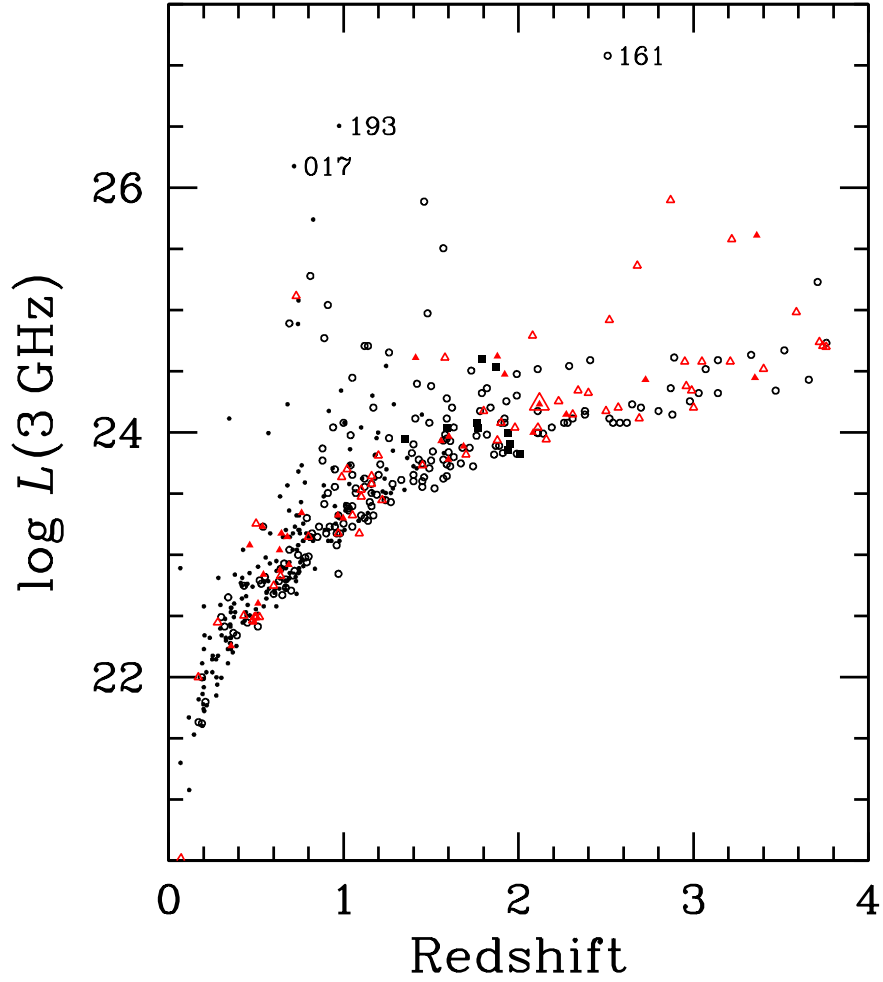


Fig. 8.— Radio power as a function of redshift for all sources that have redshifts. Red triangles denote sources with MIR colors indicating AGN emission, and black circles denote other objects. Symbols are filled if the redshift is spectroscopic. Black squares denote ULIRG sources from Huang et al. (2009, 2012a), and the large red triangle denotes the one AGN source from Huang et al. (2009). Three extreme sources are labeled with source nicknames from Table 3.

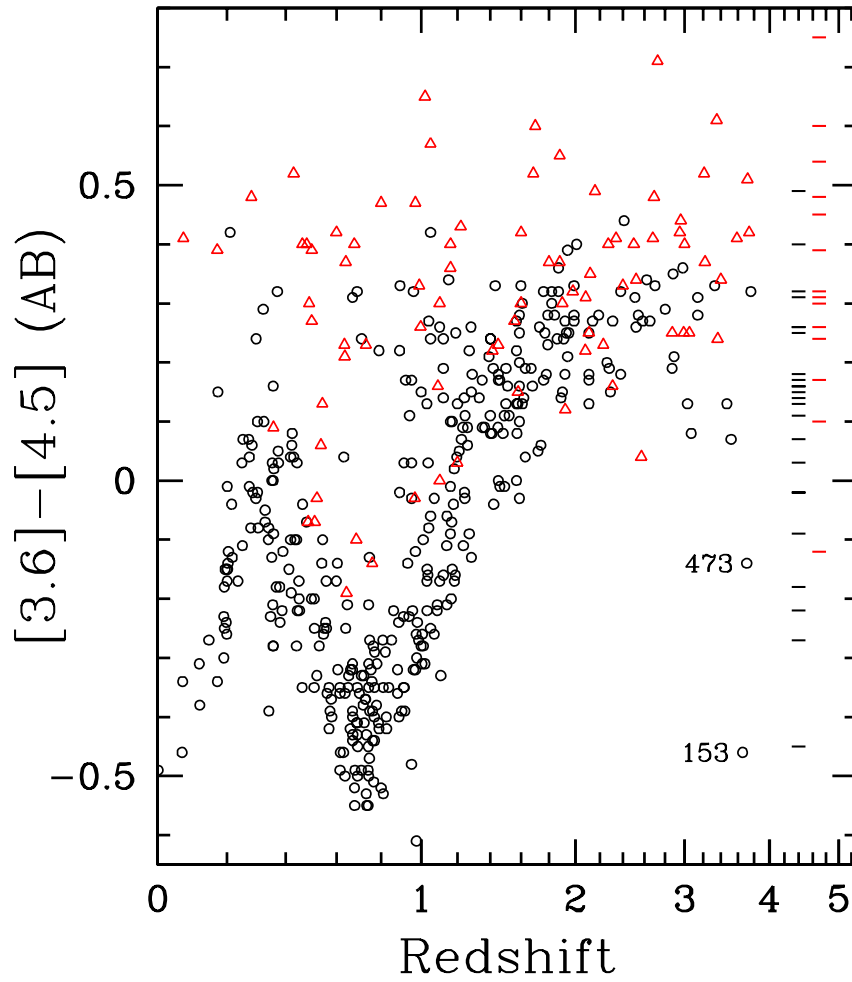


Fig. 9.— IRAC  $[3.6] - [4.5]$  color versus redshift (plotted as  $\log(1 + z)$  for clarity). Red triangles denote objects with MIR colors indicating AGN emission, and black circles denote other sources. Colors of sources without redshifts are shown as dashes, plotted arbitrarily at redshift 4.7 for those with AGN colors and 4.4 for other objects. Two outliers are labeled with their source nicknames from Table 3.

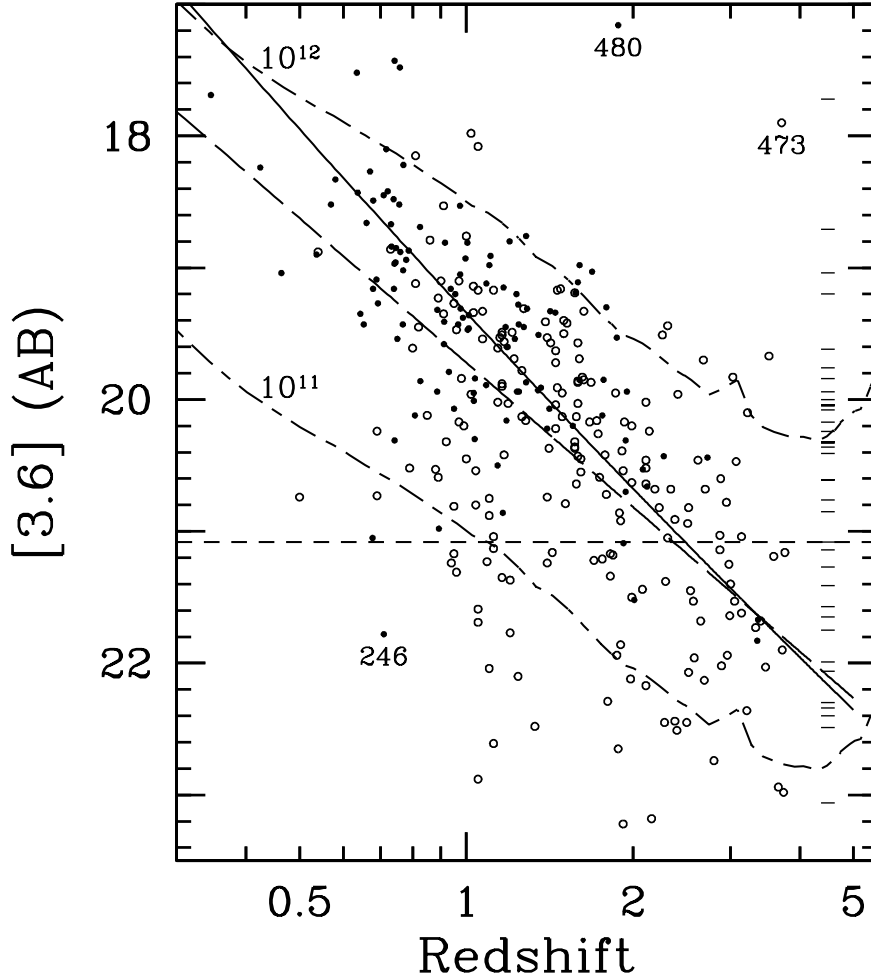


Fig. 10.— IRAC 3.6  $\mu\text{m}$  magnitude as a function of redshift. Filled circles denote objects with spectroscopic redshifts, and open circles denote objects with photometric redshifts. Objects with  $L(3\text{ GHz}) < 10^{23}\text{ W Hz}^{-1}$  are omitted; they are likely to be local starburst galaxies. Three outlying points are labeled with their source nicknames from Table 3. Magnitudes of objects with no redshift measurement are shown as dashes plotted at an arbitrary redshift of 4.5. The horizontal dashed line shows the 90% completeness limit of the IRAC catalog (Barmby et al. 2008). The solid curve shows the flux density from the  $K-z$  relation given by Willott, Rawlings, Jarvis, & Blundell (2003), i.e., assuming constant flux density from observed 2.2 to 3.6  $\mu\text{m}$ . The long-dashed line is the same but using the Bryant et al. (2009) relation. The two short-long dashed lines show the flux density of instantaneous bursts of star formation occurring at  $z = 6$  with initial masses  $10^{11}$  and  $10^{12}\text{ M}_{\odot}$ , respectively. (The actual stellar mass at relevant redshifts is 25–30% less because of assumed mass loss.) The models come from Bruzual & Charlot (2003), use a Salpeter IMF, and include no dust extinction.

Table 1. 20 cm Radio Sources with IRAC coverage

ID	AEGIS20	Flux Density (mJy)				Size (")		PA deg
		peak	unc <sup>a</sup>	int	unc <sup>a</sup>	Major	Minor <sup>b</sup>	
1	J141758.05+523134.5	0.161	0.028	0.161	0.028	0.0	0.0	0.0
2	J141736.35+523135.8	0.490	0.029	2.222	0.158	9.4	5.2	92.9
3	J141732.61+523203.3	0.850	0.032	0.910	0.057	1.7	0.0	120.6
4	J141809.94+523300.2	2.684	0.023	2.829	0.042	1.2	0.5	172.9
5	J141754.89+523307.1	0.152	0.027	0.152	0.027	0.0	0.0	0.0
6	J141824.01+523322.4	0.170	0.020	0.170	0.020	0.0	0.0	0.0
7	J141741.16+523355.5	1.033	0.029	1.033	0.029	0.0	0.0	0.0
8	J141816.25+523511.1	0.104	0.019	0.114	0.035	3.5	0.0	122.5
9	J141753.39+523539.5	1.280	0.022	1.697	0.046	3.2	0.6	16.8
10	J141831.51+523614.6	0.118	0.017	0.139	0.032	3.3	0.0	36.3
11	J141805.01+523621.5	0.106	0.019	0.106	0.019	0.0	0.0	0.0
12	J141830.15+523633.0	0.101	0.017	0.101	0.017	0.0	0.0	0.0
13	J141822.40+523633.8	0.358	0.018	0.361	0.032	1.1	0.0	16.2
14	J141755.54+523644.1	0.102	0.020	0.102	0.020	0.0	0.0	0.0
15	J141821.02+523710.9	0.169	0.017	0.195	0.033	2.7	0.0	142.7
16	J141841.95+523735.2	0.763	0.015	0.992	0.031	2.4	1.7	121.1
17	J141732.83+523816.0	43.556	0.031	127.207	0.136	8.5	-1	165.4
18	J141905.47+523859.6	0.092	0.016	0.092	0.016	0.0	0.0	0.0
19	J141906.22+523903.2	0.218	0.016	0.220	0.027	1.5	0.0	179.8
20	J141831.85+523907.3	0.089	0.015	0.089	0.015	0.0	0.0	0.0
21	J141839.58+523908.1	0.081	0.015	0.081	0.015	0.0	0.0	0.0
22	J141753.52+523934.1	0.239	0.018	0.239	0.018	0.0	0.0	0.0
23	J141814.52+523936.9	0.120	0.016	0.120	0.016	0.0	0.0	0.0
24	J141822.46+523937.7	0.119	0.015	0.119	0.015	0.0	0.0	0.0
25	J141859.89+524004.0	0.085	0.015	0.085	0.015	0.0	0.0	0.0
26	J141851.20+524004.4	0.106	0.014	0.128	0.028	2.7	0.0	119.4
27	J141857.16+524011.2	0.072	0.015	0.072	0.015	0.0	0.0	0.0
28	J141906.79+524013.9	0.088	0.015	0.098	0.028	2.8	0.0	77.9
29	J141805.51+524032.6	0.691	0.016	0.721	0.028	1.0	0.5	84.7
30	J141813.64+524038.2	0.406	0.015	0.406	0.015	0.0	0.0	0.0
31	J141841.97+524108.5	0.070	0.014	0.070	0.014	0.0	0.0	0.0
32	J141754.98+524115.0	0.314	0.018	0.319	0.031	0.9	0.0	137.8
33	J141846.26+524116.6	0.075	0.014	0.075	0.014	0.0	0.0	0.0
34	J141803.37+524127.9	0.091	0.015	0.091	0.015	0.0	0.0	0.0
35	J141850.98+524138.0	0.183	0.014	0.234	0.028	3.6	0.0	83.0
36	J141747.63+524143.4	7.146	0.018	13.089	-1	34.5	...	131.4
37	J141754.94+524144.3	0.255	0.016	0.291	0.030	2.0	0.5	17.2
38	J141817.42+524158.1	0.078	0.014	0.078	0.014	0.0	0.0	0.0
39	J141856.67+524200.7	0.087	0.014	0.087	0.014	0.0	0.0	0.0



Table 1—Continued

ID	AEGIS20	Flux Density (mJy)				Size (″)		PA deg
		peak	unc <sup>a</sup>	int	unc <sup>a</sup>	Major	Minor <sup>b</sup>	
40	J141821.21+524204.9	0.140	0.014	0.140	0.014	0.0	0.0	0.0
41	J141918.11+524233.3	0.139	0.014	0.159	0.027	1.6	1.2	128.5
42	J141833.23+524242.2	0.120	0.013	0.124	0.024	1.3	0.0	62.7
43	J141814.86+524243.7	0.336	0.014	0.344	0.025	1.0	0.0	136.3
44	J141904.34+524252.5	0.146	0.014	0.146	0.014	0.0	0.0	0.0
45	J141838.14+524307.9	0.071	0.013	0.079	0.025	1.3	1.3	138.3
46	J141855.58+524318.5	0.072	0.013	0.072	0.013	0.0	0.0	0.0
47	J141755.39+524339.5	0.086	0.014	0.086	0.014	0.0	0.0	0.0
48	J141928.05+524342.4	0.085	0.014	0.085	0.014	0.0	0.0	0.0
49	J141904.09+524346.0	0.124	0.014	0.124	0.014	0.0	0.0	0.0
50	J141826.96+524348.9	0.069	0.013	0.069	0.013	0.0	0.0	0.0
51	J141833.13+524352.4	0.171	0.014	0.171	0.014	0.0	0.0	0.0
52	J141934.05+524353.2	0.080	0.014	0.080	0.014	0.0	0.0	0.0
53	J141908.83+524400.7	0.106	0.013	0.166	0.031	4.5	0.7	175.3
54	J141853.18+524410.7	0.128	0.013	0.142	0.025	2.0	0.0	124.9
55	J141857.24+524414.1	0.241	0.013	0.260	0.024	2.0	0.0	179.9
56	J141808.93+524423.6	0.095	0.014	0.095	0.014	0.0	0.0	0.0
57	J141806.09+524452.3	0.080	0.013	0.110	0.028	3.5	0.7	41.7
58	J141845.88+524455.6	0.091	0.013	0.091	0.013	0.0	0.0	0.0
59	J141932.63+524504.4	0.097	0.013	0.097	0.013	0.0	0.0	0.0
60	J141836.70+524603.3	0.120	0.013	0.120	0.013	0.0	0.0	0.0
61	J141817.68+524615.5	0.092	0.013	0.092	0.013	0.0	0.0	0.0
62	J141852.79+524618.8	0.155	0.013	0.176	0.024	2.4	0.0	156.9
63	J141919.73+524640.1	0.121	0.012	0.159	0.026	2.8	1.4	174.7
64	J141912.82+524642.5	0.083	0.012	0.083	0.012	0.0	0.0	0.0
65	J141945.49+524647.9	10.164	0.014	10.594	0.025	1.1	0.3	2.4
66	J141830.13+524649.2	0.103	0.012	0.148	0.027	4.8	0.0	159.0
67	J141919.66+524715.4	0.089	0.012	0.098	0.023	2.5	0.0	123.3
68	J141947.91+524724.4	0.131	0.014	0.157	0.028	2.6	0.0	174.9
69	J141844.45+524735.7	0.160	0.013	0.160	0.013	0.0	0.0	0.0
70	J141820.27+524749.1	0.100	0.013	0.100	0.013	0.0	0.0	0.0
71	J141934.10+524800.3	0.444	0.013	0.444	0.013	0.0	0.0	0.0
72	J141919.02+524830.1	0.367	0.012	0.367	0.012	0.0	0.0	0.0
73	J141910.41+524830.7	2.734	0.011	6.069	0.034	6.4	2.0	39.6
74	J141829.93+524834.6	0.236	0.013	0.236	0.013	0.0	0.0	0.0
75	J141851.50+524835.9	0.263	0.012	0.263	0.012	0.0	0.0	0.0
76	J141954.81+524840.9	0.103	0.014	0.103	0.014	0.0	0.0	0.0
77	J141946.76+524844.9	0.787	0.014	1.494	0.038	5.0	-1	104.4
78	J141853.20+524855.5	0.101	0.012	0.153	0.027	3.4	2.0	28.6

Table 1—Continued

ID	AEGIS20	Flux Density (mJy)				Size (″)		PA deg
		peak	unc <sup>a</sup>	int	unc <sup>a</sup>	Major	Minor <sup>b</sup>	
79	J141914.10+524908.9	0.076	0.012	0.082	0.021	3.2	0.0	45.2
80	J141914.96+524930.0	0.270	0.012	0.270	0.012	0.0	0.0	0.0
81	J141940.04+524939.1	0.071	0.012	0.071	0.012	0.0	0.0	0.0
82	J141900.25+524948.3	0.268	0.012	0.316	0.023	2.3	0.4	8.9
83	J141907.83+524951.9	0.092	0.012	0.092	0.012	0.0	0.0	0.0
84	J141953.66+524956.9	0.082	0.014	0.082	0.014	0.0	0.0	0.0
85	J141854.51+525004.9	0.122	0.012	0.122	0.012	0.0	0.0	0.0
86	J141920.57+525024.1	0.064	0.012	0.083	0.024	4.0	0.0	63.4
87	J141947.51+525026.0	0.175	0.013	0.175	0.013	0.0	0.0	0.0
88	J141927.09+525034.5	0.059	0.011	0.102	0.028	6.8	0.0	40.5
89	J141917.32+525034.9	0.150	0.012	0.150	0.012	0.0	0.0	0.0
90	J141851.72+525044.4	0.081	0.012	0.081	0.012	0.0	0.0	0.0
91	J141937.41+525050.3	0.138	0.012	0.174	0.025	2.6	1.2	59.8
92	J141942.64+525052.7	0.174	0.013	0.174	0.013	0.0	0.0	0.0
93	J141958.24+525102.9	0.067	0.013	0.067	0.013	0.0	0.0	0.0
94	J141937.27+525103.2	0.145	0.012	0.161	0.023	2.2	0.0	120.3
95	J141952.09+525127.1	0.068	0.013	0.082	0.026	4.1	0.0	149.1
96	J141914.68+525131.0	0.066	0.012	0.066	0.012	0.0	0.0	0.0
97	J141904.88+525137.1	0.060	0.012	0.060	0.012	0.0	0.0	0.0
98	J141846.31+525141.2	0.140	0.012	0.140	0.012	0.0	0.0	0.0
99	J141910.25+525150.6	0.085	0.011	0.220	0.038	6.4	3.2	27.8
100	J141930.12+525159.1	0.470	0.012	0.478	0.020	0.6	0.4	130.7
101	J141910.11+525200.1	0.077	0.012	0.077	0.012	0.0	0.0	0.0
102	J142009.01+525214.7	0.116	0.012	0.116	0.012	0.0	0.0	0.0
103	J141915.70+525215.4	0.100	0.012	0.100	0.012	0.0	0.0	0.0
104	J141954.28+525220.7	0.437	0.013	0.468	0.024	1.7	0.0	7.4
105	J141939.21+525232.7	0.064	0.012	0.084	0.026	4.3	0.0	80.4
106	J141930.79+525235.3	0.075	0.012	0.075	0.012	0.0	0.0	0.0
107	J142004.19+525248.5	0.099	0.013	0.099	0.013	0.0	0.0	0.0
108	J141941.60+525255.3	0.101	0.013	0.101	0.013	0.0	0.0	0.0
109	J141933.34+525300.6	0.109	0.012	0.109	0.012	0.0	0.0	0.0
110	J141939.98+525327.6	0.079	0.012	0.079	0.012	0.0	0.0	0.0
111	J141912.66+525327.8	0.116	0.012	0.128	0.022	2.8	0.0	98.1
112	J141920.18+525337.3	0.087	0.012	0.087	0.012	0.0	0.0	0.0
113	J141913.64+525350.4	0.285	0.012	0.285	0.012	0.0	0.0	0.0
114	J141916.56+525352.1	0.270	0.012	0.281	0.020	1.0	0.5	162.0
115	J141938.60+525403.6	0.146	0.013	0.146	0.013	0.0	0.0	0.0
116	J142003.47+525404.4	0.146	0.013	0.158	0.023	2.9	0.0	119.6
117	J141939.58+525419.7	0.068	0.012	0.083	0.025	3.8	0.0	166.7

Table 1—Continued

ID	AEGIS20	Flux Density (mJy)				Size (″)		PA deg
		peak	unc <sup>a</sup>	int	unc <sup>a</sup>	Major	Minor <sup>b</sup>	
118	J141953.77+525421.5	0.111	0.012	0.121	0.023	3.3	0.0	165.9
119	J141922.53+525439.8	0.064	0.012	0.064	0.012	0.0	0.0	0.0
120	J142021.78+525441.9	0.091	0.012	0.114	0.025	2.9	0.0	109.9
121	J141950.44+525450.6	0.117	0.012	0.117	0.012	0.0	0.0	0.0
122	J142021.95+525511.9	0.230	0.012	0.230	0.012	0.0	0.0	0.0
123	J141922.06+525519.0	0.132	0.012	0.132	0.012	0.0	0.0	0.0
124	J141920.57+525521.3	0.530	0.012	0.560	0.022	1.2	0.6	85.9
125	J142033.15+525523.6	0.087	0.011	0.087	0.011	0.0	0.0	0.0
126	J142013.01+525533.2	0.253	0.012	0.268	0.022	1.7	0.0	128.9
127	J142009.47+525549.7	0.101	0.012	0.101	0.012	0.0	0.0	0.0
128	J141920.09+525609.0	0.077	0.012	0.111	0.027	3.9	0.5	49.0
129	J141939.82+525615.5	0.062	0.012	0.062	0.012	0.0	0.0	0.0
130	J142042.42+525631.1	0.127	0.012	0.127	0.012	0.0	0.0	0.0
131	J142037.16+525632.1	0.060	0.012	0.060	0.012	0.0	0.0	0.0
132	J141946.13+525647.0	2.882	0.012	3.115	0.022	1.3	0.8	86.7
133	J141949.25+525704.5	0.077	0.012	0.077	0.012	0.0	0.0	0.0
134	J142046.70+525711.0	0.081	0.012	0.120	0.027	4.7	0.0	52.5
135	J142002.19+525714.9	0.071	0.012	0.074	0.022	3.1	0.0	137.0
136	J142018.71+525716.7	0.073	0.011	0.073	0.011	0.0	0.0	0.0
137	J141922.33+525717.0	0.088	0.013	0.098	0.024	3.2	0.0	23.0
138	J142041.80+525724.4	0.167	0.012	0.167	0.012	0.0	0.0	0.0
139	J141928.97+525725.3	0.188	0.013	0.197	0.023	2.4	0.0	20.2
140	J141919.77+525735.0	0.089	0.013	0.089	0.013	0.0	0.0	0.0
141	J142050.36+525746.9	1.057	0.012	1.057	0.012	0.0	0.0	0.0
142	J141937.46+525800.1	0.083	0.013	0.089	0.023	3.3	0.0	39.2
143	J142033.38+525801.1	1.097	0.012	1.468	0.026	2.9	1.5	98.1
144	J142043.38+525806.2	0.069	0.013	0.069	0.013	0.0	0.0	0.0
145	J142047.54+525808.6	0.600	0.013	0.604	0.022	1.0	0.0	16.8
146	J141949.08+525811.7	0.113	0.012	0.123	0.023	1.6	0.4	54.5
147	J142031.77+525846.3	0.068	0.014	0.068	0.014	0.0	0.0	0.0
148	J142040.55+525850.4	0.106	0.013	0.106	0.013	0.0	0.0	0.0
149	J142037.25+525850.7	0.084	0.014	0.084	0.014	0.0	0.0	0.0
150	J142023.61+525858.2	0.126	0.012	0.131	0.022	1.5	0.0	77.3
151	J141943.39+525858.4	0.107	0.012	0.107	0.012	0.0	0.0	0.0
152	J141944.64+525859.4	0.119	0.012	0.119	0.012	0.0	0.0	0.0
153	J142008.19+525903.8	0.056	0.011	0.056	0.011	0.0	0.0	0.0
154	J141957.34+525926.1	0.113	0.011	0.113	0.011	0.0	0.0	0.0
155	J142053.85+525926.1	0.516	0.013	0.516	0.013	0.0	0.0	0.0
156	J141938.99+525930.0	0.076	0.013	0.076	0.013	0.0	0.0	0.0

Table 1—Continued

ID	AEGIS20	Flux Density (mJy)				Size (")		PA deg
		peak	unc <sup>a</sup>	int	unc <sup>a</sup>	Major	Minor <sup>b</sup>	
157	J142002.69+525934.0	0.084	0.011	0.087	0.019	2.4	0.0	173.1
158	J142002.82+525943.9	0.745	0.011	0.745	0.011	0.0	0.0	0.0
159	J141940.10+525945.1	0.067	0.012	0.095	0.027	3.6	1.0	67.0
160	J142002.04+525950.4	0.078	0.011	0.078	0.011	0.0	0.0	0.0
161	J142033.26+530003.7	57.500	0.015	58.546	0.027	0.6	0.4	75.8
162	J142056.20+530017.5	0.109	0.013	0.109	0.013	0.0	0.0	0.0
163	J141952.11+530022.9	0.075	0.011	0.075	0.011	0.0	0.0	0.0
164	J142011.13+530031.8	0.141	0.011	0.141	0.011	0.0	0.0	0.0
165	J142002.04+530039.0	0.067	0.011	0.067	0.011	0.0	0.0	0.0
166	J141939.79+530044.2	0.119	0.012	0.135	0.023	2.4	0.0	74.5
167	J142026.55+530045.8	0.201	0.015	0.201	0.015	0.0	0.0	0.0
168	J141951.35+530046.5	0.240	0.011	0.360	0.024	3.8	1.3	31.0
169	J142015.08+530047.4	0.078	0.012	0.113	0.026	5.1	0.0	123.6
170	J142039.58+530049.7	0.122	0.015	0.122	0.015	0.0	0.0	0.0
171	J141942.24+530110.7	0.089	0.011	0.133	0.026	4.2	0.4	170.1
172	J142006.01+530120.6	0.060	0.011	0.076	0.021	3.6	0.0	173.8
173	J142048.77+530124.4	0.082	0.013	0.082	0.013	0.0	0.0	0.0
174	J142035.21+530148.7	0.094	0.013	0.094	0.013	0.0	0.0	0.0
175	J142020.34+530156.5	0.080	0.012	0.080	0.012	0.0	0.0	0.0
176	J142018.34+530157.3	0.094	0.012	0.094	0.012	0.0	0.0	0.0
177	J142021.54+530158.6	0.138	0.012	0.138	0.012	0.0	0.0	0.0
178	J141943.43+530205.9	0.101	0.011	0.101	0.011	0.0	0.0	0.0
179	J142104.98+530209.4	3.422	0.015	6.259	0.042	5.1	-1	153.2
180	J142006.64+530210.9	0.204	0.011	0.204	0.011	0.0	0.0	0.0
181	J142025.84+530222.2	0.073	0.012	0.073	0.012	0.0	0.0	0.0
182	J142038.92+530224.2	0.083	0.012	0.083	0.012	0.0	0.0	0.0
183	J142102.66+530224.5	0.235	0.014	0.235	0.014	0.0	0.0	0.0
184	J142043.04+530226.3	0.171	0.012	0.171	0.012	0.0	0.0	0.0
185	J142041.62+530229.2	0.304	0.012	0.329	0.022	1.5	0.5	93.6
186	J142034.09+530244.9	0.068	0.012	0.068	0.012	0.0	0.0	0.0
187	J142000.01+530257.3	0.203	0.010	0.203	0.010	0.0	0.0	0.0
188	J142119.88+530310.9	0.792	0.021	0.831	0.038	1.3	0.0	175.0
189	J142003.19+530315.5	0.059	0.010	0.113	0.028	6.8	0.0	137.9
190	J142035.71+530316.8	0.105	0.011	0.105	0.011	0.0	0.0	0.0
191	J141955.30+530322.9	0.052	0.010	0.052	0.010	0.0	0.0	0.0
192	J142045.43+530329.6	0.265	0.012	0.265	0.012	0.0	0.0	0.0
193	J142118.22+530330.1	61.615	0.021	135.364	0.061	11.9	...	128.6
194	J142002.44+530331.1	0.060	0.011	0.060	0.011	0.0	0.0	0.0
195	J142044.98+530334.9	0.068	0.012	0.068	0.012	0.0	0.0	0.0

Table 1—Continued

ID	AEGIS20	Flux Density (mJy)				Size (″)		PA deg
		peak	unc <sup>a</sup>	int	unc <sup>a</sup>	Major	Minor <sup>b</sup>	
196	J142032.56+530336.9	0.057	0.011	0.057	0.011	0.0	0.0	0.0
197	J142057.28+530337.3	0.239	0.014	0.239	0.014	0.0	0.0	0.0
198	J142029.43+530339.5	0.058	0.011	0.058	0.011	0.0	0.0	0.0
199	J141947.00+530342.6	0.090	0.011	0.090	0.011	0.0	0.0	0.0
200	J142047.63+530344.4	0.118	0.012	0.118	0.012	0.0	0.0	0.0
201	J141953.03+530345.0	0.058	0.011	0.058	0.011	0.0	0.0	0.0
202	J142127.29+530406.3	0.121	0.018	0.125	0.031	3.4	0.0	122.0
203	J142011.63+530443.4	0.091	0.011	0.091	0.011	0.0	0.0	0.0
204	J142043.65+530446.8	0.093	0.012	0.093	0.012	0.0	0.0	0.0
205	J142007.92+530454.2	0.061	0.011	0.061	0.011	0.0	0.0	0.0
206	J142027.52+530454.4	0.080	0.011	0.080	0.011	0.0	0.0	0.0
207	J141957.58+530502.9	0.388	0.011	1.549	-1	47.0	...	128.0
208	J142023.35+530511.5	0.062	0.011	0.062	0.011	0.0	0.0	0.0
209	J142023.25+530519.0	0.058	0.011	0.058	0.011	0.0	0.0	0.0
210	J142035.66+530520.8	0.062	0.011	0.064	0.020	3.4	0.0	81.9
211	J142042.65+530544.4	0.061	0.012	0.061	0.012	0.0	0.0	0.0
212	J142053.96+530550.5	0.137	0.013	0.143	0.023	1.3	0.0	44.1
213	J142041.12+530551.1	0.084	0.012	0.084	0.012	0.0	0.0	0.0
214	J142116.66+530607.1	0.210	0.015	0.210	0.015	0.0	0.0	0.0
215	J142046.76+530614.1	0.082	0.012	0.082	0.012	0.0	0.0	0.0
216	J142128.04+530618.8	0.094	0.015	0.094	0.015	0.0	0.0	0.0
217	J142112.23+530621.8	0.271	0.014	0.271	0.014	0.0	0.0	0.0
218	J142048.50+530623.9	0.084	0.012	0.084	0.012	0.0	0.0	0.0
219	J142040.17+530629.7	0.076	0.011	0.076	0.011	0.0	0.0	0.0
220	J142053.38+530638.2	0.191	0.012	0.191	0.012	0.0	0.0	0.0
221	J142019.20+530642.6	0.053	0.011	0.053	0.011	0.0	0.0	0.0
222	J142100.81+530644.1	0.067	0.012	0.148	0.038	6.2	2.2	61.7
223	J142040.14+530647.6	0.088	0.011	0.088	0.011	0.0	0.0	0.0
224	J142034.18+530710.2	0.066	0.011	0.066	0.011	0.0	0.0	0.0
225	J142137.39+530716.5	0.127	0.013	0.127	0.013	0.0	0.0	0.0
226	J142012.54+530730.0	0.117	0.011	0.246	0.031	6.8	0.9	12.3
227	J142114.70+530733.9	0.065	0.012	0.065	0.012	0.0	0.0	0.0
228	J142033.18+530735.4	0.076	0.011	0.076	0.011	0.0	0.0	0.0
229	J142052.70+530745.5	0.073	0.012	0.073	0.012	0.0	0.0	0.0
230	J142043.85+530745.7	0.110	0.011	0.110	0.011	0.0	0.0	0.0
231	J142121.64+530754.0	0.177	0.012	0.177	0.012	0.0	0.0	0.0
232	J142116.68+530806.8	0.153	0.012	0.153	0.012	0.0	0.0	0.0
233	J142032.80+530815.2	2.272	0.010	12.538	0.056	15.6	-1	43.6
234	J142120.16+530816.2	0.113	0.012	0.129	0.022	1.6	1.3	0.1

Table 1—Continued

ID	AEGIS20	Flux Density (mJy)				Size (″)		PA deg
		peak	unc <sup>a</sup>	int	unc <sup>a</sup>	Major	Minor <sup>b</sup>	
235	J142015.29+530820.8	0.063	0.011	0.063	0.011	0.0	0.0	0.0
236	J142032.45+530832.5	3.000	0.010	7.398	0.034	5.4	3.9	172.5
237	J142155.14+530841.2	0.054	0.012	0.054	0.012	0.0	0.0	0.0
238	J142036.74+530902.9	0.064	0.011	0.073	0.021	2.2	0.0	45.1
239	J142056.48+530909.6	0.079	0.011	0.079	0.011	0.0	0.0	0.0
240	J142125.22+530912.5	0.062	0.012	0.062	0.012	0.0	0.0	0.0
241	J142051.61+530917.3	0.070	0.012	0.070	0.012	0.0	0.0	0.0
242	J142140.78+530924.3	0.058	0.012	0.058	0.012	0.0	0.0	0.0
243	J142148.23+530932.3	0.231	0.011	0.231	0.011	0.0	0.0	0.0
244	J142042.68+530932.8	0.943	0.011	1.049	0.021	2.0	0.0	61.2
245	J142138.35+530939.3	0.074	0.012	0.074	0.012	0.0	0.0	0.0
246	J142125.60+530949.9	0.120	0.012	0.132	0.022	1.7	0.5	60.1
247	J142058.39+530954.8	0.080	0.012	0.080	0.012	0.0	0.0	0.0
248	J142147.74+531023.3	0.329	0.011	0.370	0.021	1.8	0.7	141.8
249	J142151.45+531026.0	0.080	0.011	0.080	0.011	0.0	0.0	0.0
250	J142054.80+531045.2	0.114	0.012	0.114	0.012	0.0	0.0	0.0
251	J142141.93+531047.6	0.090	0.011	0.090	0.011	0.0	0.0	0.0
252	J142126.21+531048.9	6.314	0.011	12.615	0.033	6.6	-1	106.0
253	J142205.33+531051.5	0.064	0.011	0.080	0.022	4.7	0.0	62.9
254	J142137.87+531103.1	0.089	0.011	0.089	0.011	0.0	0.0	0.0
255	J142151.47+531105.6	0.149	0.011	0.149	0.011	0.0	0.0	0.0
256	J142150.29+531108.8	0.071	0.011	0.071	0.011	0.0	0.0	0.0
257	J142109.98+531112.8	0.197	0.012	0.197	0.012	0.0	0.0	0.0
258	J142135.25+531115.4	0.092	0.011	0.092	0.011	0.0	0.0	0.0
259	J142157.37+531119.6	0.106	0.011	0.106	0.011	0.0	0.0	0.0
260	J142200.59+531125.4	0.074	0.011	0.077	0.020	1.5	0.0	150.7
261	J142159.59+531126.1	0.103	0.011	0.134	0.022	2.5	1.7	118.6
262	J142035.94+531146.1	0.063	0.012	0.063	0.012	0.0	0.0	0.0
263	J142043.65+531150.7	0.364	0.012	0.393	0.021	1.4	0.6	89.3
264	J142046.21+531212.5	0.064	0.011	0.107	0.028	5.7	0.0	34.1
265	J142212.70+531232.5	0.059	0.011	0.059	0.011	0.0	0.0	0.0
266	J142122.43+531241.2	0.069	0.011	0.069	0.011	0.0	0.0	0.0
267	J142203.81+531248.6	0.067	0.011	0.089	0.022	4.9	0.0	42.8
268	J142153.83+531258.9	0.061	0.011	0.061	0.011	0.0	0.0	0.0
269	J142101.66+531301.2	0.079	0.012	0.079	0.012	0.0	0.0	0.0
270	J142107.11+531302.1	0.083	0.011	0.083	0.011	0.0	0.0	0.0
271	J142045.38+531305.3	0.061	0.012	0.065	0.022	2.5	0.0	68.3
272	J142056.84+531307.7	2.117	0.012	9.846	-1	78.8	...	160.2
273	J142122.37+531320.0	0.089	0.011	0.089	0.011	0.0	0.0	0.0

Table 1—Continued

ID	AEGIS20	Flux Density (mJy)				Size (″)		PA deg
		peak	unc <sup>a</sup>	int	unc <sup>a</sup>	Major	Minor <sup>b</sup>	
274	J142147.27+531322.4	0.208	0.010	0.241	0.020	2.4	0.0	173.4
275	J142157.91+531329.0	0.059	0.011	0.059	0.011	0.0	0.0	0.0
276	J142114.17+531342.8	0.161	0.011	0.161	0.011	0.0	0.0	0.0
277	J142104.82+531355.8	0.090	0.011	0.090	0.011	0.0	0.0	0.0
278	J142140.45+531355.9	0.064	0.011	0.064	0.011	0.0	0.0	0.0
279	J142158.90+531356.9	0.091	0.011	0.107	0.021	3.2	0.0	133.4
280	J142101.11+531358.5	0.059	0.012	0.059	0.012	0.0	0.0	0.0
281	J142117.09+531414.3	0.073	0.011	0.073	0.011	0.0	0.0	0.0
282	J142224.33+531424.3	0.054	0.011	0.054	0.011	0.0	0.0	0.0
283	J142155.91+531426.0	0.064	0.011	0.064	0.011	0.0	0.0	0.0
284	J142217.21+531426.6	0.121	0.011	0.141	0.021	2.6	0.0	155.9
285	J142220.39+531431.1	0.161	0.011	0.161	0.011	0.0	0.0	0.0
286	J142057.45+531440.2	0.058	0.011	0.106	0.028	8.1	0.0	10.3
287	J142226.38+531442.3	0.060	0.011	0.070	0.021	2.5	0.0	83.1
288	J142141.32+531450.0	0.092	0.011	0.092	0.011	0.0	0.0	0.0
289	J142217.06+531452.5	0.064	0.011	0.068	0.020	3.7	0.0	78.8
290	J142216.67+531457.8	0.067	0.011	0.067	0.011	0.0	0.0	0.0
291	J142150.32+531458.0	0.061	0.011	0.061	0.011	0.0	0.0	0.0
292	J142154.79+531500.5	5.843	0.011	5.965	0.019	0.8	0.0	54.2
293	J142140.70+531507.4	0.076	0.010	0.076	0.010	0.0	0.0	0.0
294	J142055.25+531513.4	0.109	0.011	0.109	0.011	0.0	0.0	0.0
295	J142221.95+531515.2	0.063	0.011	0.064	0.019	4.4	0.0	136.6
296	J142219.84+531515.9	0.086	0.011	0.086	0.011	0.0	0.0	0.0
297	J142127.92+531516.0	0.492	0.010	0.492	0.010	0.0	0.0	0.0
298	J142153.64+531521.9	0.062	0.011	0.062	0.011	0.0	0.0	0.0
299	J142148.48+531534.5	0.062	0.011	0.062	0.011	0.0	0.0	0.0
300	J142131.39+531534.9	0.163	0.010	0.170	0.018	1.1	0.2	38.5
301	J142234.35+531535.0	0.188	0.012	0.188	0.012	0.0	0.0	0.0
302	J142217.78+531535.2	0.095	0.011	0.107	0.020	2.5	0.0	144.0
303	J142201.46+531537.2	0.298	0.011	0.346	0.021	2.5	0.0	70.4
304	J142231.50+531539.3	0.069	0.011	0.069	0.011	0.0	0.0	0.0
305	J142131.71+531543.9	0.120	0.010	0.120	0.010	0.0	0.0	0.0
306	J142057.96+531544.9	0.100	0.011	0.100	0.011	0.0	0.0	0.0
307	J142156.48+531549.7	0.098	0.011	0.182	0.028	5.3	1.6	160.1
308	J142128.73+531550.6	0.051	0.010	0.051	0.010	0.0	0.0	0.0
309	J142140.37+531554.9	0.073	0.010	0.073	0.010	0.0	0.0	0.0
310	J142233.47+531555.6	0.095	0.011	0.095	0.011	0.0	0.0	0.0
311	J142154.10+531607.4	0.104	0.011	0.112	0.019	1.8	0.0	113.5
312	J142218.14+531639.0	0.080	0.010	0.080	0.010	0.0	0.0	0.0

Table 1—Continued

ID	AEGIS20	Flux Density (mJy)				Size (″)		PA deg
		peak	unc <sup>a</sup>	int	unc <sup>a</sup>	Major	Minor <sup>b</sup>	
313	J142133.11+531650.5	0.129	0.010	0.163	0.021	2.7	0.9	137.6
314	J142219.46+531657.1	0.053	0.011	0.053	0.011	0.0	0.0	0.0
315	J142159.55+531700.4	0.069	0.011	0.069	0.011	0.0	0.0	0.0
316	J142137.23+531713.2	0.057	0.010	0.057	0.010	0.0	0.0	0.0
317	J142134.11+531718.4	0.094	0.010	0.094	0.010	0.0	0.0	0.0
318	J142137.86+531721.0	0.150	0.010	0.150	0.010	0.0	0.0	0.0
319	J142217.00+531738.2	0.182	0.010	0.182	0.010	0.0	0.0	0.0
320	J142106.85+531740.9	0.062	0.011	0.062	0.011	0.0	0.0	0.0
321	J142120.26+531746.1	0.061	0.011	0.061	0.011	0.0	0.0	0.0
322	J142142.71+531753.7	0.059	0.011	0.059	0.011	0.0	0.0	0.0
323	J142240.61+531803.0	0.088	0.010	0.120	0.022	4.9	0.0	55.8
324	J142238.26+531803.6	0.066	0.011	0.083	0.021	3.9	0.0	47.1
325	J142139.93+531814.2	0.055	0.010	0.055	0.010	0.0	0.0	0.0
326	J142245.04+531817.3	0.062	0.011	0.062	0.011	0.0	0.0	0.0
327	J142118.04+531818.9	0.080	0.011	0.080	0.011	0.0	0.0	0.0
328	J142248.02+531829.0	0.084	0.011	0.084	0.011	0.0	0.0	0.0
329	J142218.08+531833.0	0.076	0.010	0.076	0.010	0.0	0.0	0.0
330	J142150.12+531838.7	0.078	0.011	0.078	0.011	0.0	0.0	0.0
331	J142249.65+531839.1	0.116	0.011	0.132	0.020	2.5	0.0	124.2
332	J142148.26+531847.0	0.082	0.011	0.082	0.011	0.0	0.0	0.0
333	J142219.11+531849.2	0.050	0.010	0.050	0.010	0.0	0.0	0.0
334	J142251.16+531858.2	0.082	0.011	0.082	0.011	0.0	0.0	0.0
335	J142155.61+531901.5	0.115	0.011	0.115	0.011	0.0	0.0	0.0
336	J142147.00+531907.4	0.057	0.011	0.057	0.011	0.0	0.0	0.0
337	J142227.11+531917.6	0.055	0.010	0.055	0.010	0.0	0.0	0.0
338	J142251.34+531929.6	0.080	0.010	0.080	0.010	0.0	0.0	0.0
339	J142145.21+531936.1	0.073	0.011	0.073	0.011	0.0	0.0	0.0
340	J142254.93+531944.8	0.107	0.010	0.107	0.010	0.0	0.0	0.0
341	J142146.30+531947.7	0.061	0.011	0.061	0.011	0.0	0.0	0.0
342	J142219.80+531949.9	0.151	0.009	0.151	0.009	0.0	0.0	0.0
343	J142154.08+531950.7	0.278	0.011	0.333	0.021	2.1	1.2	165.6
344	J142211.51+531951.1	0.063	0.010	0.063	0.010	0.0	0.0	0.0
345	J142255.14+532002.3	0.048	0.010	0.048	0.010	0.0	0.0	0.0
346	J142136.70+532003.7	0.222	0.011	0.222	0.011	0.0	0.0	0.0
347	J142134.73+532004.2	0.082	0.011	0.082	0.011	0.0	0.0	0.0
348	J142147.86+532004.3	0.060	0.011	0.060	0.011	0.0	0.0	0.0
349	J142149.84+532005.5	0.075	0.011	0.075	0.011	0.0	0.0	0.0
350	J142134.81+532010.1	0.088	0.011	0.088	0.011	0.0	0.0	0.0
351	J142155.09+532023.3	0.063	0.011	0.063	0.011	0.0	0.0	0.0



Table 1—Continued

ID	AEGIS20	Flux Density (mJy)				Size (″)		PA deg
		peak	unc <sup>a</sup>	int	unc <sup>a</sup>	Major	Minor <sup>b</sup>	
352	J142246.94+532026.1	0.417	0.010	0.417	0.010	0.0	0.0	0.0
353	J142225.48+532026.3	0.062	0.010	0.074	0.019	2.2	1.0	81.1
354	J142226.54+532028.7	0.103	0.010	0.103	0.010	0.0	0.0	0.0
355	J142210.83+532029.9	0.047	0.010	0.047	0.010	0.0	0.0	0.0
356	J142215.91+532031.4	0.062	0.010	0.062	0.010	0.0	0.0	0.0
357	J142156.66+532031.5	0.053	0.011	0.053	0.011	0.0	0.0	0.0
358	J142237.95+532039.3	0.059	0.010	0.071	0.020	5.1	0.0	60.3
359	J142256.46+532049.8	0.148	0.010	0.148	0.010	0.0	0.0	0.0
360	J142147.49+532051.9	0.106	0.010	0.553	0.060	9.2	6.5	53.5
361	J142137.15+532055.1	1.493	0.011	1.508	0.019	0.6	0.0	78.7
362	J142232.94+532103.2	0.094	0.010	0.094	0.010	0.0	0.0	0.0
363	J142151.00+532104.3	0.158	0.011	0.160	0.019	1.1	0.0	26.8
364	J142135.48+532113.3	0.211	0.011	0.211	0.011	0.0	0.0	0.0
365	J142304.09+532114.9	0.089	0.010	0.089	0.010	0.0	0.0	0.0
366	J142249.74+532116.0	0.067	0.010	0.067	0.010	0.0	0.0	0.0
367	J142244.45+532119.7	0.110	0.010	0.110	0.010	0.0	0.0	0.0
368	J142239.72+532126.4	0.068	0.010	0.068	0.010	0.0	0.0	0.0
369	J142150.24+532129.0	0.075	0.011	0.075	0.011	0.0	0.0	0.0
370	J142240.13+532138.7	0.070	0.010	0.091	0.020	4.8	0.0	57.7
371	J142228.30+532139.1	0.122	0.010	0.146	0.020	1.9	1.5	114.5
372	J142236.64+532144.2	0.050	0.010	0.060	0.019	3.8	0.0	105.2
373	J142217.62+532147.5	0.107	0.010	0.111	0.018	0.9	0.5	74.7
374	J142259.85+532152.4	0.204	0.010	0.204	0.010	0.0	0.0	0.0
375	J142222.31+532159.0	0.138	0.010	0.142	0.018	1.9	0.0	152.6
376	J142131.85+532200.2	0.063	0.011	0.063	0.011	0.0	0.0	0.0
377	J142253.40+532219.1	0.439	0.010	0.447	0.017	1.6	0.0	69.4
378	J142247.27+532221.6	0.085	0.010	0.099	0.019	3.7	0.0	148.6
379	J142158.03+532224.2	0.270	0.010	0.400	0.023	3.8	1.2	85.6
380	J142303.07+532224.5	0.325	0.010	0.951	0.020	11.4	-1	36.3
381	J142249.82+532234.1	0.073	0.010	0.073	0.010	0.0	0.0	0.0
382	J142150.80+532242.5	0.070	0.011	0.070	0.011	0.0	0.0	0.0
383	J142230.62+532244.4	0.085	0.010	0.085	0.010	0.0	0.0	0.0
384	J142238.43+532251.2	0.073	0.010	0.073	0.010	0.0	0.0	0.0
385	J142249.96+532257.6	0.122	0.010	0.124	0.017	2.4	0.0	162.6
386	J142159.33+532314.6	0.065	0.011	0.065	0.011	0.0	0.0	0.0
387	J142305.81+532326.0	0.050	0.010	0.052	0.017	3.6	0.0	107.2
388	J142233.77+532328.5	0.059	0.009	0.059	0.009	0.0	0.0	0.0
389	J142229.50+532333.5	0.067	0.009	0.067	0.009	0.0	0.0	0.0
390	J142233.49+532338.1	0.061	0.009	0.067	0.018	4.0	0.0	161.6

Table 1—Continued

ID	AEGIS20	Flux Density (mJy)				Size (″)		PA deg
		peak	unc <sup>a</sup>	int	unc <sup>a</sup>	Major	Minor <sup>b</sup>	
391	J142245.65+532342.3	0.070	0.009	0.070	0.009	0.0	0.0	0.0
392	J142320.15+532350.6	0.089	0.010	0.089	0.010	0.0	0.0	0.0
393	J142151.18+532400.5	0.073	0.012	0.073	0.012	0.0	0.0	0.0
394	J142302.75+532407.5	0.054	0.010	0.054	0.010	0.0	0.0	0.0
395	J142239.03+532414.3	0.362	0.009	0.379	0.017	1.6	0.0	102.1
396	J142301.16+532418.7	0.090	0.010	0.090	0.010	0.0	0.0	0.0
397	J142208.34+532420.3	0.078	0.010	0.085	0.019	3.4	0.0	152.0
398	J142206.74+532426.6	0.051	0.010	0.051	0.010	0.0	0.0	0.0
399	J142237.85+532428.4	0.047	0.009	0.085	0.024	6.5	0.0	62.6
400	J142226.09+532437.3	0.288	0.009	0.288	0.009	0.0	0.0	0.0
401	J142300.02+532440.5	0.113	0.010	0.123	0.018	1.7	0.0	68.0
402	J142153.11+532441.0	0.106	0.011	0.106	0.011	0.0	0.0	0.0
403	J142225.41+532450.5	0.448	0.009	0.449	0.016	1.0	0.0	100.3
404	J142203.96+532451.3	0.078	0.010	0.078	0.010	0.0	0.0	0.0
405	J142317.68+532452.0	0.105	0.010	0.109	0.018	1.8	0.0	80.1
406	J142302.02+532458.9	0.106	0.010	0.106	0.010	0.0	0.0	0.0
407	J142222.95+532526.3	0.209	0.010	0.209	0.010	0.0	0.0	0.0
408	J142252.92+532528.3	0.096	0.009	0.096	0.009	0.0	0.0	0.0
409	J142210.40+532545.1	0.303	0.010	0.303	0.010	0.0	0.0	0.0
410	J142316.85+532558.2	0.054	0.010	0.054	0.010	0.0	0.0	0.0
411	J142321.84+532558.9	0.209	0.010	0.209	0.010	0.0	0.0	0.0
412	J142156.32+532601.2	0.081	0.011	0.109	0.023	4.1	0.0	57.8
413	J142237.03+532608.9	0.077	0.010	0.077	0.010	0.0	0.0	0.0
414	J142156.51+532613.4	0.063	0.011	0.063	0.011	0.0	0.0	0.0
415	J142217.38+532618.7	0.052	0.010	0.052	0.010	0.0	0.0	0.0
416	J142312.40+532623.6	0.069	0.010	0.088	0.019	3.2	0.0	64.0
417	J142231.78+532624.2	0.072	0.010	0.072	0.010	0.0	0.0	0.0
418	J142302.89+532624.3	0.047	0.009	0.048	0.016	4.1	0.0	25.9
419	J142205.75+532626.9	0.051	0.010	0.051	0.010	0.0	0.0	0.0
420	J142234.75+532633.1	0.052	0.010	0.054	0.017	2.7	0.0	177.7
421	J142220.65+532642.2	0.059	0.010	0.059	0.010	0.0	0.0	0.0
422	J142234.71+532642.4	0.056	0.010	0.056	0.010	0.0	0.0	0.0
423	J142231.49+532643.5	0.132	0.009	0.132	0.009	0.0	0.0	0.0
424	J142241.36+532646.4	0.092	0.010	0.092	0.010	0.0	0.0	0.0
425	J142231.05+532649.2	0.057	0.009	0.057	0.009	0.0	0.0	0.0
426	J142223.27+532659.5	0.083	0.010	0.083	0.010	0.0	0.0	0.0
427	J142242.08+532715.3	0.047	0.010	0.047	0.010	0.0	0.0	0.0
428	J142321.16+532718.3	6.587	0.010	34.281	-1	27.3	...	133.4
429	J142251.13+532721.6	0.119	0.009	0.119	0.009	0.0	0.0	0.0

Table 1—Continued

ID	AEGIS20	Flux Density (mJy)				Size (″)		PA deg
		peak	unc <sup>a</sup>	int	unc <sup>a</sup>	Major	Minor <sup>b</sup>	
430	J142303.38+532745.4	0.059	0.010	0.059	0.010	0.0	0.0	0.0
431	J142312.68+532756.8	4.253	0.010	4.410	0.018	0.8	0.6	7.1
432	J142221.76+532758.5	0.216	0.010	0.216	0.010	0.0	0.0	0.0
433	J142214.97+532806.9	0.152	0.011	0.159	0.019	1.8	0.0	93.4
434	J142213.25+532817.5	0.050	0.011	0.050	0.011	0.0	0.0	0.0
435	J142327.21+532819.6	0.062	0.010	0.062	0.010	0.0	0.0	0.0
436	J142237.54+532819.8	0.064	0.010	0.064	0.010	0.0	0.0	0.0
437	J142330.80+532823.2	0.300	0.010	0.318	0.018	1.4	0.0	168.0
438	J142341.00+532824.5	0.192	0.010	0.192	0.010	0.0	0.0	0.0
439	J142340.83+532829.7	0.066	0.010	0.066	0.010	0.0	0.0	0.0
440	J142231.08+532838.6	0.050	0.009	0.067	0.020	5.0	0.0	36.7
441	J142252.38+532841.2	0.105	0.010	0.105	0.010	0.0	0.0	0.0
442	J142222.54+532841.9	0.361	0.010	0.361	0.010	0.0	0.0	0.0
443	J142210.53+532847.9	0.065	0.011	0.065	0.011	0.0	0.0	0.0
444	J142339.43+532853.9	0.058	0.010	0.074	0.021	4.7	0.0	7.8
445	J142227.71+532903.3	0.060	0.010	0.060	0.010	0.0	0.0	0.0
446	J142230.17+532915.2	0.073	0.010	0.073	0.010	0.0	0.0	0.0
447	J142255.04+532916.2	0.068	0.010	0.068	0.010	0.0	0.0	0.0
448	J142258.89+532925.6	0.051	0.010	0.051	0.010	0.0	0.0	0.0
449	J142238.85+532938.8	0.153	0.010	0.153	0.010	0.0	0.0	0.0
450	J142347.78+532940.0	0.072	0.011	0.073	0.020	2.1	0.0	83.4
451	J142351.24+532942.2	0.061	0.011	0.061	0.011	0.0	0.0	0.0
452	J142256.07+533002.3	0.125	0.010	0.149	0.019	2.4	0.6	137.0
453	J142226.98+533004.5	0.061	0.010	0.061	0.010	0.0	0.0	0.0
454	J142318.78+533009.0	0.132	0.010	0.138	0.017	2.2	0.0	133.8
455	J142325.39+533010.2	0.058	0.010	0.058	0.010	0.0	0.0	0.0
456	J142253.33+533025.5	0.240	0.010	0.240	0.010	0.0	0.0	0.0
457	J142324.62+533048.7	0.061	0.010	0.061	0.010	0.0	0.0	0.0
458	J142327.59+533049.6	0.070	0.010	0.070	0.010	0.0	0.0	0.0
459	J142316.00+533051.7	0.384	0.010	0.384	0.010	0.0	0.0	0.0
460	J142232.17+533059.5	0.067	0.010	0.067	0.010	0.0	0.0	0.0
461	J142324.77+533059.8	0.098	0.010	0.098	0.010	0.0	0.0	0.0
462	J142348.44+533106.1	0.055	0.011	0.055	0.011	0.0	0.0	0.0
463	J142338.88+533121.2	0.102	0.011	0.105	0.019	2.3	0.0	93.7
464	J142311.98+533131.9	0.050	0.010	0.050	0.010	0.0	0.0	0.0
465	J142349.42+533134.3	0.131	0.011	0.156	0.021	2.3	0.9	122.2
466	J142323.81+533134.3	0.111	0.010	0.115	0.018	1.6	0.0	42.0
467	J142303.81+533148.7	0.094	0.010	0.094	0.010	0.0	0.0	0.0
468	J142252.67+533200.5	0.064	0.010	0.064	0.010	0.0	0.0	0.0

Table 1—Continued

ID	AEGIS20	Flux Density (mJy)				Size (″)		PA deg
		peak	unc <sup>a</sup>	int	unc <sup>a</sup>	Major	Minor <sup>b</sup>	
469	J142400.77+533200.6	0.083	0.012	0.083	0.012	0.0	0.0	0.0
470	J142247.52+533202.8	0.198	0.010	0.198	0.010	0.0	0.0	0.0
471	J142301.53+533222.2	0.069	0.010	0.069	0.010	0.0	0.0	0.0
472	J142352.36+533227.8	0.072	0.011	0.072	0.011	0.0	0.0	0.0
473	J142317.03+533240.2	0.324	0.010	0.347	0.018	1.8	0.0	96.8
474	J142339.30+533243.3	0.337	0.011	0.337	0.011	0.0	0.0	0.0
475	J142243.37+533246.2	0.098	0.011	0.098	0.011	0.0	0.0	0.0
476	J142254.52+533303.8	0.056	0.011	0.056	0.011	0.0	0.0	0.0
477	J142341.19+533306.5	0.054	0.011	0.054	0.011	0.0	0.0	0.0
478	J142328.10+533308.3	0.058	0.011	0.058	0.011	0.0	0.0	0.0
479	J142236.55+533309.3	0.083	0.011	0.083	0.011	0.0	0.0	0.0
480	J142301.07+533311.8	0.367	0.011	0.386	0.019	1.3	0.0	51.1
481	J142234.21+533314.4	0.121	0.011	0.121	0.011	0.0	0.0	0.0
482	J142345.74+533319.5	0.183	0.011	0.255	0.024	3.6	0.6	98.5
483	J142327.06+533331.1	0.080	0.011	0.081	0.019	1.9	0.0	70.3
484	J142316.88+533339.5	0.103	0.011	0.112	0.019	1.7	0.0	135.6
485	J142350.38+533343.0	0.076	0.011	0.076	0.011	0.0	0.0	0.0
486	J142400.41+533347.0	0.124	0.012	0.124	0.012	0.0	0.0	0.0
487	J142412.21+533347.5	0.223	0.012	0.223	0.012	0.0	0.0	0.0
488	J142306.17+533351.8	0.062	0.011	0.062	0.011	0.0	0.0	0.0
489	J142400.60+533403.2	0.086	0.011	0.104	0.022	2.8	0.0	92.7
490	J142259.42+533407.2	0.072	0.012	0.072	0.012	0.0	0.0	0.0
491	J142324.13+533419.9	0.077	0.011	0.088	0.021	2.2	0.0	27.4
492	J142311.81+533422.2	0.056	0.011	0.056	0.011	0.0	0.0	0.0
493	J142338.53+533432.3	0.067	0.011	0.067	0.011	0.0	0.0	0.0
494	J142256.53+533449.5	0.161	0.012	0.161	0.012	0.0	0.0	0.0
495	J142324.25+533511.2	0.168	0.011	0.168	0.011	0.0	0.0	0.0
496	J142247.51+533513.8	0.078	0.013	0.078	0.013	0.0	0.0	0.0
497	J142338.67+533520.0	0.124	0.011	0.124	0.011	0.0	0.0	0.0
498	J142341.88+533525.3	0.451	0.012	0.451	0.012	0.0	0.0	0.0
499	J142345.88+533628.3	0.177	0.012	0.224	0.023	2.1	1.8	3.1
500	J142334.45+533633.9	0.224	0.011	0.224	0.011	0.0	0.0	0.0
501	J142401.11+533639.0	3.324	0.012	5.690	0.030	4.5	1.8	147.9
502	J142301.56+533640.0	0.083	0.013	0.083	0.013	0.0	0.0	0.0
503	J142301.71+533655.3	0.120	0.013	0.151	0.026	2.9	0.3	56.7
504	J142332.62+533738.5	0.124	0.012	0.124	0.012	0.0	0.0	0.0
505	J142325.09+533758.4	0.185	0.012	0.185	0.012	0.0	0.0	0.0
506	J142340.86+533818.4	0.182	0.012	0.182	0.012	0.0	0.0	0.0
507	J142326.22+533857.3	0.118	0.012	0.118	0.012	0.0	0.0	0.0

Table 1—Continued

ID	AEGIS20	Flux Density (mJy)				Size (")		PA deg
		peak	unc <sup>a</sup>	int	unc <sup>a</sup>	Major	Minor <sup>b</sup>	
508	J142316.06+533912.2	0.085	0.013	0.085	0.013	0.0	0.0	0.0
509	J142332.20+533913.8	0.090	0.013	0.090	0.013	0.0	0.0	0.0
510	J142326.02+533942.1	0.156	0.013	0.163	0.023	2.0	0.0	115.3
511	J142328.02+534102.9	0.075	0.014	0.086	0.026	3.4	0.0	5.3

<sup>a</sup>Tabulated uncertainties in flux density are  $1\sigma$ . Values of  $-1$  in integrated uncertainty indicate that the source was poorly fit by a Gaussian. In these cases, integrated flux density was measured in a square that included the entire source, and minor axis sizes are not given.

<sup>b</sup>Value  $-1$  indicates source unresolved in the minor axis direction.

Table 2: Radio Sources with No IRAC Identification

ID	AEGIS20	Comment
002	J141736.35+523135.8	Radio source is hot spot in jet from 003
434	J142213.25+532817.5	Radio source $<5\sigma$ , nearest IRAC source $1''.6$ away
488	J142306.17+533351.8	near saturated star

Table 3. IRAC Counterparts of EGS 20 cm Radio Sources

ID	RA	Dec	EGSIRAC	Offset <sup>a</sup>	Exposure <sup>b</sup>	irac <sup>c</sup>	Offset <sup>d</sup>	Comment
001	214.49231	52.52630	J141758.15+523134.6	0.9	54	...	...	companion 3''2 NE
003	214.38602	52.53422	J141732.64+523203.1	0.3	56	166271	0.16	
004	214.54145	52.55013	J141809.94+523300.4	0.2	50	158078	0.04	
005	214.47884	52.55180	J141754.92+523306.4	0.7	58	160802_1	0.23	
006	214.60013	52.55620	J141824.03+523322.3	0.2	48	155105	0.18	
007	214.42157	52.56538	J141741.17+523355.3	0.3	50	162660_1	0.50	
008	214.56741	52.58661	J141816.17+523511.7	1.0	49	154917	0.10	
009	214.47249	52.59434	J141753.39+523539.6	0.1	55	158749	0.10	
010	214.63114	52.60408	J141831.47+523614.6	0.4	56	151178_2	0.17	
011	214.52096	52.60604	J141805.03+523621.7	0.2	49	155871	0.06	
012	214.62569	52.60914	J141830.16+523632.8	0.2	55	151190_2	0.17	
013	214.59332	52.60942	J141822.39+523633.9	0.1	49	152559	0.07	
014	214.48136	52.61227	J141755.52+523644.1	0.2	47	157331	0.09	companion 4''1 SW
015	214.58743	52.61979	J141820.98+523711.2	0.5	49	152264	0.07	
016	214.67476	52.62641	J141841.94+523735.0	0.2	50	147805	0.50	good ID
017	214.38552	52.63837	J141732.52+523818.1	3.5	21	160192	0.56	good ID
018	214.77288	52.64978	J141905.49+523859.1	0.4	12	141847	0.23	
019	214.77607	52.65071	J141906.25+523902.5	0.7	12	141631	0.14	double 1''4 sep in R
020	214.63302	52.65198	J141831.92+523907.1	0.7	47	148319	0.12	
021	214.66499	52.65225	J141839.59+523908.0	0.1	51	146745	0.10	
022	214.47267	52.65959	J141753.44+523934.5	0.9	52	...	...	near bright star
023	214.56055	52.66009	J141814.53+523936.3	0.6	50	151274_2	0.23	fainter companion 3''5 S
024	214.59366	52.66049	J141822.47+523937.7	0.1	58	149658	0.18	
025	214.74954	52.66782	J141859.89+524004.1	0.1	42	141916_1	0.26	
026	214.71357	52.66790	J141851.25+524004.4	0.5	52	143621_2	0.51	
027	214.73819	52.66971	J141857.16+524010.9	0.3	44	142336_1	0.25	
028	214.77839	52.67034	J141906.81+524013.2	0.7	27	140385	0.22	
029	214.52311	52.67579	J141805.54+524032.8	0.3	49	152178_1	0.42	
030	214.55692	52.67727	J141813.66+524038.1	0.1	49	150435	0.14	
031	214.67491	52.68560	J141841.97+524108.1	0.4	56	144420_1	0.27	
032	214.47897	52.68755	J141754.95+524115.1	0.4	38	153384	0.51	
033	214.69299	52.68828	J141846.31+524117.7	1.3	48	143420	0.05	big offset
034	214.51401	52.69110	J141803.36+524127.9	0.2	55	151682	0.13	
035	214.71205	52.69387	J141850.89+524137.9	0.9	49	142182	0.08	
036	214.44844	52.69538	...	0.1	9	...	...	large galaxy
037	214.47885	52.69563	J141754.92+524144.2	0.2	28	152964	0.41	
038	214.57266	52.69943	J141817.43+524157.9	0.2	49	148432	0.02	
039	214.73592	52.70017	J141856.62+524200.6	0.5	52	140679	0.09	
040	214.58840	52.70138	J141821.21+524204.9	0.0	53	147555	0.03	
041	214.82562	52.70920	J141918.14+524233.1	0.4	35	135943	0.46	

Table 3—Continued

ID	RA	Dec	EGSIRAC	Offset <sup>a</sup>	Exposure <sup>b</sup>	irac <sup>c</sup>	Offset <sup>d</sup>	Comment
042	214.63838	52.71162	J141833.21+524241.8	0.4	58	144645	0.23	
043	214.56192	52.71216	J141814.86+524243.7	0.0	50	148192	0.08	
044	214.76821	52.71450	J141904.37+524252.2	0.4	54	138319	0.14	companion 3''1 E
045	214.65910	52.71867	J141838.18+524307.1	0.8	58	143254	0.24	
046	214.73153	52.72186	J141855.56+524318.6	0.2	52	139629	0.15	
047	214.48089	52.72763	...	0.2	6	151150	0.37	
048	214.86710	52.72837	J141928.10+524342.1	0.6	17	132884_1	0.27	
049	214.76713	52.72943	J141904.11+524345.9	0.2	55	137529	0.13	extended in R
050	214.61249	52.73041	J141826.99+524349.4	0.6	53	144758	0.09	
051	214.63804	52.73118	J141833.12+524352.2	0.2	55	143536	0.07	companion 4''7 E
052	214.89215	52.73134	...	0.7	6	131509	0.42	
053	214.78693	52.73350	J141908.86+524400.6	0.3	51	...	...	extended in R with bright nucleus
054	214.72156	52.73634	J141853.17+524410.8	0.1	53	139257	0.07	
055	214.73866	52.73726	J141857.27+524414.1	0.3	59	138423	0.11	
056	214.53719	52.73984	J141808.92+524423.4	0.3	29	147748	0.44	
057	214.52524	52.74805	...	0.7	11	147837	0.61	resolved spiral in R
058	214.69126	52.74880	J141845.90+524455.6	0.2	56	140017	0.02	
059	214.88599	52.75119	J141932.63+524504.2	0.1	32	130651	0.34	
060	214.65302	52.76776	J141836.72+524603.9	0.6	57	140699_3	0.13	
061	214.57359	52.77097	J141817.66+524615.4	0.2	25	144273	0.49	
062	214.71989	52.77179	J141852.77+524618.4	0.5	51	137316	0.26	
063	214.83235	52.77775	J141919.76+524639.9	0.3	51	131678_2	0.44	
064	214.80328	52.77831	...	0.7	51	133033	0.56	
065	214.93967	52.77990	J141945.52+524647.6	0.4	17	126349	0.34	
066	214.62568	52.78019	J141830.16+524648.6	0.7	50	141289_1	0.23	companions
067	214.83180	52.78768	J141919.63+524715.6	0.3	55	131111	0.12	
068	214.94973	52.79011	J141947.93+524724.3	0.2	28	125331	0.32	
069	214.68512	52.79331	J141844.42+524735.9	0.3	48	137716	0.29	
070	214.58458	52.79700	...	0.2	3	...	...	near bright star
071	214.89220	52.80007	J141934.12+524800.2	0.2	51	127470_1	0.27	
072	214.82921	52.80844	J141919.01+524830.3	0.2	55	129998	0.15	fainter companion 4''1 S
073	214.79347	52.80856	J141910.43+524830.8	0.1	68	131725	0.13	extended in IR
074	214.62450	52.80979	J141829.87+524835.2	0.8	17	139616	0.47	fainter companion 3''1 N
075	214.71457	52.80999	J141851.49+524835.9	0.1	51	135434	0.23	
076	214.97826	52.81149	...	0.5	35	122794	0.35	fainter companion 2''5 E
077	214.94612	52.81227	J141947.06+524844.1	2.9	51	124199	0.10	good ID
078	214.72165	52.81552	J141853.19+524855.8	0.4	52	134760	0.19	extended spiral in R
079	214.80868	52.81914	J141914.08+524908.9	0.2	62	130374	0.18	
080	214.81237	52.82494	J141914.96+524929.7	0.2	65	129840_1	0.43	
081	214.91697	52.82735	J141940.07+524938.4	0.8	51	124711	0.03	

Table 3—Continued

ID	RA	Dec	EGSIRAC	Offset <sup>a</sup>	Exposure <sup>b</sup>	irac <sup>c</sup>	Offset <sup>d</sup>	Comment
082	214.75103	52.83010	J141900.24+524948.3	0.1	49	132499_2	0.27	
083	214.78264	52.83102	J141907.83+524951.6	0.3	56	130927	0.12	extended in R
084	214.97392	52.83237	J141953.74+524956.5	0.8	47	121851	0.28	
085	214.72704	52.83472	J141854.49+525004.9	0.2	53	133380	0.14	
086	214.83587	52.84010	J141920.61+525024.3	0.4	55	127824	0.25	
087	214.94800	52.84061	J141947.52+525026.2	0.2	53	122569	0.01	
088	214.86261	52.84285	J141927.02+525034.2	0.7	58	126382_2	0.45	radio may be faint extension to
089	214.82228	52.84307	J141917.34+525035.0	0.2	53	128336	0.12	
090	214.71539	52.84596	J141851.69+525045.4	1.1	42	133299	0.29	
091	214.90572	52.84731	J141937.37+525050.3	0.4	53	124112	0.13	
092	214.92763	52.84796	J141942.63+525052.6	0.1	52	...	...	
093	214.99282	52.85072	J141958.27+525102.5	0.4	45	119960	0.07	
094	214.90525	52.85093	J141937.26+525103.3	0.2	53	123914	0.01	
095	214.96715	52.85768	J141952.11+525127.6	0.5	50	120741	0.11	
096	214.81118	52.85846	J141914.68+525130.4	0.6	50	127954_1	0.58	two sources in R
097	214.77034	52.86042	J141904.88+525137.4	0.4	56	129786_3	0.33	
098	214.69271	52.86144	...	0.5	11	133463_1	0.31	
099	214.79281	52.86421	J141910.27+525151.1	0.5	54	128722	0.10	good ID
100	214.87554	52.86642	J141930.12+525159.1	0.1	64	124408	0.21	
101	214.79212	52.86669	J141910.10+525200.0	0.1	53	...	...	
102	215.03774	52.87073	J142009.05+525214.6	0.4	45	...	...	
103	214.81541	52.87093	J141915.69+525215.3	0.2	48	126987	0.28	companion 3''2 SE
104	214.97619	52.87244	J141954.28+525220.7	0.1	56	119484	0.16	
105E	214.91438	52.87594	J141939.45+525233.3	0.1	60	122166	0.09	two sources
105W	214.91285	52.87568	...	0.0	57	122244_2	0.46	
106	214.87814	52.87647	J141930.75+525235.3	0.4	52	123738_2	0.21	
107	215.01731	52.88022	...	0.4	49	117132	0.56	
108	214.92323	52.88214	J141941.57+525255.6	0.4	56	121436_1	0.38	
109	214.88896	52.88351	J141933.34+525300.6	0.1	56	122889	0.12	
110	214.91645	52.89099	...	0.4	59	...	...	
111	214.80274	52.89105	J141912.65+525327.7	0.1	48	126421	0.08	
112	214.83428	52.89376	J141920.22+525337.5	0.5	50	124812	0.01	
113	214.80693	52.89733	J141913.66+525350.3	0.2	50	125889	0.08	
114	214.81902	52.89779	J141916.56+525352.0	0.1	47	125306	0.08	
115	214.91084	52.90091	J141938.60+525403.2	0.3	57	120933	0.25	
116	215.01442	52.90123	J142003.46+525404.4	0.1	51	116102	0.11	
117	214.91478	52.90545	J141939.54+525419.6	0.3	58	120477	0.19	
118	214.97409	52.90596	J141953.78+525421.4	0.2	48	117673	0.15	
119	214.84368	52.91096	J141922.48+525439.4	0.6	49	123412	0.01	
120	215.09079	52.91178	J142021.79+525442.4	0.5	45	112048	0.12	



Table 3—Continued

ID	RA	Dec	EGSIRAC	Offset <sup>a</sup>	Exposure <sup>b</sup>	irac <sup>c</sup>	Offset <sup>d</sup>	Comment
121	214.96036	52.91404	J141950.48+525450.5	0.4	54	117861	0.15	
122	215.09147	52.91998	J142021.95+525511.9	0.1	51	111604	0.14	
123	214.84184	52.92197	J141922.04+525519.1	0.2	51	122906	0.14	
124	214.83575	52.92264	J141920.57+525521.4	0.2	49	123130	0.16	
125	215.13824	52.92316	J142033.17+525523.3	0.4	27	109224	0.40	
126	215.05419	52.92591	J142013.00+525533.2	0.1	55	112964	0.11	
127	215.03929	52.93040	J142009.42+525549.4	0.5	53	113429	0.05	
128	214.83371	52.93583	J141920.09+525609.0	0.0	48	122489	0.54	
129	214.91604	52.93738	J141939.84+525614.5	1.0	49	118588	0.10	
130	215.17697	52.94193	J142042.47+525630.9	0.5	16	106401	0.60	
131	215.15508	52.94236	J142037.21+525632.4	0.6	37	107382	0.38	
132	214.94201	52.94640	J141946.08+525647.0	0.5	49	116892_1	0.40	
133	214.95537	52.95127	J141949.28+525704.5	0.3	53	116023	0.14	
134	215.19474	52.95300	J142046.73+525710.7	0.4	15	104964	0.52	companion 3''5 W
135	215.00915	52.95422	J142002.19+525715.1	0.3	62	113602	0.17	good ID
136	215.07794	52.95474	J142018.70+525717.0	0.3	50	110236	0.07	
137	214.84303	52.95507	J141922.32+525718.2	1.3	29	121016	0.41	
138	215.17432	52.95678	J142041.83+525724.4	0.3	33	105665	0.45	
139	214.87071	52.95703	J141928.97+525725.3	0.1	43	119633	0.24	
140	214.83203	52.95982	J141919.68+525735.3	0.8	18	121257	0.50	
141	215.20995	52.96293	J142050.38+525746.5	0.5	15	103679	0.67	
142	214.90614	52.96687	J141937.47+525800.7	0.6	49	117406	0.07	
143	215.13916	52.96687	J142033.39+525800.7	0.5	50	106730_1	0.32	good ID
144	215.18074	52.96840	J142043.37+525806.2	0.1	39	104762	0.32	
145	215.19819	52.96891	J142047.56+525808.0	0.6	29	103890	0.36	slightly extended
146	214.95442	52.96992	J141949.05+525811.7	0.2	53	115081	0.12	
147	215.13242	52.97963	J142031.78+525846.6	0.3	54	106367	0.05	
148	215.16901	52.98077	J142040.56+525850.7	0.4	44	104612	0.07	
149	215.15517	52.98084	J142037.24+525851.0	0.3	47	105214_1	0.22	
150	215.09824	52.98300	J142023.57+525858.7	0.6	54	107715	0.11	
151	214.93090	52.98288	J141943.41+525858.3	0.2	55	115413_2	0.22	
152	214.93585	52.98313	J141944.60+525859.2	0.4	54	115167	0.36	multiple in R
153	215.03413	52.98438	J142008.19+525903.7	0.1	56	110596_1	0.23	
154	214.98888	52.99061	J141957.33+525926.1	0.1	51	112363	0.24	
155	215.22445	52.99056	J142053.86+525926.0	0.2	35	101453	0.35	
156	214.91253	52.99171	J141939.00+525930.1	0.2	50	115743	0.28	
157	215.01106	52.99256	J142002.65+525933.2	0.9	50	111242	0.21	
158	215.01181	52.99552	J142002.83+525943.8	0.1	50	111029	0.14	
159	214.91660	52.99605	J141939.98+525945.7	1.2	48	115339	0.33	
160	215.00853	52.99735	J142002.04+525950.4	0.0	49	111088	0.16	

Table 3—Continued

ID	RA	Dec	EGSIRAC	Offset <sup>a</sup>	Exposure <sup>b</sup>	irac <sup>c</sup>	Offset <sup>d</sup>	Comment
161	215.13853	53.00099	J142033.24+530003.5	0.3	52	104891_2	0.24	
162	215.23446	53.00490	J142056.27+530017.6	0.6	36	100113	0.40	
163	214.96709	53.00638	J141952.10+530022.9	0.1	50	112472_2	0.18	
164	215.04649	53.00884	J142011.15+530031.8	0.2	49	108641	0.12	blended in R
165	215.00834	53.01083	J142002.00+530039.0	0.4	54	110296	0.11	
166	214.91581	53.01243	J141939.79+530044.7	0.5	30	114497	0.32	
167	215.11082	53.01278	...	0.4	56	105474_1	0.40	companion 2''0 W
168	214.96369	53.01280	...	0.8	47	...	...	multiple IRAC within 3
169	215.06263	53.01333	J142015.03+530048.0	0.7	51	107650_1	0.06	blended IRAC
170	215.16499	53.01396	J142039.59+530050.2	0.5	50	102918	0.19	
171	214.92583	53.01967	J141942.19+530110.7	0.4	27	113644	0.27	
172	215.02490	53.02247	J142005.97+530120.8	0.4	57	108890	0.18	
173	215.20334	53.02367	J142048.80+530125.2	0.8	53	100510	0.14	
174	215.14657	53.03029	J142035.17+530149.0	0.4	52	102858	0.02	
175	215.08464	53.03237	J142020.31+530156.5	0.3	59	105580	0.28	
176	215.07652	53.03261	J142018.36+530157.3	0.2	54	105945	0.15	
177	215.08987	53.03318	J142021.56+530159.4	0.8	60	105311_2	0.50	
178	214.93066	53.03501	J141943.35+530206.0	0.7	14	112545	0.31	
179	215.27131	53.03532	J142105.11+530207.1	2.6	40	096535	0.10	good ID
180	215.02777	53.03635	J142006.66+530210.8	0.1	51	107978	0.09	
181	215.10764	53.03949	J142025.83+530222.1	0.1	58	104140	0.17	
182	215.16234	53.04021	J142038.96+530224.7	0.6	51	101624_3	0.33	
183	215.26120	53.04016	J142102.68+530224.5	0.3	50	096731	0.05	R blended
184	215.17926	53.04073	J142043.02+530226.6	0.3	56	100682	0.09	
185	215.17338	53.04150	J142041.61+530229.3	0.2	57	100921	0.08	
186	215.14192	53.04575	J142034.06+530244.7	0.4	55	102184_3	0.07	
187	215.00000	53.04928	J141959.99+530257.4	0.1	52	108553	0.17	
188	215.33290	53.05299	J142119.89+530310.7	0.2	19	092562_1	0.25	
189	215.01375	53.05399	J142003.30+530314.3	1.5	51	107638_1	0.32	
190	215.14885	53.05470	J142035.72+530316.9	0.1	53	101360	0.11	
191	214.98044	53.05645	J141955.30+530323.2	0.2	28	109045	0.24	
192	215.18929	53.05827	J142045.43+530329.7	0.2	53	...	...	
193	215.32691	53.05800	J142118.45+530328.7	2.5	31	092556	0.53	good ID
194	215.01022	53.05862	J142002.45+530331.0	0.2	52	107549	0.24	
195	215.18718	53.05966	J142044.92+530334.7	0.6	54	...	...	
196	215.13546	53.06014	...	0.6	54	101681_2	0.37	red source
197	215.23860	53.06039	J142057.26+530337.3	0.2	52	096647_1	0.18	
198	215.12254	53.06105	J142029.40+530339.7	0.4	50	102222	0.12	
199	214.94571	53.06186	...	0.3	3	110318_1	0.37	
200	215.19844	53.06246	J142047.62+530344.8	0.4	55	...	...	

Table 3—Continued

ID	RA	Dec	EGSIRAC	Offset <sup>a</sup>	Exposure <sup>b</sup>	irac <sup>c</sup>	Offset <sup>d</sup>	Comment
201	214.97078	53.06254	J141952.98+530345.1	0.4	17	109128	0.38	
202	215.36422	53.06817	...	1.4	7	...	...	ch2 offset smaller
203	215.04842	53.07878	J142011.62+530443.5	0.2	44	104694	0.12	companion 4''1 E
204	215.18187	53.07971	...	0.2	54	098284	0.71	companion 2''5 NW
205	215.03267	53.08179	J142007.84+530454.4	0.8	45	105228	0.28	
206	215.11460	53.08182	J142027.50+530454.5	0.2	54	101414	0.14	
207	214.99226	53.08304	J141958.14+530458.9	6.4	11	107020_1	0.32	good ID
208	215.09734	53.08651	J142023.36+530511.4	0.1	52	101935	0.14	
209	215.09676	53.08848	...	0.6	52	...	...	
210	215.14901	53.08926	J142035.76+530521.3	1.0	49	099291_1	0.38	
211	215.17776	53.09570	J142042.66+530544.5	0.1	50	097528	0.27	
212	215.22482	53.09735	J142053.95+530550.4	0.1	54	095161	0.08	
213	215.17153	53.09743	J142041.16+530550.7	0.6	56	097722	0.23	
214	215.31952	53.10200	J142116.68+530607.2	0.2	52	090482	0.08	
215	215.19466	53.10408	J142046.71+530614.6	0.7	57	096219	0.22	
216	215.36696	53.10511	J142128.07+530618.4	0.5	41	088486	0.03	fainter companion 4''0 S
217	215.30095	53.10606	J142112.22+530621.8	0.1	51	091054	0.05	
218	215.20256	53.10660	J142048.61+530623.7	1.0	51	095727	0.25	
219	215.16740	53.10829	J142040.17+530629.8	0.1	51	097273	0.12	
220	215.22233	53.11067	J142053.35+530638.4	0.3	55	094556_1	0.24	
221	215.08012	53.11179	J142019.22+530642.4	0.3	46	101350	0.14	
222E	215.25432	53.11241	J142101.03+530644.6	0.0	62	092894	0.12	two sources
222W	215.25222	53.11198	J142100.53+530643.1	0.1	62	093015	0.05	
223	215.16736	53.11310	J142040.16+530647.1	0.5	49	096986	0.13	
224	215.14252	53.11940	J142034.20+530709.8	0.5	50	097828	0.20	
225	215.40585	53.12115	J142137.40+530716.1	0.4	38	086566_1	0.18	
226	215.05203	53.12494	J142012.48+530729.7	0.6	14	000003	0.27	big galaxy
227	215.31121	53.12614	J142114.69+530734.1	0.2	53	089648	0.22	
228	215.13814	53.12642	J142033.15+530735.1	0.5	50	097628	0.10	
229	215.21962	53.12930	...	0.1	53	093595	0.10	
230	215.18255	53.12945	J142043.81+530746.0	0.5	53	095351	0.29	
231	215.34034	53.13176	J142121.68+530754.3	0.5	48	088287_1	0.05	
232	215.31942	53.13522	J142116.66+530806.7	0.2	53	088921	0.17	
233	215.13885	53.13924	J142033.32+530821.2	7.6	47	096846	0.14	jet
234	215.33395	53.13793	J142120.14+530816.5	0.3	50	088250	0.02	
235	215.06354	53.13917	...	0.5	7	100482	0.32	
236	215.13421	53.14134	J142032.20+530828.8	4.3	48	096952	0.05	doubtful ID, dbl with 233??
237	215.47945	53.14469	...	0.8	6	...	...	
238	215.15291	53.15074	J142036.69+530902.6	0.5	51	095527	0.09	
239	215.23528	53.15283	J142056.46+530910.2	0.6	49	091468	0.08	

Table 3—Continued

ID	RA	Dec	EGSIRAC	Offset <sup>a</sup>	Exposure <sup>b</sup>	irac <sup>c</sup>	Offset <sup>d</sup>	Comment
240	215.35508	53.15349	J142125.21+530912.5	0.1	49	086907	0.10	
241	215.21498	53.15482	J142051.59+530917.3	0.2	47	092306	0.14	
242	215.42013	53.15679	...	0.4	50	...	...	brighter (bluer) companion 2''2 E
243	215.45115	53.15891	J142148.27+530932.0	0.5	35	084237	0.18	
244	215.17747	53.15923	J142042.59+530933.2	0.9	49	093886_2	0.59	companion 1''6 NW
245	215.40995	53.16082	J142138.38+530938.9	0.4	52	085247	0.04	
246	215.35650	53.16384	J142125.55+530949.8	0.4	54	086507	0.11	
247	215.24316	53.16525	J142058.35+530954.9	0.3	54	090467	0.11	
248	215.44900	53.17318	J142147.75+531023.4	0.2	47	083886	0.08	
249	215.46459	53.17395	J142151.50+531026.2	0.5	44	083488	0.18	
250	215.22848	53.17929	J142054.83+531045.4	0.3	48	090347	0.03	
251	215.42464	53.17980	J142141.91+531047.2	0.4	53	084269	0.17	
252	215.36028	53.18031	J142126.46+531049.1	2.2	50	085902	0.44	radio double
253	215.52259	53.18100	...	0.7	7	...	...	companion 4''5 NE
254	215.40803	53.18423	J142137.92+531103.2	0.5	56	084564_1	0.42	companions 1''9 E (blended)
255	215.46452	53.18492	J142151.48+531105.7	0.2	47	083145	0.17	
256	215.45953	53.18575	J142150.28+531108.6	0.2	49	083246	0.13	
257	215.29162	53.18689	J142109.98+531112.8	0.1	53	087651	0.08	
258	215.39713	53.18770	J142135.31+531115.7	0.6	55	084755	0.17	
259	215.48904	53.18879	...	0.0	42	082414_1	0.21	bright companion 2''9 W
260	215.50264	53.19045	J142200.63+531125.6	0.4	40	082053	0.16	
261	215.49853	53.19062	J142159.64+531126.2	0.5	40	...	...	
262	215.15002	53.19637	J142036.00+531146.9	0.9	12	093001	0.79	edge of ch 1/3
263	215.18171	53.19746	J142043.60+531150.8	0.4	34	091431	0.05	
264	215.19222	53.20334	J142046.13+531212.0	0.9	36	090668	0.09	
265	215.55325	53.20887	J142212.77+531231.9	1.0	12	...	...	
266	215.34312	53.21154	J142122.34+531241.5	0.8	52	085372	0.17	
267	215.51598	53.21351	J142203.83+531248.6	0.2	40	081052	0.12	companion 3''0 SW
268	215.47420	53.21629	J142153.80+531258.6	0.4	50	081987	0.18	double in R
269	215.25671	53.21705	J142101.61+531301.3	0.5	53	087589	0.15	
270	215.27973	53.21728	J142107.13+531302.2	0.2	54	086859	0.09	
271	215.18881	53.21824	J142045.31+531305.6	0.7	19	090135	0.20	galaxy slightly extended
272	215.23677	53.21886	J142056.82+531307.8	0.3	50	088226	0.09	big radio dbl with central radio so
273	215.34320	53.22214	J142122.36+531319.7	0.3	53	085055	0.18	
274	215.44687	53.22295	J142147.24+531322.6	0.3	52	082445	0.08	double at R
275	215.49154	53.22489	J142157.96+531329.6	0.7	52	081317	0.06	
276	215.30917	53.22855	J142114.20+531342.7	0.2	51	085703	0.01	companion 4''9 W
277	215.26985	53.23214	J142104.76+531355.7	0.5	47	...	...	
278	215.41858	53.23226	...	0.2	62	082848	0.72	blended or extended
279	215.49543	53.23252	J142158.90+531357.0	0.1	47	080986	0.13	

Table 3—Continued

ID	RA	Dec	EGSIRAC	Offset <sup>a</sup>	Exposure <sup>b</sup>	irac <sup>c</sup>	Offset <sup>d</sup>	Comment
280	215.25466	53.23293	J142101.11+531358.5	0.1	45	...	...	
281	215.32118	53.23722	J142117.08+531413.9	0.4	50	085154	0.17	
282	215.60174	53.24024	...	0.9	11	...	...	
283	215.48344	53.24046	J142156.02+531425.6	1.0	49	081057	0.19	
284	215.57170	53.24076	J142217.20+531426.7	0.1	37	078862	0.21	
285	215.58523	53.24192	J142220.45+531430.9	0.6	22	078484	0.29	
286	215.23928	53.24394	J142057.42+531438.1	2.1	28	087108	0.22	companion 4''0 N
287	215.61013	53.24501	J142226.43+531442.0	0.5	12	...	...	
288	215.42216	53.24731	J142141.31+531450.3	0.3	59	082332.1	0.20	
289	215.57082	53.24803	J142216.99+531452.9	0.7	41	078656	0.31	double 1''6 sep in R
290	215.56945	53.24939	J142216.66+531457.8	0.1	40	078653	0.20	
291	215.45987	53.24963	J142150.36+531458.6	0.8	56	...	...	companions 2''7 N
292	215.47830	53.25018	J142154.79+531500.6	0.1	54	...	...	
293	215.41957	53.25211	J142140.69+531507.5	0.2	56	082253	0.12	
294	215.23015	53.25377	J142055.23+531513.5	0.2	12	...	...	
295N	215.59148	53.25441	J142221.95+531515.8	0.6	36	077979	0.12	companion 2''8 SE has some rad
296	215.58281	53.25442	J142219.87+531515.9	0.2	43	078174	0.13	
297	215.36615	53.25448	J142127.87+531516.1	0.5	52	083523	0.06	
298	215.47352	53.25622	J142153.64+531522.3	0.4	56	080824.1	0.46	
299	215.45205	53.25959	J142148.49+531534.5	0.1	61	081261	0.04	
300	215.38082	53.25976	J142131.39+531535.1	0.1	51	082969	0.05	
301	215.64326	53.25958	...	0.6	4	...	...	
302	215.57401	53.25994	J142217.76+531535.7	0.6	52	078220	0.19	
303	215.50610	53.26046	J142201.46+531537.6	0.4	48	079884	0.17	
304	215.63129	53.26085	J142231.50+531539.0	0.3	12	002162	0.17	
305	215.38219	53.26224	J142131.72+531544.0	0.1	50	082855.1	0.08	
306	215.24146	53.26262	J142057.94+531545.4	0.5	14	...	...	fainter companion 3''3 NE
307	215.48517	53.26391	J142156.44+531550.0	0.5	52	080322	0.09	companions 5'' N & S
308	215.36988	53.26391	J142128.77+531550.0	0.7	47	083122	0.07	
309	215.41823	53.26536	J142140.37+531555.2	0.4	49	081905	0.09	triple in R
310	215.63967	53.26540	...	0.4	9	002125	0.19	blended in R
311	215.47548	53.26854	J142154.11+531606.7	0.8	54	080431.1	0.35	
312	215.57568	53.27759	J142218.16+531639.3	0.3	51	077695	0.00	
313	215.38786	53.28079	J142133.08+531650.8	0.3	51	082186	0.16	
314	215.58093	53.28256	J142219.42+531657.2	0.4	51	077418.1	0.46	
315	215.49825	53.28350	J142159.58+531700.5	0.3	59	079404.1	0.37	
316	215.40523	53.28691	J142137.25+531712.8	0.4	51	081579	0.17	
317	215.39230	53.28852	J142134.15+531718.6	0.4	53	081843	0.08	
318	215.40787	53.28922	J142137.88+531721.1	0.3	55	081458	0.17	
319	215.57069	53.29403	J142216.96+531738.4	0.4	49	...	...	

Table 3—Continued

ID	RA	Dec	EGSIRAC	Offset <sup>a</sup>	Exposure <sup>b</sup>	irac <sup>c</sup>	Offset <sup>d</sup>	Comment
320	215.27851	53.29471	...	0.1	4	...	...	
321	215.33421	53.29632	J142120.21+531746.7	0.8	39	083017	0.11	
322	215.42792	53.29828	J142142.69+531753.8	0.2	51	080702	0.16	
323	215.66919	53.30082	J142240.60+531802.9	0.1	22	074652	0.25	companions 2''4 NE
324	215.65939	53.30078	J142238.25+531802.8	0.9	31	074918	0.17	companion 2''7 NE
325	215.41618	53.30412	J142139.88+531814.8	0.7	51	080808	0.09	
326	215.68780	53.30479	J142245.07+531817.2	0.3	14	001985	0.04	
327	215.32501	53.30542	J142118.00+531819.5	0.7	23	...	...	
328	215.70018	53.30784	...	0.8	9	...	...	
329	215.57523	53.30923	J142218.05+531833.2	0.3	48	076745	0.08	red companion 4''8 NE
330	215.45901	53.31067	J142150.16+531838.4	0.4	50	079546	0.10	
331	215.70721	53.31069	...	1.0	6	...	...	
332	215.45124	53.31301	J142148.29+531846.8	0.4	48	079666	0.10	
333	215.57956	53.31369	J142219.09+531849.2	0.2	52	076499	0.12	
334	215.71341	53.31599	...	0.8	6	...	...	companion 4''9 SE
335	215.48175	53.31702	J142155.62+531901.2	0.3	54	078812	0.11	
336	215.44583	53.31891	J142146.99+531908.0	0.6	52	079626	0.08	
337	215.61312	53.32162	J142227.14+531917.8	0.3	47	...	...	fainter companion 4''8 E
338	215.71425	53.32486	J142251.41+531929.5	0.6	12	072899	0.15	
339	215.43837	53.32674	J142145.20+531936.2	0.1	51	079590_1	0.28	
340	215.72864	53.32932	...	0.9	8	001807	0.16	
341	215.44266	53.32988	J142146.23+531947.5	0.6	52	079379	0.10	
342	215.58254	53.33064	J142219.81+531950.3	0.4	51	075903_1	0.31	
343	215.47537	53.33075	J142154.08+531950.7	0.0	49	078537	0.09	
344	215.54781	53.33084	J142211.47+531951.0	0.4	61	076790	0.09	
345	215.73004	53.33402	...	0.6	12	...	...	brighter companion 2''1 SW
346	215.40288	53.33443	J142136.69+532003.9	0.2	48	080243	0.02	
347	215.39449	53.33460	J142134.67+532004.5	0.6	46	080453	0.06	
348	215.44924	53.33451	J142147.81+532004.2	0.5	53	079101	0.10	
349	215.45763	53.33479	J142149.83+532005.2	0.3	54	078879	0.07	
350	215.39480	53.33612	J142134.75+532010.0	0.6	45	080397	0.06	
351	215.47978	53.33992	J142155.14+532023.7	0.6	54	078168	0.03	
352	215.69571	53.34054	J142246.97+532025.9	0.3	45	072889	0.16	
353	215.60587	53.34079	J142225.40+532026.8	0.9	52	075056	0.14	
354	215.61062	53.34128	J142226.54+532028.6	0.2	51	074916	0.10	
355	215.54500	53.34165	J142210.80+532029.9	0.3	54	076513	0.16	
356	215.56624	53.34227	J142215.89+532032.1	0.8	58	075969	0.14	companion 4''3 NW
357	215.48598	53.34189	J142156.63+532030.8	0.8	53	077980	0.10	
358W	215.65829	53.34432	J142237.98+532039.5	0.4	52	...	...	companion 2''8 E has some radi
359	215.73548	53.34724	J142256.51+532050.0	0.5	17	071736	0.16	

Table 3—Continued

ID	RA	Dec	EGSIRAC	Offset <sup>a</sup>	Exposure <sup>b</sup>	irac <sup>c</sup>	Offset <sup>d</sup>	Comment
360	215.44747	53.34792	J142147.39+532052.5	1.1	51	078728	0.10	radio triple
361	215.40475	53.34868	J142137.13+532055.2	0.2	32	079750	0.22	
362	215.63717	53.35093	J142232.91+532103.3	0.2	53	074041	0.15	
363	215.46246	53.35114	J142150.99+532104.1	0.3	58	078266	0.21	
364	215.39782	53.35375	J142135.47+532113.5	0.2	29	079770	0.07	
365	215.76711	53.35426	...	0.4	9	...	...	
366	215.70719	53.35445	J142249.72+532116.0	0.2	51	072214	0.24	
367	215.68519	53.35553	J142244.44+532119.8	0.1	50	072710	0.18	
368	215.66549	53.35753	J142239.71+532127.1	0.6	52	073127_1	0.23	
369	215.45905	53.35781	J142150.17+532128.1	1.1	57	078150	0.15	
370E	215.66749	53.36098	...	0.0	53	072980	0.08	370=two sources
370W	215.66616	53.36035	...	0.0	51	073032_1	0.21	double 1''5 sep in R
371	215.61802	53.36095	J142228.32+532139.4	0.4	52	074188_2	0.61	double or triple 1''4 sep at R
372	215.65283	53.36222	J142236.67+532143.9	0.4	54	073304	0.11	
373	215.57341	53.36320	J142217.61+532147.5	0.1	58	075193	0.05	
374	215.74949	53.36456	J142259.87+532152.4	0.2	35	070913_1	0.73	double 1''5 sep in R
375	215.59285	53.36645	J142222.28+532159.2	0.3	57	074592	0.38	
376	215.38250	53.36698	...	1.0	5	...	...	
377	215.72270	53.37206	J142253.44+532219.4	0.5	49	...	...	
378	215.69688	53.37272	J142247.25+532221.7	0.3	50	071933	0.08	
379	215.49178	53.37342	J142158.02+532224.2	0.1	49	076917	0.08	
380	215.76290	53.37351	J142303.09+532224.6	0.3	35	070313	0.17	radio double
381	215.70756	53.37616	J142249.81+532234.1	0.1	48	071568	0.09	
382	215.46148	53.37838	...	0.6	50	077529	0.78	
383	215.62752	53.37907	J142230.60+532244.6	0.3	61	073424	0.11	
384	215.65995	53.38087	J142238.38+532251.1	0.4	51	072580	0.18	
385	215.70820	53.38273	J142249.96+532257.8	0.2	51	071390	0.09	
386	215.49721	53.38745	J142159.32+532314.8	0.1	54	076314	0.16	
387	215.77510	53.39051	J142306.02+532325.8	1.9	38	069467	0.06	
388	215.64071	53.39121	J142233.76+532328.3	0.2	60	072738	0.27	companions 4''1 E
389	215.62296	53.39272	J142229.51+532333.7	0.3	60	073124	0.23	
390	215.63943	53.39397	...	0.3	59	072695	0.16	
391	215.69019	53.39517	J142245.64+532342.6	0.3	48	071448	0.12	
392	215.83382	53.39707	...	1.2	7	...	...	
393	215.46337	53.40021	J142151.20+532400.7	0.3	29	076802	0.11	
394	215.76195	53.40221	J142302.86+532407.9	1.1	41	069441	0.14	
395	215.66259	53.40402	...	0.2	56	071861	0.27	double at R
396	215.75484	53.40527	J142301.16+532418.9	0.2	44	069544	0.08	
397	215.53477	53.40567	J142208.34+532420.4	0.1	55	074859	0.18	
398	215.52790	53.40749	J142206.69+532426.9	0.6	54	074982	0.38	

Table 3—Continued

ID	RA	Dec	EGSIRAC	Offset <sup>a</sup>	Exposure <sup>b</sup>	irac <sup>c</sup>	Offset <sup>d</sup>	Comment
399	215.65718	53.40784	J142237.72+532428.2	1.2	54	072036	0.21	IR extended
400	215.60865	53.41045	...	0.3	45	072968	0.17	
401	215.74997	53.41124	J142259.99+532440.4	0.3	48	069479	0.04	
402	215.47135	53.41140	J142153.12+532441.0	0.1	27	076235_1	0.36	
403	215.60578	53.41404	J142225.38+532450.5	0.3	47	072925	0.09	
404	215.51617	53.41422	J142203.88+532451.1	0.7	53	075091_1	0.20	
405	215.82397	53.41447	J142317.75+532452.0	0.6	30	067554	0.22	
406	215.75852	53.41645	J142302.04+532459.2	0.3	54	069095_1	0.35	
407	215.59558	53.42397	J142222.93+532526.2	0.1	45	072882	0.24	
408	215.72031	53.42459	J142252.87+532528.5	0.4	52	069823	0.01	
409	215.54319	53.42914	...	0.4	52	...	...	near bright star
410	215.82028	53.43290	J142316.86+532558.4	0.3	46	067078_1	0.03	
411	215.84130	53.43310	...	0.6	30	066542_1	0.18	companions 4''6 E
412	215.48432	53.43383	J142156.23+532601.7	1.0	15	...	...	
413	215.65450	53.43585	J142237.07+532609.0	0.4	50	071125	0.04	
414	215.48553	53.43725	...	0.7	6	...	...	
415	215.57211	53.43852	J142217.30+532618.6	0.7	48	073019	0.28	
416	215.80164	53.43995	J142312.39+532623.8	0.2	49	067357	0.08	companion 4''0 NE
417	215.63235	53.43999	J142231.76+532623.9	0.3	54	071535_1	0.09	
418S	215.76186	53.44003	J142302.84+532624.1	0.4	47	068295	0.18	3 companion 3''9 NE has some r
419	215.52403	53.44081	...	0.1	37	...	...	
420N	215.64515	53.44264	J142234.83+532633.5	0.9	47	071152	0.08	1 companion 2''8 S has some rad
421	215.58609	53.44508	...	0.1	48	072479	0.68	
422	215.64447	53.44510	J142234.67+532642.3	0.5	50	071103	0.09	R blended or extended
423	215.63116	53.44543	J142231.47+532643.5	0.2	54	071419	0.08	
424	215.67242	53.44627	J142241.38+532646.5	0.2	50	070383	0.12	
425	215.62942	53.44704	J142231.06+532649.3	0.1	55	071409	0.08	companion 4''9 NW
426	215.59690	53.44995	J142223.25+532659.8	0.3	53	072100	0.22	
427	215.67553	53.45430	J142242.12+532715.4	0.4	46	070047_1	0.11	
428	215.83444	53.45589	J142320.26+532721.2	8.5	52	066050	0.15	complex radio
429	215.71318	53.45605	J142251.16+532721.7	0.3	61	069045	0.15	
430	215.76402	53.46274	J142303.36+532745.8	0.4	54	067605	0.12	
431	215.80288	53.46581	J142312.69+532756.9	0.1	49	066530	0.08	
432	215.59065	53.46630	J142221.75+532758.6	0.2	53	071780	0.19	
433	215.56222	53.46864	J142214.93+532807.0	0.4	35	072378	0.24	
435	215.86362	53.47197	J142327.26+532819.0	0.7	46	064885	0.33	R companion 0''8 SE
436	215.65645	53.47213	J142237.54+532819.6	0.1	54	069989	0.04	
437	215.87793	53.47319	J142330.70+532823.4	1.0	37	216288_2	0.46	large merging pair
438	215.92101	53.47350	J142341.04+532824.6	0.3	20	063794	0.26	
439	215.92019	53.47512	...	0.7	20	216220	0.67	faint source



Table 3—Continued

ID	RA	Dec	EGSIRAC	Offset <sup>a</sup>	Exposure <sup>b</sup>	irac <sup>c</sup>	Offset <sup>d</sup>	Comment
440	215.62923	53.47750	J142231.01+532839.0	0.7	51	070537	0.07	
441	215.71828	53.47813	J142252.38+532841.2	0.0	52	068240	0.15	
442	215.59377	53.47833	J142222.50+532842.0	0.4	47	071366	0.11	
443	215.54383	53.48018	J142210.51+532848.6	0.7	8	...	...	
444	215.91462	53.48192	J142339.50+532854.9	1.2	30	063738	0.27	
445	215.61516	53.48439	J142227.63+532903.8	0.8	49	070686	0.08	
446	215.62548	53.48766	J142230.11+532915.5	0.6	51	...	...	
447	215.72964	53.48786	J142255.11+532916.2	0.6	49	067693	0.10	
448	215.74542	53.49066	J142258.89+532926.3	0.7	50	067219	0.05	R extended or multiple
449	215.66193	53.49409	J142238.86+532938.7	0.2	54	069181	0.02	
450	215.94974	53.49456	J142347.93+532940.4	1.4	11	000979	0.18	
451	215.96374	53.49520	...	0.7	2	...	...	
452	215.73378	53.50066	J142256.10+533002.3	0.3	50	067209	0.13	
453	215.61220	53.50135	J142226.92+533004.8	0.6	44	070231	0.13	
454	215.82798	53.50264	J142318.71+533009.5	0.8	53	064859	0.10	IR slightly extended
455	215.85569	53.50311	J142325.36+533011.1	0.9	52	064287	0.17	
456	215.72231	53.50708	J142253.35+533025.4	0.2	50	067323	0.18	
457	215.85235	53.51354	...	0.6	49	...	...	brighter companion 3''6 W
458	215.86519	53.51383	J142327.64+533049.7	0.5	48	063927	0.09	
459	215.81664	53.51442	J142315.99+533051.8	0.2	55	064798	0.22	
460	215.63404	53.51658	J142232.16+533059.6	0.2	39	069202	0.22	
461	215.85311	53.51671	J142324.74+533100.1	0.3	50	064059	0.07	
462	215.95212	53.51843	J142348.50+533106.3	0.6	20	062071	0.48	
463	215.91198	53.52279	J142338.87+533122.0	0.8	32	062924	0.12	companion 3''6 NE
464	215.79976	53.52561	J142311.94+533132.1	0.4	58	064869	0.07	companion 3''0 SW
465	215.95608	53.52633	J142349.45+533134.7	0.5	22	061706	0.19	
466	215.84939	53.52625	J142323.85+533134.4	0.4	50	063944	0.07	
467	215.76607	53.53044	J142303.85+533149.5	0.9	47	065554	0.16	
468	215.71966	53.53340	...	0.5	49	066571	0.19	multiple or extended in R
469	216.00302	53.53370	...	0.8	4	...	...	ch1-2 maps shifted
470	215.69792	53.53416	J142247.50+533202.9	0.2	48	067104	0.09	
471	215.75624	53.53957	J142301.49+533222.4	0.4	50	065529	0.16	
472	215.96796	53.54104	J142352.31+533227.7	0.5	25	060872	0.32	
473	215.82102	53.54460	...	0.3	49	064063	0.19	IR slightly extended
474	215.91367	53.54549	J142339.28+533243.7	0.5	31	062224	0.04	
475	215.68069	53.54633	J142243.36+533246.7	0.6	37	067161	0.29	
476	215.72701	53.55117	J142254.48+533304.2	0.5	50	065873	0.09	
477	215.92167	53.55206	J142341.20+533307.4	0.8	23	061800	0.62	
478	215.86706	53.55250	...	0.7	31	063124	0.15	brighter companions 2''8 SE
479	215.65210	53.55288	J142236.50+533310.3	1.2	13	...	...	

Table 3—Continued

ID	RA	Dec	EGSIRAC	Offset <sup>a</sup>	Exposure <sup>b</sup>	irac <sup>c</sup>	Offset <sup>d</sup>	Comment
480	215.75453	53.55334	J142301.08+533312.0	0.2	50	216316	0.19	
481	215.64240	53.55412	...	0.5	8	...	...	
482	215.94081	53.55547	J142345.79+533319.7	0.5	27	061154	0.22	
483	215.86278	53.55877	J142327.06+533331.5	0.4	32	063059	0.15	
484	215.82031	53.56112	...	0.5	28	...	...	near bright star
485	215.95988	53.56209	...	0.5	25	060357	0.41	companion 2''1 W
486	216.00167	53.56315	J142400.39+533347.3	0.3	23	059238	0.25	
487	216.05112	53.56355	...	1.3	5	...	...	ch1-2 maps shifted
489	216.00278	53.56757	J142400.66+533403.2	0.6	23	059080	0.18	
490	215.74749	53.56864	...	0.3	46	064883	0.04	
491	215.85048	53.57240	...	0.7	26	...	...	
492	215.79941	53.57292	...	0.5	34	...	...	
493	215.91026	53.57565	J142338.46+533432.3	0.6	27	061341	0.24	
494	215.73557	53.58050	J142256.53+533449.7	0.3	41	064827	0.46	companion 3''1 SE
495	215.85104	53.58656	...	0.4	29	...	...	
496	215.69769	53.58724	...	0.7	7	...	...	companion 4''6 N
497	215.91111	53.58898	J142338.66+533520.3	0.3	25	060858	0.28	companion 2''9 S
498	215.92450	53.59049	...	0.4	27	060400	0.26	
499	215.94101	53.60801	J142345.84+533628.8	0.6	26	059408	0.17	
500	215.89351	53.60955	J142334.44+533634.3	0.5	26	060636	0.56	brighter companion 2''2 NW
501	216.00461	53.61102	J142401.10+533639.6	0.7	14	...	...	
502	215.75602	53.61127	J142301.44+533640.5	1.2	13	...	...	
503	215.75694	53.61553	J142301.66+533655.9	0.7	12	...	...	extended or multiple
504	215.88593	53.62738	J142332.62+533738.5	0.1	25	215864	0.50	big galaxy in R
505	215.85448	53.63302	J142325.07+533758.8	0.5	25	060958	0.11	extended in R
506	215.92032	53.63853	J142340.87+533818.7	0.3	18	059019	0.24	
507	215.85893	53.64941	J142326.14+533857.8	0.9	24	060249	0.28	
508	215.81670	53.65336	...	0.5	19	...	...	brighter companion 2''7 SW
509	215.88398	53.65397	J142332.15+533914.2	0.6	21	059449	0.28	
510	215.85818	53.66189	J142325.96+533942.7	0.8	24	059888	0.40	
511	215.86671	53.68442	...	1.0	9	...	...	

<sup>a</sup>Radial offset from IRAC to radio position. Where a source name is shown, IRAC names and positions are from the published catalog (Barmby et al. 2008). For counterparts not in the published catalog, source positions were measured on the published images.

<sup>b</sup>Number of useful images in whichever IRAC wavelength has the fewest in units of 200 s (one image at 3.6–5.8  $\mu\text{m}$ ; 4 images at 8.0  $\mu\text{m}$ ; see Barmby et al. 2008).

<sup>c</sup>Source name in Rainbow database (Barro et al. 2011a)

<sup>d</sup>Radial offset from IRAC position measured here to source position in Rainbow database.

Table 4.  $R$  Magnitudes and Redshifts of Radio Source Counterparts

ID	RA <sup>a</sup>	Dec <sup>a</sup>	Offset <sup>b</sup>	Mag type <sup>c</sup>	$R$	$\pm^d$	$z$	$z$ source <sup>e</sup>	$L(3\text{ GHz})$
001	...	...	...	5	23.77	0.02	0.95	6	3.6E+23
003	214.38594	52.53426	0.23	1	23.13	0.01	0.9859	2	2.2E+24
004	214.54142	52.55020	0.28	1	25.14	0.09	2.87	6	7.9E+25
005	214.47884	52.55183	0.12	1	25.30	0.10	1.84	6	1.6E+24
006	214.59998	52.55628	0.43	1	23.35	0.02	1.20	6	6.5E+23
007	214.42169	52.56540	0.28	1	23.73	0.02	3.3630	5	4.1E+25
008	214.56735	52.58665	0.18	4	20.95	0.01	0.3264	2	2.1E+22
009	214.47244	52.59435	0.12	3	21.27	0.01	0.6791	2	1.7E+24
010	...	...	...	5	24.69	0.05	1.63	6	1.1E+24
011	214.52084	52.60600	0.29	1	24.43	0.05	2.11	6	1.5E+24
012	214.62560	52.60917	0.22	1	24.23	0.04	1.76	6	9.4E+23
013	214.59319	52.60945	0.31	1	24.83	0.07	1.73	6	3.2E+24
014	214.48129	52.61232	0.23	1	25.53	0.13	3.07	7	3.3E+24
015	214.58739	52.61983	0.17	1	21.40	0.00	0.4207	2	6.5E+22
016	214.67462	52.62652	0.49	1	23.32	0.02	1.05	6	2.8E+24
017	214.38566	52.63827	0.48	2	20.82	0.00	0.7168	2	1.5E+26
018	...	...	...	5	26.74	-5	0.43	8	3.2E+22
019	214.77600	52.65094	0.83	1	23.44	0.02	1.79	6	2.1E+24
020	...	...	...	5	23.60	0.02	1.68	6	7.5E+23
021	214.66485	52.65236	0.50	4	22.93	0.03	1.40	6	4.5E+23
022	...	...	...	5	17.91	0.00	...	0	...
023	...	...	...	5	25.31	0.07	1.57	6	8.6E+23
024	214.59365	52.66062	0.47	1	24.76	0.06	1.77	4	1.1E+24
025	214.74947	52.66800	0.67	1	21.43	0.00	0.6798	3	8.6E+22
026	...	...	...	5	24.59	0.03	2.95	6	3.8E+24
027	214.73804	52.66980	0.46	1	25.01	0.08	2.11	6	1.0E+24
028	214.77824	52.67048	0.59	1	19.17	0.00	0.1979	2	6.0E+21
029	214.52314	52.67575	0.17	1	22.50	0.01	1.4127	2	4.1E+24
030	214.55690	52.67738	0.41	4	22.15	0.01	0.7602	1	5.4E+23
031	214.67472	52.68554	0.48	1	25.17	0.09	2.11	6	9.9E+23
032	214.47903	52.68756	0.13	4	18.10	0.00	0.0679	3	2.0E+21
033	...	...	...	5	26.94	0.29	2.38	9	1.4E+24
034	214.51403	52.69111	0.06	1	20.32	0.00	1.6866	3	7.7E+23
035	214.71213	52.69399	0.48	1	23.26	0.02	2.11	6	3.3E+24
036	214.44881	52.69538	0.80	4	15.08	0.00	0.0662	3	7.8E+22
037	...	...	...	5	21.95	0.00	0.4635	1	1.2E+23
038	...	...	...	5	26.34	0.16	2.11	6	1.1E+24
039	214.73582	52.70029	0.50	1	23.05	0.01	0.6469	1	7.9E+22
040	214.58835	52.70149	0.40	1	24.49	0.05	1.0319	1	3.8E+23
041	214.82543	52.70937	0.74	1	22.52	0.01	1.2819	1	7.1E+23

Table 4—Continued

ID	RA <sup>a</sup>	Dec <sup>a</sup>	Offset <sup>b</sup>	Mag type <sup>c</sup>	$R$	$\pm^d$	$z$	$z$ source <sup>e</sup>	$L(3\text{ GHz})$
042	214.63832	52.71175	0.48	1	26.03	0.20	1.76	4	1.2E+24
043	214.56180	52.71213	0.28	5	26.73	−5	1.04	7	9.5E+23
044	214.76803	52.71462	0.58	1	24.83	0.07	1.40	6	8.0E+23
045	214.65907	52.71868	0.08	1	25.94	0.19	1.88	9	8.6E+23
046	214.73144	52.72196	0.40	1	25.85	0.17	1.40	6	4.0E+23
047	214.48091	52.72761	0.08	1	24.12	0.03	1.28	6	3.8E+23
048	214.86693	52.72839	0.38	4	24.20	0.06	1.94	4	9.9E+23
049	214.76713	52.72953	0.37	1	21.73	0.00	0.7471	3	1.6E+23
050	214.61257	52.73038	0.20	3	22.41	0.01	0.7603	1	9.1E+22
051	214.63797	52.73129	0.43	3	20.11	0.00	0.4625	1	7.1E+22
052	...	...	...	5	26.51	−5	3.40	6	3.3E+24
053	214.78673	52.73367	0.74	3	19.83	0.00	0.2948	2	2.5E+22
054	214.72154	52.73642	0.30	1	19.44	0.00	0.2483	2	1.4E+22
055	214.73866	52.73740	0.49	1	19.51	0.00	0.2957	2	3.9E+22
056	214.53733	52.73988	0.34	1	26.15	0.23	1.82	6	9.6E+23
057	214.52546	52.74806	0.49	3	19.16	0.00	0.2497	2	1.1E+22
058	214.69116	52.74892	0.49	1	21.60	0.00	0.5693	2	6.1E+22
059	214.88590	52.75136	0.64	1	24.29	0.04	1.3993	1	5.3E+23
060	...	...	...	5	25.12	0.06	2.12	4	1.7E+24
061	214.57373	52.77102	0.36	2	23.14	0.02	1.50	6	5.9E+23
062	214.71978	52.77198	0.73	1	22.88	0.01	1.1774	1	6.5E+23
063	...	...	...	5	26.18	0.12	1.99	6	2.0E+24
064	...	...	...	5	26.71	−5	1.33	6	4.1E+23
065	214.93963	52.78011	0.76	1	20.75	0.00	0.73	8	1.3E+25
066	...	...	...	5	24.48	0.04	0.1714	3	6.6E+21
067	214.83168	52.78774	0.35	1	21.76	0.00	0.5468	2	6.0E+22
068	214.94967	52.79032	0.76	1	21.56	0.00	0.6530	1	1.4E+23
069	214.68505	52.79336	0.22	1	23.96	0.03	1.93	6	1.8E+24
070	...	...	...	5	20.70	0.01	...	0	...
071	214.89225	52.80011	0.19	1	24.54	0.05	1.42	6	2.5E+24
072	214.82916	52.80849	0.21	1	25.52	0.12	1.50	6	2.4E+24
073	214.79335	52.80861	0.32	4	18.73	0.00	0.3459	2	1.3E+24
074	214.62451	52.80973	0.20	1	23.18	0.01	0.9371	1	5.1E+23
075	214.71444	52.81001	0.28	1	24.01	0.03	1.9217	2	3.0E+24
076	214.97812	52.81175	0.98	1	25.54	0.12	1.43	7	6.0E+23
077	214.94611	52.81240	0.47	1	24.83	0.06	1.14	9	5.1E+24
078	214.72162	52.81563	0.39	4	20.81	0.00	0.4411	3	5.7E+22
079	214.80858	52.81923	0.39	1	21.81	0.00	0.8250	3	1.3E+23
080	214.81218	52.82497	0.43	1	22.67	0.01	1.1970	2	1.0E+24
081	214.91690	52.82744	0.37	1	23.53	0.02	1.2318	2	2.9E+23

Table 4—Continued

ID	RA <sup>a</sup>	Dec <sup>a</sup>	Offset <sup>b</sup>	Mag type <sup>c</sup>	$R$	$\pm^d$	$z$	$z$ source <sup>e</sup>	$L(3\text{ GHz})$
082	214.75109	52.82996	0.52	5	24.10	0.02	1.87	4	3.4E+24
083	214.78247	52.83109	0.45	4	18.88	0.00	0.4409	2	3.4E+22
084	214.97388	52.83251	0.49	1	20.04	0.00	0.4345	5	2.9E+22
085	214.72703	52.83476	0.13	2	21.39	0.00	0.4797	2	5.5E+22
086	214.83573	52.84019	0.46	1	21.00	0.00	0.6904	2	8.7E+22
087	214.94785	52.84072	0.50	1	24.65	0.05	1.35	4	8.9E+23
088	214.86263	52.84297	0.42	1	26.20	0.22	3.74	9	5.1E+24
089	214.82216	52.84316	0.42	1	20.98	0.00	0.6603	3	1.4E+23
090	...	...	...	5	23.47	0.02	2.87	9	2.3E+24
091	214.90569	52.84749	0.64	1	21.78	0.00	0.7312	1	2.1E+23
092	214.92755	52.84802	0.27	2	23.95	0.04	0.99	7	4.3E+23
093	214.99291	52.85091	0.72	1	26.30	0.24	0.96	7	1.5E+23
094	214.90524	52.85095	0.08	4	20.09	0.00	0.6702	2	1.6E+23
095	214.96719	52.85779	0.39	2	20.17	0.00	0.2029	2	5.3E+21
096	214.81098	52.85843	0.45	1	24.21	0.03	0.49	7	3.1E+22
097	214.77047	52.86040	0.29	5	24.71	0.04	1.05	7	1.7E+23
098	214.69280	52.86150	0.29	1	25.17	0.08	0.79	7	2.0E+23
099	214.79276	52.86428	0.27	4	16.21	0.00	0.34	9	4.5E+22
100	214.87549	52.86654	0.46	2	19.55	0.00	0.2840	3	6.5E+22
101	214.79202	52.86677	0.36	1	19.89	0.00	0.39	8	2.2E+22
102	215.03775	52.87084	0.39	1	21.29	0.00	0.5422	3	6.9E+22
103	214.81531	52.87104	0.45	2	20.80	0.00	0.4518	3	3.9E+22
104	...	...	...	5	26.71	−5	1.00	7	1.2E+24
105E	214.91442	52.87600	0.25	1	21.30	0.00	0.7315	2	4.8E+22
105W	...	...	...	5	26.58	−5	1.09	9	1.5E+23
106	...	...	...	5	25.09	0.06	1.59	9	5.5E+23
107	...	...	...	5	26.42	0.15	3.76	9	5.0E+24
108	214.92309	52.88233	0.75	1	23.07	0.01	1.0106	2	2.6E+23
109	214.88902	52.88366	0.55	1	23.31	0.02	1.07	8	3.2E+23
110	...	...	...	5	26.34	0.17	...	0	...
111	214.80271	52.89113	0.30	4	19.43	0.00	0.3794	2	3.4E+22
112	214.83429	52.89388	0.44	1	21.80	0.00	0.7328	1	1.1E+23
113	214.80697	52.89741	0.29	1	20.95	0.00	0.5365	2	1.7E+23
114	214.81906	52.89789	0.38	1	21.80	0.00	0.7788	2	3.9E+23
115	214.91071	52.90104	0.54	1	24.31	0.04	0.32	7	2.6E+22
116	215.01446	52.90132	0.32	1	19.88	0.00	0.3739	3	4.0E+22
117	214.91479	52.90558	0.47	1	20.30	0.00	0.3379	2	1.7E+22
118	214.97418	52.90606	0.42	1	24.59	0.05	2.34	7	2.2E+24
119	214.84369	52.91103	0.24	1	24.18	0.03	0.67	7	6.3E+22
120	...	...	...	5	26.55	−5	3.14	9	3.9E+24

Table 4—Continued

ID	RA <sup>a</sup>	Dec <sup>a</sup>	Offset <sup>b</sup>	Mag type <sup>c</sup>	$R$	$\pm^d$	$z$	$z$ source <sup>e</sup>	$L(3\text{ GHz})$
121	214.96053	52.91421	0.70	1	24.95	0.07	1.20	7	4.5E+23
122	215.09151	52.92012	0.50	1	24.04	0.03	0.17	7	1.0E+22
123	214.84189	52.92203	0.24	1	22.14	0.01	0.7690	2	1.8E+23
124	214.83571	52.92270	0.23	1	23.28	0.01	1.58	7	4.1E+24
125	215.13819	52.92341	0.92	4	22.15	0.01	0.64	7	7.7E+22
126	215.05429	52.92602	0.45	1	24.65	0.05	1.0369	1	7.3E+23
127	215.03931	52.93048	0.30	4	22.01	0.01	0.7400	2	1.2E+23
128	214.83380	52.93589	0.29	5	24.54	0.03	3.72	9	5.5E+24
129	214.91606	52.93748	0.35	1	22.72	0.01	0.7455	2	7.8E+22
130	215.17687	52.94209	0.63	1	23.94	0.03	0.7420	1	1.6E+23
131	215.15515	52.94245	0.37	2	22.91	0.01	1.91	7	6.8E+23
132	214.94177	52.94623	0.80	1	25.98	0.18	0.89	7	5.9E+24
133	214.95544	52.95141	0.53	1	24.59	0.05	1.2823	1	3.5E+23
134	215.19481	52.95322	0.82	1	22.87	0.01	0.7506	1	1.5E+23
135	215.00929	52.95437	0.61	4	20.12	0.00	0.3559	1	1.7E+22
136	215.07793	52.95481	0.25	1	25.34	0.10	2.28	7	1.2E+24
137	214.84325	52.95511	0.51	1	23.43	0.02	0.7680	1	1.3E+23
138	215.17437	52.95696	0.65	2	22.04	0.01	0.7451	2	2.1E+23
139	214.87089	52.95710	0.46	1	23.44	0.02	1.0352	2	5.4E+23
140	214.83225	52.95992	0.60	5	24.86	0.04	1.16	7	3.2E+23
141	215.20982	52.96297	0.32	5	23.71	0.01	3.22	7	3.8E+25
142	214.90625	52.96697	0.42	1	24.69	0.05	1.98	7	1.1E+24
143	215.13916	52.96694	0.24	1	20.82	0.00	0.5699	2	9.9E+23
144	215.18085	52.96842	0.26	1	23.76	0.02	0.7633	1	9.2E+22
145	215.19818	52.96914	0.82	4	18.53	0.00	0.2008	1	3.8E+22
146	214.95448	52.97002	0.37	1	20.43	0.00	0.3728	2	3.1E+22
147	215.13253	52.97966	0.26	2	22.65	0.01	0.7522	2	8.7E+22
148	215.16902	52.98085	0.31	1	23.86	0.03	1.16	7	3.8E+23
149	215.15522	52.98091	0.27	1	21.30	0.00	2.2723	3	1.4E+24
150	215.09835	52.98309	0.40	4	18.08	0.00	0.2006	3	8.3E+21
151	214.93100	52.98295	0.33	5	24.35	0.04	1.16	7	3.8E+23
152	214.93604	52.98331	0.77	1	23.99	0.03	3.05	7	3.8E+24
153	215.03424	52.98447	0.40	1	25.53	0.12	3.66	9	2.7E+24
154	214.98880	52.99068	0.30	1	19.78	0.00	0.2703	3	1.4E+22
155	215.22442	52.99060	0.17	1	26.18	0.21	0.94	7	1.1E+24
156	214.91272	52.99173	0.42	1	23.18	0.01	1.70	7	6.6E+23
157	215.01107	52.99266	0.35	1	23.32	0.02	1.03	7	2.3E+23
158	215.01188	52.99567	0.54	1	22.52	0.01	0.9155	1	1.5E+24
159	214.91676	52.99607	0.36	1	22.92	0.01	0.8076	2	1.4E+23
160	215.00858	52.99744	0.36	1	23.10	0.01	0.9122	2	1.6E+23

Table 4—Continued

ID	RA <sup>a</sup>	Dec <sup>a</sup>	Offset <sup>b</sup>	Mag type <sup>c</sup>	$R$	$\pm^d$	$z$	$z$ source <sup>e</sup>	$L(3\text{ GHz})$
161	...	...	...	5	26.73	–5	2.51	9	1.2E+27
162	215.23459	53.00507	0.65	1	24.24	0.04	1.12	7	3.6E+23
163	214.96715	53.00649	0.42	5	24.13	0.02	0.95	8	1.7E+23
164	215.04653	53.00897	0.47	1	23.40	0.02	1.21	7	5.5E+23
165	215.00840	53.01090	0.27	1	23.94	0.03	1.3477	1	3.4E+23
166	214.91595	53.01247	0.34	4	19.16	0.00	0.4187	2	4.4E+22
167	215.11099	53.01291	0.59	1	20.91	0.00	0.30	7	3.1E+22
168	...	...	...	5	22.69	0.01	...	0	...
169	215.06256	53.01351	0.68	1	23.50	0.02	0.9502	1	2.5E+23
170	215.16505	53.01395	0.13	4	20.22	0.00	0.3513	2	2.7E+22
171	214.92598	53.01951	0.66	5	23.74	0.02	1.1060	2	4.2E+23
172	215.02496	53.02243	0.19	4	20.70	0.00	0.4639	3	3.2E+22
173	215.20352	53.02369	0.40	1	25.51	0.12	0.92	7	1.7E+23
174	215.14670	53.03033	0.31	1	23.90	0.03	1.5737	1	6.8E+23
175	215.08475	53.03244	0.36	1	22.20	0.01	0.9551	2	1.8E+23
176	215.07640	53.03271	0.44	4	19.40	0.00	0.3557	2	2.1E+22
177	215.08982	53.03312	0.24	5	23.07	0.01	0.89	8	2.6E+23
178	214.93078	53.03503	0.27	1	23.88	0.03	1.2347	1	4.2E+23
179	215.27132	53.03544	0.42	2	21.49	0.00	0.7392	3	7.7E+24
180	215.02776	53.03647	0.44	1	24.38	0.04	2.29	7	3.5E+24
181	...	...	...	5	26.38	–5	1.87	9	7.8E+23
182	215.16208	53.04002	0.89	5	24.70	0.04	1.19	7	3.1E+23
183	215.26134	53.04024	0.42	1	23.50	0.02	1.4476	2	1.4E+24
184	215.17940	53.04078	0.35	4	19.99	0.00	0.4185	2	5.6E+22
185	215.17350	53.04156	0.34	4	19.56	0.00	0.4245	3	1.1E+23
186	...	...	...	5	26.39	0.18	1.67	7	5.6E+23
187	...	...	...	5	25.49	0.08	2.41	9	3.9E+24
188	215.33294	53.05310	0.41	1	23.62	0.02	1.2432	1	3.5E+24
189	215.01381	53.05395	0.20	1	23.86	0.03	1.1814	1	4.2E+23
190	...	...	...	5	26.66	–5	3.21	9	3.8E+24
191	...	...	...	5	26.50	0.17	2.01	4	6.6E+23
192	215.18941	53.05829	0.28	2	19.54	0.00	0.3787	3	6.9E+22
193	215.32693	53.05804	0.14	3	21.10	0.00	0.9739	2	3.2E+26
194	215.01033	53.05864	0.25	2	22.04	0.01	0.79	7	8.7E+22
195	...	...	...	5	24.30	0.04	...	0	...
196	215.13568	53.06023	0.58	5	22.83	0.01	0.52	9	3.1E+22
197	215.23866	53.06043	0.18	1	23.86	0.03	1.1882	1	9.0E+23
198	215.12247	53.06105	0.15	1	24.76	0.06	1.17	7	2.1E+23
199	214.94582	53.06187	0.24	1	24.24	0.04	0.21	7	6.3E+21
200	...	...	...	5	23.84	0.02	1.07	8	3.5E+23

Table 4—Continued

ID	RA <sup>a</sup>	Dec <sup>a</sup>	Offset <sup>b</sup>	Mag type <sup>c</sup>	$R$	$\pm^d$	$z$	$z$ source <sup>e</sup>	$L(3\text{ GHz})$
201	214.97075	53.06266	0.42	1	22.99	0.01	0.7468	2	7.3E+22
202	...	...	...	5	25.35	0.07	1.39	7	6.8E+23
203	215.04853	53.07882	0.27	1	26.10	0.20	1.45	9	5.4E+23
204	215.18198	53.07965	0.31	1	25.75	0.14	0.37	7	2.3E+22
205	...	...	...	5	26.30	−5	3.14	9	2.1E+24
206	215.11462	53.08187	0.17	1	20.99	0.00	0.9966	3	2.0E+23
207	214.99241	53.08304	0.31	1	25.72	0.14	1.12	7	5.1E+24
208	215.09743	53.08658	0.33	1	23.88	0.03	1.12	7	2.0E+23
209	...	...	...	5	26.54	0.25	...	0	...
210	215.14906	53.08930	0.17	1	23.82	0.02	0.72	7	7.4E+22
211	215.17780	53.09591	0.77	1	24.45	0.04	1.27	7	2.7E+23
212	215.22481	53.09729	0.20	1	23.74	0.02	2.89	7	4.1E+24
213	215.17149	53.09751	0.30	1	19.70	0.00	0.2729	3	1.0E+22
214	215.31956	53.10202	0.12	1	20.24	0.00	0.28	9	2.8E+22
215	215.19475	53.10413	0.26	1	21.26	0.00	0.74	7	1.0E+23
216	215.36698	53.10512	0.07	2	21.72	0.00	0.7092	2	1.1E+23
217	215.30103	53.10606	0.18	4	18.49	0.00	0.2014	2	1.7E+22
218	215.20266	53.10662	0.22	4	19.09	0.00	0.3546	2	1.9E+22
219	215.16748	53.10828	0.17	1	25.89	0.16	0.64	7	6.7E+22
220	215.22258	53.11077	0.65	5	24.74	0.08	1.49	9	1.2E+24
221	215.08026	53.11183	0.34	1	22.88	0.01	0.9765	2	1.3E+23
222E	215.25439	53.11239	0.16	2	23.11	0.02	1.2700	2	3.2E+23
222W	215.25229	53.11197	0.15	3	19.95	0.00	0.3009	3	9.9E+21
223	215.16743	53.11319	0.35	3	18.31	0.00	0.1996	3	5.5E+21
224	215.14245	53.11932	0.32	1	25.47	0.11	1.10	7	2.1E+23
225	215.40593	53.12112	0.21	1	25.61	0.13	1.12	7	4.2E+23
226	215.05226	53.12491	0.51	4	16.63	0.00	0.1157	3	4.7E+21
227	...	...	...	5	26.68	−5	0.48	9	2.9E+22
228	215.13819	53.12647	0.20	1	20.89	0.00	2.0835	3	1.0E+24
229	...	...	...	5	26.09	0.17	2.50	9	1.5E+24
230	...	...	...	5	26.68	−5	2.40	9	2.1E+24
231	215.34034	53.13180	0.13	1	22.98	0.01	1.1830	1	6.6E+23
232	215.31951	53.13517	0.28	4	20.73	0.00	0.5107	1	8.0E+22
233	215.13888	53.13923	0.07	1	21.41	0.00	0.81	7	1.9E+25
234	215.33395	53.13787	0.23	1	21.43	0.00	0.6925	1	1.4E+23
235	215.06368	53.13919	0.31	1	21.53	0.00	0.6706	2	6.2E+22
236	215.13416	53.14135	0.12	1	24.32	0.04	0.69	7	7.8E+24
237	...	...	...	5	26.56	−5	...	0	...
238	215.15292	53.15060	0.51	1	23.95	0.03	2.57	7	1.6E+24
239	215.23530	53.15283	0.04	1	21.64	0.00	0.6704	2	7.8E+22



Table 4—Continued

ID	RA <sup>a</sup>	Dec <sup>a</sup>	Offset <sup>b</sup>	Mag type <sup>c</sup>	$R$	$\pm^d$	$z$	$z$ source <sup>e</sup>	$L(3\text{ GHz})$
240	215.35505	53.15354	0.20	1	21.47	0.00	0.6910	3	6.5E+22
241	215.21492	53.15483	0.14	1	25.12	0.08	1.22	7	2.8E+23
242	215.42022	53.15682	0.22	5	22.41	0.01	...	0	...
243	215.45110	53.15891	0.10	1	24.14	0.03	1.41	9	1.3E+24
244	215.17778	53.15915	0.74	2	24.66	0.07	1.26	7	4.5E+24
245	215.40959	53.16081	0.77	1	25.88	0.16	0.60	9	5.6E+22
246	215.35657	53.16386	0.17	5	25.01	0.05	0.7099	5	1.5E+23
247	215.24316	53.16523	0.09	1	22.05	0.00	0.6863	2	8.3E+22
248	215.44895	53.17313	0.22	2	21.64	0.00	0.6787	3	3.7E+23
249	215.46436	53.17402	0.56	1	25.68	0.14	1.49	9	5.1E+23
250	...	...	...	5	26.58	-5	1.92	9	1.3E+24
251	215.42471	53.17976	0.20	1	21.64	0.00	1.4177	2	5.1E+23
252	...	...	...	5	23.64	0.02	1.46	9	7.7E+25
253	215.52238	53.18105	0.49	1	22.96	0.01	1.6004	2	6.0E+23
254	215.40781	53.18410	0.66	4	22.38	0.01	1.05	8	2.5E+23
255	215.46442	53.18499	0.34	4	19.69	0.00	0.2150	2	1.1E+22
256	215.45942	53.18580	0.29	1	25.07	0.08	1.89	9	7.8E+23
257	215.29152	53.18685	0.25	1	22.78	0.01	0.8866	2	3.7E+23
258	215.39712	53.18756	0.51	2	21.24	0.00	0.6168	2	7.4E+22
259	...	...	...	5	23.10	0.01	3.52	9	4.7E+24
260	215.50249	53.19053	0.42	1	19.95	0.00	0.5609	3	5.0E+22
261	...	...	...	5	25.02	0.05	...	0	...
262	215.15021	53.19622	0.68	4	20.63	0.00	0.5434	2	3.8E+22
263	...	...	...	5	26.78	-5	2.52	9	8.3E+24
264	215.19234	53.20324	0.44	1	25.65	0.13	1.10	8	3.4E+23
265	215.55296	53.20893	0.66	1	24.86	0.06	...	0	...
266	215.34310	53.21155	0.06	1	23.86	0.03	1.16	9	2.5E+23
267	215.51592	53.21358	0.28	1	23.72	0.02	1.03	8	2.4E+23
268	...	...	...	5	23.86	0.03	1.45	9	3.6E+23
269	215.25671	53.21699	0.20	4	19.00	0.00	0.2168	2	5.9E+21
270	215.27964	53.21738	0.41	1	25.29	0.09	2.38	9	1.5E+24
271	215.18896	53.21817	0.41	4	19.01	0.00	0.3660	1	1.6E+22
272	215.23677	53.21874	0.45	3	19.58	0.00	0.7423	2	1.2E+25
273	215.34308	53.22210	0.29	1	22.50	0.01	0.9667	2	2.1E+23
274	215.44713	53.22292	0.57	5	24.94	0.05	1.99	9	3.0E+24
275	215.49150	53.22497	0.29	1	26.36	0.26	2.98	9	1.8E+24
276	215.30912	53.22849	0.26	1	22.79	0.01	0.8858	2	3.0E+23
277	...	...	...	5	19.66	0.00	0.66	8	8.5E+22
278	...	...	...	5	25.73	0.13	2.70	9	1.6E+24
279	...	...	...	5	26.56	0.27	3.76	9	5.4E+24

Table 4—Continued

ID	RA <sup>a</sup>	Dec <sup>a</sup>	Offset <sup>b</sup>	Mag type <sup>c</sup>	$R$	$\pm^d$	$z$	$z$ source <sup>e</sup>	$L(3\text{ GHz})$
280	215.25468	53.23273	0.72	1	25.76	0.15	...	0	...
281	...	...	...	5	26.69	−5	1.05	9	2.1E+23
282	...	...	...	5	25.59	0.07	...	0	...
283	215.48345	53.24047	0.04	3	20.16	0.00	0.3874	2	1.8E+22
284	215.57158	53.24085	0.41	4	18.29	0.00	0.3028	2	2.2E+22
285	215.58507	53.24201	0.46	1	19.71	0.00	0.3575	2	3.7E+22
286	215.23916	53.24386	0.40	1	23.77	0.02	2.7256	3	2.7E+24
287	...	...	...	5	26.79	−5	...	0	...
288	215.42204	53.24733	0.26	1	25.35	0.10	1.60	9	6.9E+23
289	215.57063	53.24808	0.45	4	20.78	0.00	0.5583	3	4.4E+22
290	215.56933	53.24947	0.39	4	20.75	0.00	0.6060	2	5.2E+22
291	...	...	...	5	21.25	0.00	...	0	...
292	...	...	...	5	23.34	0.02	...	0	...
293	215.41949	53.25212	0.18	1	21.05	0.00	0.5592	2	4.9E+22
294	215.23028	53.25364	0.54	1	24.41	0.04	...	0	...
295N	215.59114	53.25456	0.91	5	22.11	0.00	0.60	8	4.8E+22
296	215.58270	53.25447	0.29	1	21.07	0.00	0.6361	2	7.5E+22
297	215.36609	53.25452	0.20	1	22.99	0.01	1.0045	2	1.2E+24
298	215.47366	53.25636	0.58	1	23.29	0.02	0.9113	2	1.3E+23
299	215.45210	53.25962	0.15	1	26.85	0.40	1.94	4	7.2E+23
300	215.38079	53.25983	0.25	4	21.65	0.01	0.6438	2	1.5E+23
301	...	...	...	5	25.54	0.07	...	0	...
302	215.57404	53.25999	0.20	1	25.01	0.07	0.69	9	1.1E+23
303	215.50609	53.26049	0.12	3	20.81	0.00	0.6367	2	3.0E+23
304	215.63143	53.26095	0.45	1	25.64	0.13	1.61	9	5.3E+23
305	215.38207	53.26232	0.38	1	23.86	0.03	1.3638	2	6.2E+23
306	215.24159	53.26246	0.64	5	24.76	0.05	...	0	...
307	215.48515	53.26398	0.24	2	22.97	0.02	1.59	9	1.3E+24
308	215.36995	53.26386	0.25	1	25.57	0.12	2.88	9	1.4E+24
309	215.41803	53.26535	0.42	1	23.77	0.02	2.31	9	1.3E+24
310	215.63955	53.26561	0.80	1	22.04	0.00	0.86	8	1.7E+23
311	215.47553	53.26853	0.11	1	23.93	0.03	1.61	9	8.5E+23
312	215.57567	53.27766	0.25	3	19.70	0.00	0.3562	3	1.8E+22
313	215.38785	53.28079	0.03	4	19.29	0.00	0.3557	3	3.7E+22
314	215.58098	53.28254	0.12	1	24.18	0.03	1.52	9	3.5E+23
315	215.49833	53.28355	0.25	1	24.77	0.06	2.19	9	1.1E+24
316	215.40512	53.28694	0.26	3	22.20	0.01	0.7422	2	7.1E+22
317	215.39220	53.28857	0.27	1	24.37	0.04	1.02	9	2.5E+23
318	215.40784	53.28927	0.18	1	21.10	0.00	0.4504	2	5.8E+22
319	...	...	...	5	26.76	0.28	...	0	...

Table 4—Continued

ID	RA <sup>a</sup>	Dec <sup>a</sup>	Offset <sup>b</sup>	Mag type <sup>c</sup>	$R$	$\pm^d$	$z$	$z$ source <sup>e</sup>	$L(3\text{ GHz})$
320	215.27858	53.29476	0.24	1	24.40	0.04	1.0861	2	1.9E+23
321	215.33431	53.29629	0.23	3	23.01	0.02	0.71	8	6.8E+22
322	215.42788	53.29833	0.21	4	19.21	0.00	0.1169	2	1.2E+21
323	...	...	...	5	25.74	0.10	1.59	9	8.9E+23
324	215.65932	53.30088	0.41	1	24.13	0.03	1.57	9	6.0E+23
325	215.41615	53.30414	0.11	1	22.92	0.01	0.67	8	5.4E+22
326	215.68772	53.30492	0.49	1	24.77	0.06	1.86	9	6.6E+23
327	...	...	...	5	25.69	0.07	...	0	...
328	215.70020	53.30785	0.06	1	25.63	0.13	...	0	...
329	215.57529	53.30925	0.15	1	23.50	0.02	1.2412	2	3.2E+23
330	215.45897	53.31072	0.21	1	21.46	0.00	0.5736	3	5.3E+22
331	215.70706	53.31087	0.71	1	21.33	0.00	0.6344	2	1.1E+23
332	215.45123	53.31306	0.18	1	24.47	0.05	2.31	9	1.4E+24
333	215.57960	53.31369	0.09	1	22.11	0.01	0.51	8	2.6E+22
334	215.71344	53.31612	0.47	1	24.42	0.04	...	0	...
335	215.48169	53.31711	0.34	2	21.07	0.00	0.52	8	6.2E+22
336	215.44585	53.31896	0.19	1	21.71	0.00	0.6684	2	5.6E+22
337	...	...	...	5	26.34	–5	...	0	...
338	...	...	...	5	26.69	–5	2.96	9	2.4E+24
339	215.43841	53.32676	0.12	1	21.49	0.00	0.6369	2	6.4E+22
340	215.72862	53.32945	0.49	1	21.61	0.00	0.55	8	6.6E+22
341	215.44261	53.32994	0.24	1	22.11	0.01	0.6882	3	6.4E+22
342	215.58272	53.33064	0.39	1	22.88	0.01	1.59	4	1.1E+24
343	215.47538	53.33082	0.24	4	18.11	0.00	0.2045	3	2.2E+22
344	215.54796	53.33083	0.32	4	19.79	0.00	0.3387	2	1.3E+22
345	215.73015	53.33411	0.40	5	26.93	0.27	...	0	...
346	215.40296	53.33444	0.19	1	22.57	0.01	0.6884	3	2.3E+23
347	215.39454	53.33458	0.14	1	20.52	0.00	0.4227	3	2.8E+22
348	215.44936	53.33458	0.36	1	23.73	0.02	0.9301	2	1.3E+23
349	215.45762	53.33484	0.19	4	17.62	0.00	0.19	9	4.2E+21
350	215.39478	53.33610	0.08	1	22.55	0.01	1.1671	2	3.2E+23
351	215.47980	53.33998	0.21	1	22.48	0.01	1.0867	2	1.9E+23
352	...	...	...	5	24.22	0.03	1.79	4	4.0E+24
353	215.60587	53.34082	0.12	2	20.06	0.00	0.4984	3	3.6E+22
354	215.61066	53.34133	0.21	2	20.96	0.00	0.53	8	5.8E+22
355	215.54494	53.34169	0.20	1	22.76	0.01	0.8359	2	7.7E+22
356	215.56626	53.34228	0.04	3	22.47	0.01	1.0057	2	1.6E+23
357	215.48602	53.34188	0.10	4	22.74	0.02	0.6694	2	5.2E+22
358W	...	...	...	5	24.61	0.04	...	0	...
359	...	...	...	5	25.41	0.07	1.80	9	1.5E+24

Table 4—Continued

ID	RA <sup>a</sup>	Dec <sup>a</sup>	Offset <sup>b</sup>	Mag type <sup>c</sup>	$R$	$\pm^d$	$z$	$z$ source <sup>e</sup>	$L(3\text{ GHz})$
360	215.44742	53.34796	0.19	1	23.85	0.03	1.1643	2	2.0E+24
361	215.40481	53.34872	0.20	1	23.15	0.01	1.48	9	9.4E+24
362	215.63723	53.35100	0.29	1	24.81	0.06	1.45	9	5.6E+23
363	215.46250	53.35126	0.43	2	21.94	0.01	0.91	8	3.2E+23
364	215.39790	53.35377	0.18	1	22.94	0.01	1.62	9	1.6E+24
365	215.76713	53.35430	0.13	1	23.67	0.02	...	0	...
366	215.70724	53.35457	0.45	1	20.80	0.00	0.6919	3	7.1E+22
367	...	...	...	5	26.64	−5	3.33	9	4.3E+24
368	215.66547	53.35766	0.48	1	22.29	0.01	0.7652	2	9.1E+22
369	215.45910	53.35776	0.23	1	18.10	0.00	0.0013	3	1.6E+17
370E	215.66751	53.36102	0.16	1	21.93	0.00	0.80	8	9.7E+22
370W	215.66619	53.36039	0.15	1	22.84	0.01	0.97	8	7.0E+22
371	215.61805	53.36096	0.07	4	21.62	0.01	0.7213	3	1.7E+23
372	215.65287	53.36228	0.24	1	21.83	0.00	0.7697	2	8.1E+22
373	215.57347	53.36317	0.17	3	20.79	0.00	0.6157	3	8.9E+22
374	215.74938	53.36459	0.26	3	22.08	0.01	0.7566	2	2.7E+23
375	215.59293	53.36648	0.21	1	19.35	0.00	0.2518	3	1.5E+22
376	215.38233	53.36675	0.91	1	22.05	0.00	0.6046	2	4.9E+22
377	...	...	...	5	23.71	0.02	...	0	...
378	215.69694	53.37276	0.19	1	19.16	0.00	0.17	8	4.3E+21
379	215.49185	53.37348	0.24	1	24.62	0.05	0.88	8	7.4E+23
380	215.76273	53.37357	0.41	1	24.50	0.05	2.68	9	2.3E+25
381	215.70760	53.37621	0.20	1	21.28	0.00	0.6153	2	5.9E+22
382	215.46148	53.37858	0.74	1	23.40	0.02	2.99	9	2.2E+24
383	215.62757	53.37910	0.15	4	19.20	0.00	0.3500	3	1.9E+22
384	215.66005	53.38090	0.24	3	20.24	0.00	0.45	8	2.8E+22
385	215.70823	53.38279	0.23	1	21.53	0.00	0.4428	3	4.6E+22
386	215.49723	53.38747	0.08	1	24.56	0.05	0.97	9	1.5E+23
387	215.77523	53.39063	0.51	1	25.75	0.15	3.00	9	1.6E+24
388	215.64063	53.39128	0.29	1	25.45	0.11	1.59	9	4.4E+23
389	...	...	...	7	20.29	0.00	0.2774	3	8.7E+21
390	215.63945	53.39396	0.05	1	24.53	0.05	2.14	9	9.8E+23
391	215.69017	53.39534	0.61	1	24.46	0.04	1.46	9	4.3E+23
392	215.83378	53.39718	0.42	1	19.05	0.00	...	0	...
393	215.46346	53.40017	0.23	1	22.66	0.01	1.00	8	1.8E+23
394	...	...	...	5	25.85	0.14	2.54	9	1.2E+24
395	215.66240	53.40412	0.55	1	24.02	0.03	1.2872	2	1.7E+24
396	215.75489	53.40535	0.31	1	21.68	0.00	0.81	9	1.4E+23
397	215.53494	53.40564	0.38	1	25.02	0.07	1.72	9	7.5E+23
398	215.52801	53.40746	0.26	1	22.60	0.01	0.7280	2	6.1E+22

Table 4—Continued

ID	RA <sup>a</sup>	Dec <sup>a</sup>	Offset <sup>b</sup>	Mag type <sup>c</sup>	$R$	$\pm^d$	$z$	$z$ source <sup>e</sup>	$L(3\text{ GHz})$
399	215.65735	53.40794	0.51	4	19.92	0.00	0.4443	3	3.2E+22
400	215.60872	53.41040	0.23	5	22.10	0.00	0.54	8	1.7E+23
401	215.75001	53.41129	0.19	3	20.16	0.00	0.5783	3	8.5E+22
402	215.47143	53.41136	0.22	1	24.60	0.05	1.90	9	1.2E+24
403	215.60596	53.41409	0.42	1	24.65	0.05	1.17	9	1.6E+24
404	215.51610	53.41423	0.14	1	23.13	0.01	1.15	9	2.7E+23
405	215.82387	53.41456	0.39	4	19.65	0.00	0.3266	2	2.0E+22
406	215.75859	53.41647	0.16	1	25.19	0.09	1.51	9	7.0E+23
407	215.59562	53.42397	0.09	1	24.46	0.04	1.26	9	9.0E+23
408	215.72037	53.42461	0.15	1	23.24	0.01	0.82	8	1.5E+23
409	...	...	...	5	23.67	0.03	...	0	...
410	215.82018	53.43298	0.36	1	24.87	0.07	1.99	9	6.7E+23
411	215.84153	53.43300	0.62	1	23.94	0.03	3.59	9	9.6E+24
412	215.48450	53.43373	0.53	4	17.08	0.00	0.1443	3	3.4E+21
413	215.65444	53.43590	0.22	1	21.08	0.00	0.5114	2	4.0E+22
414	...	...	...	6	22.05	0.00	0.50	8	3.1E+22
415	215.57220	53.43855	0.23	2	21.67	0.00	0.65	8	4.7E+22
416	215.80156	53.43990	0.24	1	22.96	0.01	1.0315	3	2.4E+23
417	215.63236	53.44001	0.08	1	23.47	0.02	3.3522	2	2.8E+24
418S	215.76183	53.44005	0.09	3	20.64	0.00	0.6155	2	3.8E+22
419	215.52416	53.44080	0.29	1	23.25	0.01	0.96	8	1.2E+23
420N	215.64518	53.44279	0.53	1	23.85	0.03	3.47	9	2.2E+24
421	...	...	...	5	26.64	−5	2.16	9	8.8E+23
422	215.64451	53.44523	0.47	1	24.05	0.03	1.14	8	1.9E+23
423	...	...	...	5	25.24	0.06	1.58	9	9.6E+23
424	...	...	...	5	21.81	0.00	0.80	8	1.4E+23
425	215.62945	53.44705	0.08	4	19.94	0.00	0.2723	2	7.1E+21
426	215.59690	53.44997	0.07	1	23.93	0.03	1.2236	2	3.3E+23
427	215.67538	53.45438	0.44	1	23.07	0.01	0.70	8	5.1E+22
428	215.83442	53.45595	0.22	1	22.72	0.01	0.8260	2	5.5E+25
429	215.71321	53.45598	0.27	1	23.87	0.03	1.2443	2	5.0E+23
430	215.76413	53.46274	0.24	1	25.51	0.12	1.57	9	4.2E+23
431	215.80268	53.46571	0.56	5	24.50	0.03	1.57	9	3.2E+25
432	215.59076	53.46628	0.25	4	21.18	0.01	0.5804	3	1.5E+23
433	...	...	...	5	19.95	0.00	0.43	8	5.6E+22
435	215.86389	53.47187	0.67	1	21.54	0.00	0.6320	3	5.3E+22
436	215.65639	53.47218	0.23	1	21.43	0.00	0.5091	2	3.3E+22
437	215.87838	53.47322	0.98	4	18.07	0.00	0.88	8	5.9E+23
438	215.92105	53.47363	0.49	3	22.09	0.01	1.02	9	5.0E+23
439	215.92032	53.47513	0.28	1	23.10	0.01	1.1387	2	2.2E+23

Table 4—Continued

ID	RA <sup>a</sup>	Dec <sup>a</sup>	Offset <sup>b</sup>	Mag type <sup>c</sup>	$R$	$\pm^d$	$z$	$z$ source <sup>e</sup>	$L(3\text{ GHz})$
440	215.62918	53.47763	0.49	1	24.78	0.06	3.03	9	2.1E+24
441	...	...	...	5	26.76	–5	1.90	9	1.2E+24
442	...	...	...	5	25.52	0.08	0.50	9	1.8E+23
443	215.54408	53.48018	0.53	1	24.89	0.07	...	0	...
444	215.91434	53.48203	0.72	1	23.11	0.01	0.90	8	1.5E+23
445	215.61519	53.48440	0.09	1	25.86	0.16	2.52	9	1.3E+24
446	...	...	...	5	25.00	0.04	...	0	...
447	...	...	...	5	22.91	0.01	0.78	8	9.5E+22
448	215.74524	53.49056	0.53	1	25.10	0.08	2.62	9	1.2E+24
449	215.66194	53.49406	0.10	1	23.92	0.03	1.78	9	1.5E+24
450	215.94968	53.49461	0.21	1	26.01	0.19	2.65	9	1.7E+24
451	...	...	...	5	23.61	0.01	...	0	...
452	215.73370	53.50071	0.23	1	20.30	0.00	0.3551	2	3.4E+22
453	215.61225	53.50132	0.14	1	20.42	0.00	0.4854	2	2.8E+22
454	215.82824	53.50285	0.92	1	23.38	0.02	0.6775	2	1.4E+23
455	215.85562	53.50313	0.16	1	24.45	0.04	2.80	9	1.5E+24
456	215.72217	53.50711	0.33	4	18.88	0.00	0.2350	2	2.1E+22
457	...	...	...	5	24.90	0.05	...	0	...
458	215.86511	53.51384	0.18	4	18.63	0.00	0.1923	3	4.0E+21
459	215.81661	53.51447	0.21	1	22.43	0.01	0.7415	3	4.8E+23
460	215.63397	53.51661	0.18	1	25.28	0.10	1.45	9	4.0E+23
461	215.85308	53.51672	0.08	2	22.10	0.01	0.7697	2	1.3E+23
462	215.95189	53.51838	0.53	1	25.29	0.10	2.58	9	1.2E+24
463	215.91188	53.52272	0.32	1	25.50	0.12	1.92	9	1.2E+24
464	...	...	...	5	23.58	0.01	0.07	9	3.3E+20
465	215.95602	53.52630	0.17	4	18.76	0.00	0.1998	2	9.7E+21
466	215.84909	53.52613	0.78	1	24.82	0.06	2.23	9	1.8E+24
467	...	...	...	5	25.05	0.05	1.10	9	3.0E+23
468	215.71940	53.53347	0.61	1	23.93	0.03	0.98	8	1.5E+23
469	216.00303	53.53359	0.40	1	22.89	0.01	0.9752	2	2.0E+23
470	215.69782	53.53416	0.22	1	24.74	0.06	1.04	8	5.4E+23
471	215.75590	53.53955	0.73	1	23.27	0.02	1.95	4	8.1E+23
472	215.96793	53.54106	0.11	3	21.13	0.00	0.63	8	6.1E+22
473	...	...	...	5	18.43	0.00	3.71	9	1.7E+25
474	215.91362	53.54543	0.23	1	23.03	0.01	1.1004	2	1.1E+24
475	215.68062	53.54641	0.33	1	20.45	0.00	0.3504	3	2.1E+22
476	215.72692	53.55115	0.19	1	22.61	0.01	0.7258	3	6.6E+22
477	...	...	...	5	26.59	–5	2.69	9	1.3E+24
478	215.86682	53.55227	0.98	1	24.89	0.07	1.74	9	5.3E+23
479	215.65193	53.55291	0.37	1	23.55	0.02	0.8921	2	1.6E+23

Table 4—Continued

ID	RA <sup>a</sup>	Dec <sup>a</sup>	Offset <sup>b</sup>	Mag type <sup>c</sup>	$R$	$\pm^d$	$z$	$z$ source <sup>e</sup>	$L(3\text{ GHz})$
480	215.75440	53.55334	0.28	1	18.23	0.00	1.8802	2	4.2E+24
481	215.64226	53.55403	0.46	1	22.03	0.00	1.5575	2	8.5E+23
482	215.94073	53.55545	0.19	1	24.89	0.07	1.59	9	1.9E+24
483	215.86266	53.55869	0.40	3	22.99	0.02	1.63	9	6.3E+23
484	...	...	...	5	20.34	0.00	0.2816	3	1.5E+22
485	...	...	...	5	26.59	–5	...	0	...
486	216.00156	53.56311	0.28	1	20.17	0.00	1.6015	2	9.3E+23
487	...	...	...	5	23.05	0.02	0.95	8	5.0E+23
489	216.00267	53.56755	0.26	1	21.64	0.00	0.7871	2	1.5E+23
490	...	...	...	5	23.91	0.03	2.26	9	1.2E+24
491	...	...	...	5	21.44	0.00	1.0107	3	2.3E+23
492	215.79935	53.57280	0.47	1	23.17	0.01	...	0	...
493	215.91069	53.57569	0.92	1	25.44	0.11	1.24	9	2.8E+23
494	...	...	...	5	18.50	0.00	1.05	9	4.5E+23
495	215.85083	53.58649	0.52	1	20.26	0.00	0.7587	2	2.2E+23
496	215.69761	53.58725	0.18	1	25.70	0.14	...	0	...
497	...	...	...	5	25.71	0.10	1.16	9	4.4E+23
498	215.92410	53.59058	0.92	1	23.89	0.03	2.08	9	6.2E+24
499	...	...	...	7	18.99	0.01	0.1915	2	1.3E+22
500	...	...	...	5	26.00	0.14	1.82	9	2.3E+24
501	...	...	...	5	...	...	0.91	8	1.1E+25
502	215.75591	53.61117	0.43	1	24.08	0.03	0.85	8	1.4E+23
503	215.75680	53.61541	0.52	4	19.96	0.00	0.5550	3	9.5E+22
504	215.88596	53.62740	0.10	5	19.57	0.00	0.1940	3	7.3E+21
505	215.85428	53.63299	0.45	2	20.83	0.00	0.4123	2	5.9E+22
506	...	...	...	5	...	...	0.19	8	1.0E+22
507	...	...	...	5	...	...	0.3535	3	2.6E+22
508	...	...	...	5	24.29	0.04	...	0	...
509	...	...	...	5	...	...	0.97	8	2.1E+23
510	...	...	...	5	...	...	0.3225	3	3.0E+22
511	...	...	...	5	...	...	...	0	...

<sup>a</sup>J2000 position of counterpart if measured independently on  $R$  image.

<sup>b</sup>Distance in arcseconds from  $R$  to IRAC position of counterpart.

<sup>c</sup>Magnitude type: 1–3 = SExtractor aperture magnitudes in 1''53, 2''14, or 3''06 radii respectively, 4 = magnitude in Kron aperture as measured by SExtractor, 5–7 = APPHOT magnitude with same aperture sizes as 1–3 respectively measured at  $R$  position if available, otherwise IRAC position.

<sup>d</sup>Magnitude uncertainties given here are statistical only, estimated from sky fluctuations. See text for discussion of systematic uncertainties. “–5” indicates magnitude given is  $5\sigma$  upper limit.

<sup>e</sup>Redshift source (in priority order if more than one redshifts exists): 1 = DEEP3 (Cooper et al. 2011, 2012), 2 = DEEP2 (Davis et al. 2003; Newman et al. 2012, <http://deep.berkeley.edu/DR3/>), 3 = MMT Hectospec (Coil et al. 2009), 4 = *Spitzer*/IRS (Huang et al. 2009, 2012a), 5 = spectroscopic redshift from Rainbow (Barro et al. 2011a), 6 = photometric redshift from NMBS (Whitaker et al. 2011), 7 = photometric redshift from CFHTLS (Coupon et al. 2009: [http://terapix.iap.fr/cplt/CFHTLS\\_deep\\_ugriz\\_T0004\\_zphot\\_1.4.tgz](http://terapix.iap.fr/cplt/CFHTLS_deep_ugriz_T0004_zphot_1.4.tgz)), 8 = photometric redshift from Huang et al. (2012b), 9 = photometric redshift from Rainbow (Barro et al. 2011a).



Table 5. IRAC Magnitudes

ID	Mag type <sup>a</sup>	3.6 $\mu\text{m}$	$\pm$	4.5 $\mu\text{m}$	$\pm$	5.8 $\mu\text{m}$	$\pm$	8.0 $\mu\text{m}$	$\pm$
001	1	21.17	0.01	21.14	0.01	21.34	0.11	21.46	0.12
003	1	19.38	0.00	19.65	0.00	19.85	0.02	20.09	0.03
004	1	21.03	0.01	20.78	0.01	20.56	0.05	20.31	0.04
005	1	21.18	0.01	20.90	0.01	20.87	0.06	21.11	0.08
006	1	21.77	0.02	21.74	0.03	21.57	0.13	21.32	0.11
007	1	21.67	0.02	21.43	0.02	21.24	0.10	20.69	0.06
008	4	18.96	0.01	19.01	0.01	19.34	0.06	18.35	0.03
009	3	18.49	0.00	19.04	0.00	19.16	0.02	19.83	0.04
010	1	19.85	0.00	19.81	0.00	20.03	0.03	19.88	0.03
011	1	20.64	0.01	20.51	0.01	20.29	0.04	20.69	0.05
012	1	21.21	0.01	21.04	0.01	20.93	0.07	21.31	0.10
013	1	20.26	0.01	20.00	0.01	20.25	0.04	20.55	0.05
014	1	20.47	0.01	20.39	0.01	20.24	0.04	20.59	0.05
015	1	19.61	0.00	19.80	0.00	19.84	0.03	19.01	0.01
016	1	19.17	0.00	19.23	0.00	19.16	0.01	18.94	0.01
017	2	18.10	0.00	18.48	0.00	18.50	0.02	18.70	0.01
018	1	22.00	0.05	21.48	0.04	20.83	0.13	20.87	0.14
019	1	20.72	0.02	20.44	0.02	20.20	0.08	20.35	0.09
020	1	19.87	0.00	19.71	0.00	19.89	0.03	20.12	0.04
021	4	19.53	0.02	19.45	0.02	19.91	0.06	19.93	0.10
022	1	21.41	0.01	21.31	0.02	20.45	0.12	20.64	0.09
023	1	20.37	0.01	20.10	0.01	20.27	0.04	20.69	0.06
024	1	19.85	0.00	19.60	0.00	19.42	0.02	19.77	0.02
025	1	18.58	0.00	19.07	0.00	19.19	0.02	19.79	0.03
026	1	20.78	0.01	20.36	0.01	19.88	0.03	19.43	0.02
027	1	20.46	0.01	20.29	0.01	20.09	0.03	20.78	0.07
028	1	19.10	0.00	19.34	0.00	19.52	0.02	17.66	0.00
029	1	20.07	0.00	19.85	0.00	19.65	0.02	19.42	0.02
030	4	18.88	0.01	19.27	0.02	19.47	0.06	19.25	0.05
031	1	20.02	0.00	19.77	0.00	19.56	0.02	19.89	0.03
032	4	17.47	0.00	17.81	0.01	17.50	0.02	15.66	0.00
033	1	22.44	0.04	22.12	0.04	21.79	0.16	22.19	0.22
034	1	19.03	0.00	18.51	0.00	18.04	0.01	17.50	0.00

Table 5—Continued

ID	Mag type <sup>a</sup>	3.6 $\mu\text{m}$	$\pm$	4.5 $\mu\text{m}$	$\pm$	5.8 $\mu\text{m}$	$\pm$	8.0 $\mu\text{m}$	$\pm$
035	1	20.52	0.01	20.34	0.01	20.16	0.04	20.43	0.05
036	4	14.82	0.00	15.28	0.00	16.07	0.01	16.30	0.00
037	1	19.04	0.00	18.64	0.00	18.17	0.01	17.67	0.00
038	1	22.17	0.03	21.92	0.03	21.74	0.16	21.52	0.13
039	1	19.94	0.00	20.15	0.01	19.84	0.03	19.57	0.02
040	1	20.01	0.00	20.16	0.01	20.52	0.05	20.38	0.04
041	1	18.76	0.00	18.61	0.00	18.92	0.01	18.65	0.01
042	1	20.12	0.00	19.80	0.00	19.80	0.02	19.73	0.02
043	1	20.80	0.01	20.53	0.01	20.32	0.04	20.59	0.05
044	1	20.74	0.01	20.50	0.01	20.67	0.06	20.70	0.06
045	1	22.65	0.05	22.28	0.04	21.68	0.14	21.51	0.11
046	1	21.24	0.01	21.00	0.01	21.03	0.08	21.18	0.09
047	1	20.16	0.01	19.90	0.01	20.16	0.11	20.02	0.09
048	4	20.70	0.04	20.49	0.04	20.27	0.15	20.45	0.25
049	1	18.85	0.00	19.24	0.00	19.14	0.01	19.42	0.02
050	3	19.17	0.00	19.61	0.01	19.67	0.04	19.98	0.05
051	3	18.54	0.00	18.89	0.00	19.15	0.02	19.80	0.04
052	1	21.68	0.03	21.34	0.03	20.86	0.14	20.93	0.17
053	3	18.16	0.00	18.19	0.00	18.51	0.01	17.43	0.01
054	1	18.56	0.00	18.53	0.00	18.87	0.01	16.96	0.00
055	1	18.61	0.00	18.37	0.00	18.67	0.01	16.94	0.00
056	1	21.17	0.02	20.85	0.01	20.77	0.09	20.95	0.08
057	3	18.46	0.00	18.57	0.00	18.96	0.04	17.27	0.01
058	1	19.76	0.00	20.11	0.01	20.14	0.03	20.11	0.03
059	1	20.22	0.01	20.11	0.01	20.24	0.05	20.50	0.06
060	1	20.66	0.01	20.31	0.01	19.87	0.03	19.62	0.02
061	2	19.40	0.00	19.21	0.00	19.43	0.03	19.67	0.03
062	1	19.45	0.00	19.49	0.00	19.75	0.02	19.78	0.02
063	1	20.63	0.01	20.35	0.01	20.17	0.04	20.66	0.06
064	1	22.48	0.04	22.34	0.04	21.99	0.18	22.11	0.20
065	1	18.86	0.00	18.63	0.00	18.12	0.01	17.55	0.01
066	1	21.10	0.01	20.95	0.01	21.24	0.10	20.72	0.06
067	1	19.26	0.00	19.52	0.00	19.38	0.02	19.00	0.01

Table 5—Continued

ID	Mag type <sup>a</sup>	3.6 $\mu\text{m}$	$\pm$	4.5 $\mu\text{m}$	$\pm$	5.8 $\mu\text{m}$	$\pm$	8.0 $\mu\text{m}$	$\pm$
068	1	19.43	0.00	19.76	0.01	19.37	0.02	19.08	0.02
069	1	20.17	0.01	19.92	0.00	19.73	0.03	20.14	0.04
070	1	18.71	0.01	18.89	0.01	19.36	0.08	19.32	0.04
071	1	19.57	0.00	19.61	0.00	19.94	0.03	20.29	0.04
072	1	19.50	0.00	19.37	0.00	19.59	0.02	19.38	0.02
073	4	17.69	0.01	17.92	0.01	18.40	0.03	18.84	0.06
074	1	19.16	0.00	19.39	0.00	19.47	0.03	19.63	0.03
075	1	21.09	0.01	20.97	0.01	20.34	0.04	19.23	0.02
076	1	21.16	0.01	20.83	0.01	20.22	0.04	20.58	0.06
077	1	20.02	0.00	20.23	0.01	20.65	0.06	21.10	0.09
078	4	18.45	0.01	18.55	0.01	18.83	0.03	17.91	0.02
079	1	18.69	0.00	19.09	0.00	19.21	0.01	19.57	0.02
080	1	18.80	0.00	18.76	0.00	19.04	0.01	18.84	0.01
081	1	19.20	0.00	19.11	0.00	19.21	0.02	18.87	0.01
082	1	19.53	0.00	19.21	0.00	19.10	0.01	19.17	0.01
083	4	17.83	0.01	18.11	0.01	18.37	0.02	18.34	0.03
084	1	18.72	0.00	18.82	0.00	19.03	0.01	18.26	0.01
085	2	19.22	0.00	19.29	0.00	19.33	0.02	18.46	0.01
086	1	19.45	0.00	19.80	0.00	19.76	0.02	19.89	0.03
087	1	19.51	0.00	19.42	0.00	19.49	0.02	19.16	0.01
088	1	22.98	0.06	22.56	0.05	22.01	0.19	21.84	0.16
089	1	18.66	0.00	18.98	0.00	18.73	0.01	18.79	0.01
090	1	21.14	0.01	20.95	0.01	20.59	0.06	20.73	0.06
091	1	18.67	0.00	19.20	0.00	19.36	0.02	19.83	0.03
092	2	20.20	0.01	19.87	0.01	19.64	0.03	18.71	0.01
093	1	21.31	0.02	20.99	0.01	20.87	0.07	21.55	0.13
094	4	18.27	0.01	18.70	0.02	18.79	0.10	19.12	0.12
095	2	19.25	0.00	19.39	0.00	19.63	0.03	17.75	0.00
096	1	22.24	0.03	21.94	0.03	21.52	0.13	21.38	0.11
097	1	21.59	0.02	21.35	0.02	21.02	0.08	21.35	0.10
098	1	20.52	0.01	20.30	0.01	20.57	0.11	21.03	0.12
099	4	15.81	0.00	16.20	0.00	16.57	0.01	15.45	0.01
100	2	18.17	0.00	18.19	0.00	18.51	0.01	17.16	0.00

Table 5—Continued

ID	Mag type <sup>a</sup>	3.6 $\mu\text{m}$	$\pm$	4.5 $\mu\text{m}$	$\pm$	5.8 $\mu\text{m}$	$\pm$	8.0 $\mu\text{m}$	$\pm$
101	1	18.34	0.00	18.46	0.00	18.85	0.01	17.74	0.00
102	1	18.62	0.00	18.49	0.00	17.79	0.00	17.26	0.00
103	2	19.10	0.00	19.32	0.00	19.42	0.02	19.16	0.02
104	1	20.45	0.01	20.30	0.01	20.25	0.04	20.69	0.06
105E	1	19.13	0.00	19.56	0.00	19.46	0.02	19.66	0.02
105W	1	21.23	0.01	21.07	0.01	20.82	0.06	20.44	0.04
106	1	19.87	0.00	19.62	0.00	19.72	0.02	20.03	0.03
107	1	23.93	0.10	22.90	0.05	22.05	0.19	20.86	0.06
108	1	19.36	0.00	19.46	0.00	19.74	0.02	19.57	0.02
109	1	19.33	0.00	19.59	0.00	20.00	0.03	20.41	0.04
110	1	22.34	0.02	22.02	0.03	21.71	0.13	21.31	0.08
111	4	18.28	0.01	18.52	0.01	18.95	0.07	19.25	0.10
112	1	18.84	0.00	19.39	0.00	19.57	0.02	20.18	0.04
113	1	18.90	0.00	18.84	0.00	18.44	0.01	17.98	0.00
114	1	18.94	0.00	19.32	0.00	19.33	0.02	19.18	0.01
115	1	20.75	0.01	20.46	0.01	20.01	0.03	20.18	0.03
116	1	18.61	0.00	18.58	0.00	18.83	0.01	17.52	0.00
117	1	19.07	0.00	19.17	0.00	19.48	0.02	18.52	0.01
118	1	20.68	0.01	20.27	0.01	19.55	0.02	18.90	0.01
119	1	20.33	0.01	20.02	0.01	19.66	0.02	19.77	0.03
120	1	21.04	0.01	20.73	0.01	20.40	0.04	20.38	0.05
121	1	21.37	0.02	21.24	0.02	21.49	0.12	21.14	0.09
122	1	21.11	0.01	20.72	0.01	19.58	0.02	18.06	0.01
123	1	19.02	0.00	19.37	0.00	19.28	0.02	19.13	0.01
124	1	20.64	0.01	20.49	0.01	19.97	0.03	19.92	0.03
125	4	19.35	0.02	19.60	0.02	19.36	0.09	19.61	0.11
126	1	19.84	0.00	19.81	0.00	19.68	0.02	19.08	0.01
127	4	19.16	0.02	19.65	0.04	20.02	0.11	20.88	0.16
128	1	21.90	0.03	21.39	0.02	20.98	0.08	20.55	0.05
129	1	19.55	0.00	19.68	0.00	19.41	0.02	19.02	0.01
130	1	20.31	0.01	20.62	0.02	20.75	0.10	20.75	0.11
131	2	20.39	0.01	20.15	0.01	20.05	0.04	20.32	0.06
132	1	20.59	0.01	20.37	0.01	20.16	0.04	20.55	0.05

Table 5—Continued

ID	Mag type <sup>a</sup>	3.6 $\mu\text{m}$	$\pm$	4.5 $\mu\text{m}$	$\pm$	5.8 $\mu\text{m}$	$\pm$	8.0 $\mu\text{m}$	$\pm$
133	1	19.87	0.00	20.00	0.01	20.37	0.04	20.66	0.05
134	1	19.54	0.00	0.00	0.00	20.07	0.05	20.50	0.08
135	4	18.19	0.01	18.28	0.01	18.52	0.05	17.94	0.03
136	1	22.45	0.04	22.26	0.04	22.35	0.27	22.01	0.19
137	1	19.43	0.00	19.83	0.01	19.96	0.04	20.11	0.04
138	2	18.96	0.00	19.43	0.01	19.59	0.03	20.15	0.05
139	1	20.30	0.01	20.46	0.01	20.66	0.06	20.06	0.03
140	1	19.51	0.01	19.52	0.00	19.84	0.05	19.88	0.03
141	1	20.10	0.01	19.73	0.01	19.29	0.03	18.88	0.02
142	1	22.12	0.03	21.80	0.03	21.49	0.13	20.89	0.07
143	1	18.52	0.00	18.94	0.00	19.11	0.01	19.80	0.03
144	1	19.67	0.00	19.95	0.01	19.75	0.03	19.87	0.03
145	4	17.39	0.01	17.40	0.01	17.42	0.02	16.81	0.01
146	1	18.70	0.00	18.65	0.00	18.87	0.01	17.55	0.00
147	2	19.59	0.00	19.91	0.01	19.84	0.03	20.01	0.04
148	1	19.88	0.00	19.48	0.00	18.74	0.01	18.10	0.01
149	1	20.43	0.01	20.03	0.01	19.48	0.02	19.13	0.01
150	4	17.40	0.00	17.57	0.01	17.85	0.02	15.94	0.01
151	1	19.90	0.00	19.80	0.00	20.06	0.03	19.96	0.03
152	1	21.53	0.02	21.28	0.02	21.01	0.08	20.17	0.04
153	1	22.94	0.05	23.40	0.11	23.19	0.51	22.41	0.24
154	1	19.20	0.00	19.13	0.00	19.41	0.02	17.68	0.00
155	1	21.24	0.02	21.13	0.02	21.28	0.12	21.68	0.18
156	1	21.22	0.01	20.62	0.01	19.66	0.02	18.79	0.01
157	1	19.14	0.00	19.01	0.00	19.24	0.02	19.42	0.02
158	1	18.81	0.00	19.20	0.00	19.35	0.02	19.50	0.02
159	1	20.12	0.01	20.39	0.01	20.42	0.05	20.58	0.05
160	1	19.41	0.00	19.76	0.00	19.99	0.03	20.28	0.04
161	1	20.94	0.01	20.63	0.01	20.44	0.05	20.65	0.06
162	1	21.13	0.01	20.89	0.01	20.70	0.07	20.86	0.08
163	1	20.81	0.01	20.64	0.01	20.30	0.04	20.38	0.05
164	1	19.49	0.00	19.44	0.00	19.71	0.02	19.70	0.02
165	1	19.93	0.00	19.76	0.00	19.94	0.03	19.95	0.03

Table 5—Continued

ID	Mag type <sup>a</sup>	3.6 $\mu\text{m}$	$\pm$	4.5 $\mu\text{m}$	$\pm$	5.8 $\mu\text{m}$	$\pm$	8.0 $\mu\text{m}$	$\pm$
166	4	18.08	0.01	18.18	0.01	18.52	0.05	17.40	0.03
167	1	19.02	0.00	18.92	0.00	19.06	0.01	17.54	0.00
168	1	19.20	0.00	19.22	0.00	18.92	0.01	19.23	0.02
169	1	20.07	0.00	20.10	0.01	20.14	0.04	20.22	0.04
170	4	18.55	0.01	18.52	0.01	18.88	0.04	17.60	0.01
171	1	18.91	0.00	19.24	0.00	19.47	0.03	19.80	0.03
172	4	18.91	0.01	18.95	0.01	19.07	0.07	18.39	0.04
173	1	20.32	0.01	20.15	0.01	20.39	0.04	20.81	0.06
174	1	19.19	0.00	19.11	0.00	19.40	0.02	19.84	0.03
175	1	19.20	0.00	19.42	0.00	19.34	0.02	19.09	0.01
176	4	18.43	0.01	18.71	0.01	19.16	0.07	19.24	0.09
177	1	19.23	0.00	19.25	0.00	19.19	0.01	19.60	0.02
178	1	19.94	0.01	20.05	0.01	20.14	0.07	20.29	0.06
179	2	18.48	0.00	19.03	0.00	19.14	0.02	19.75	0.03
180	1	21.38	0.02	21.23	0.02	21.07	0.08	21.02	0.08
181	1	21.94	0.02	21.58	0.02	21.18	0.09	21.67	0.13
182	1	20.03	0.00	19.78	0.00	19.80	0.03	20.20	0.04
183	1	19.34	0.00	19.25	0.00	19.34	0.02	19.27	0.02
184	4	18.69	0.01	18.65	0.01	18.86	0.04	17.76	0.02
185	4	18.24	0.01	18.16	0.01	18.38	0.02	17.04	0.01
186	1	20.17	0.00	19.98	0.00	20.09	0.03	20.29	0.04
187	1	19.96	0.00	19.52	0.00	19.49	0.02	19.71	0.02
188	1	19.43	0.00	19.46	0.01	19.71	0.04	20.10	0.06
189	1	20.16	0.00	20.14	0.01	20.38	0.04	20.29	0.04
190	1	22.36	0.04	21.84	0.03	21.37	0.11	20.98	0.07
191	1	21.52	0.02	21.12	0.02	20.71	0.08	20.77	0.07
192	2	18.36	0.00	18.54	0.00	18.93	0.01	19.44	0.02
193	3	18.53	0.00	18.79	0.00	19.03	0.03	18.72	0.02
194	2	18.53	0.00	18.95	0.00	18.96	0.01	19.28	0.02
195	1	20.61	0.01	20.31	0.01	20.24	0.04	19.91	0.03
196	1	20.23	0.00	20.26	0.01	19.99	0.03	18.98	0.01
197	1	19.60	0.00	19.76	0.00	20.25	0.04	20.41	0.05
198	1	20.42	0.01	20.32	0.01	20.57	0.05	20.48	0.05

Table 5—Continued

ID	Mag type <sup>a</sup>	3.6 $\mu\text{m}$	$\pm$	4.5 $\mu\text{m}$	$\pm$	5.8 $\mu\text{m}$	$\pm$	8.0 $\mu\text{m}$	$\pm$
199	1	20.37	0.01	19.95	0.01	19.57	0.07	19.70	0.05
200	1	19.54	0.00	19.57	0.00	19.67	0.02	19.15	0.01
201	1	19.90	0.01	20.17	0.01	20.31	0.07	20.36	0.06
202	1	19.41	0.00	19.20	0.01	19.38	0.03	19.94	0.08
203	1	20.04	0.00	19.81	0.00	19.59	0.02	18.91	0.01
204	1	21.04	0.01	20.72	0.01	20.36	0.04	20.45	0.05
205	1	21.62	0.02	21.34	0.02	21.25	0.10	21.10	0.09
206	1	18.93	0.00	18.67	0.00	18.21	0.01	17.72	0.00
207	1	21.04	0.02	20.85	0.02	21.00	0.17	21.01	0.12
208	1	19.17	0.00	19.33	0.00	19.49	0.02	19.30	0.02
209	1	21.65	0.02	21.11	0.02	20.48	0.05	19.46	0.02
210	1	20.14	0.00	20.47	0.01	20.48	0.05	20.58	0.05
211	1	19.31	0.00	19.09	0.00	18.94	0.01	19.11	0.01
212	1	22.02	0.03	21.81	0.03	21.57	0.13	21.82	0.16
213	1	19.16	0.00	19.12	0.00	19.44	0.02	17.75	0.00
214	1	17.95	0.00	17.47	0.00	17.04	0.00	16.66	0.00
215	1	18.38	0.00	18.83	0.00	18.74	0.01	19.04	0.01
216	2	18.45	0.00	18.94	0.00	18.90	0.01	19.23	0.02
217	4	17.72	0.00	17.87	0.00	18.17	0.02	16.39	0.01
218	4	17.96	0.01	18.24	0.02	18.67	0.10	19.23	0.14
219	1	21.23	0.01	20.86	0.01	20.42	0.05	20.46	0.05
220	1	19.95	0.00	19.96	0.00	20.18	0.04	20.02	0.03
221	1	19.31	0.00	19.61	0.00	19.90	0.03	20.35	0.04
222E	2	19.45	0.00	19.54	0.00	19.89	0.03	19.62	0.02
222W	3	18.89	0.00	18.91	0.00	19.26	0.02	17.96	0.01
223	3	17.24	0.00	17.50	0.00	17.96	0.01	16.65	0.00
224	1	20.75	0.01	20.49	0.01	20.27	0.04	20.66	0.06
225	1	22.61	0.06	22.47	0.06	22.27	0.26	22.27	0.29
226	4	15.94	0.01	16.25	0.01	16.55	0.03	14.99	0.01
227	1	22.42	0.04	22.02	0.03	21.47	0.12	21.39	0.11
228	1	20.53	0.01	20.22	0.01	19.56	0.02	18.75	0.01
229	1	22.45	0.04	22.05	0.04	21.60	0.13	20.32	0.04
230	1	22.51	0.04	22.18	0.04	21.67	0.14	20.59	0.05

Table 5—Continued

ID	Mag type <sup>a</sup>	3.6 $\mu\text{m}$	$\pm$	4.5 $\mu\text{m}$	$\pm$	5.8 $\mu\text{m}$	$\pm$	8.0 $\mu\text{m}$	$\pm$
231	1	19.60	0.00	19.77	0.00	20.16	0.04	19.81	0.03
232	4	18.38	0.01	18.63	0.01	18.75	0.03	18.16	0.02
233	1	18.15	0.00	18.68	0.00	18.78	0.01	19.32	0.02
234	1	19.27	0.00	19.72	0.00	19.62	0.02	19.84	0.03
235	1	18.91	0.00	19.35	0.00	19.58	0.05	20.14	0.06
236	1	20.73	0.01	21.14	0.01	21.47	0.13	21.53	0.13
237	1	21.57	0.04	21.09	0.04	21.12	0.26	20.45	0.13
238	1	21.53	0.02	21.49	0.02	21.00	0.08	20.45	0.05
239	1	19.27	0.00	19.67	0.00	19.58	0.02	19.75	0.02
240	1	19.06	0.00	19.49	0.00	19.27	0.02	19.49	0.02
241	1	19.69	0.00	19.26	0.00	18.94	0.01	18.57	0.01
242	1	20.36	0.01	20.63	0.01	20.44	0.05	20.53	0.05
243	1	20.37	0.01	20.29	0.01	20.49	0.05	20.86	0.08
244	2	20.13	0.01	20.04	0.01	19.85	0.03	20.07	0.04
245	1	21.15	0.01	20.73	0.01	20.16	0.04	20.14	0.04
246	1	21.78	0.02	21.54	0.02	21.13	0.09	21.26	0.10
247	1	20.28	0.01	20.38	0.01	19.85	0.03	19.41	0.02
248	2	19.16	0.00	19.68	0.01	19.81	0.03	20.42	0.06
249	1	20.13	0.01	20.02	0.01	20.19	0.04	20.14	0.04
250	1	23.22	0.09	22.95	0.08	23.04	0.47	...	...
251	1	19.33	0.00	19.14	0.00	19.14	0.01	19.03	0.01
252	1	19.17	0.00	19.18	0.00	19.52	0.02	19.91	0.03
253	1	19.85	0.01	19.55	0.01	19.32	0.03	18.97	0.03
254	4	18.08	0.01	18.33	0.01	18.65	0.04	19.14	0.06
255	4	18.39	0.01	18.43	0.01	18.72	0.03	16.52	0.01
256	1	20.86	0.01	20.72	0.01	20.68	0.06	21.23	0.10
257	1	19.32	0.00	19.72	0.00	20.03	0.03	20.64	0.06
258	2	18.61	0.00	19.07	0.00	19.24	0.02	19.94	0.03
259	1	19.67	0.00	19.60	0.00	19.61	0.02	19.56	0.02
260	1	18.22	0.00	18.58	0.00	18.78	0.01	19.36	0.02
261	1	20.41	0.01	20.01	0.01	20.04	0.04	20.19	0.04
262	4	19.75	0.05	19.85	0.04	19.40	0.31	19.56	0.14
263	1	22.07	0.03	21.73	0.03	21.26	0.12	21.24	0.11



Table 5—Continued

ID	Mag type <sup>a</sup>	3.6 $\mu\text{m}$	$\pm$	4.5 $\mu\text{m}$	$\pm$	5.8 $\mu\text{m}$	$\pm$	8.0 $\mu\text{m}$	$\pm$
264	1	20.88	0.01	20.88	0.01	20.62	0.07	19.83	0.03
265	1	20.08	0.01	20.05	0.01	20.18	0.07	20.13	0.07
266	1	19.49	0.00	19.58	0.00	19.99	0.03	20.11	0.03
267	1	19.34	0.00	19.51	0.00	19.79	0.02	20.03	0.04
268	1	20.22	0.01	20.04	0.01	20.09	0.03	20.39	0.04
269	4	18.25	0.01	18.38	0.01	18.61	0.05	16.83	0.01
270	1	20.91	0.01	20.73	0.01	20.65	0.06	20.96	0.08
271	4	18.09	0.01	18.27	0.01	18.58	0.09	18.25	0.07
272	3	17.43	0.00	17.93	0.00	17.99	0.01	18.41	0.01
273	1	19.43	0.00	19.46	0.00	19.16	0.01	18.56	0.01
274	1	21.50	0.02	21.17	0.01	21.02	0.08	21.24	0.10
275	1	21.25	0.01	20.89	0.01	20.59	0.05	20.78	0.06
276	1	19.94	0.00	20.18	0.01	20.05	0.03	19.43	0.02
277	1	18.66	0.00	19.08	0.00	19.10	0.01	19.30	0.02
278	1	20.68	0.01	20.35	0.01	20.25	0.04	20.31	0.04
279	1	21.16	0.01	20.84	0.01	20.69	0.06	20.92	0.07
280	1	21.75	0.02	21.51	0.02	21.02	0.08	20.43	0.05
281	1	21.69	0.02	21.12	0.01	20.68	0.06	20.55	0.05
282	1	21.08	0.02	20.92	0.02	20.97	0.14	21.03	0.17
283	3	18.91	0.00	19.13	0.00	19.45	0.03	19.22	0.03
284	4	17.54	0.01	17.62	0.01	18.02	0.04	16.82	0.02
285	1	18.43	0.00	18.41	0.00	18.77	0.01	17.58	0.00
286	1	20.44	0.01	19.73	0.01	19.15	0.02	18.12	0.01
287	1	22.06	0.05	21.57	0.05	21.12	0.18	21.49	0.23
288	1	19.69	0.00	19.36	0.00	19.30	0.02	19.37	0.02
289	4	19.75	0.03	19.92	0.04	20.02	0.10	19.67	0.12
290	4	18.74	0.01	19.06	0.01	18.95	0.04	18.74	0.05
291	1	19.76	0.00	19.88	0.00	0.00	0.00	19.40	0.02
292	1	19.04	0.00	19.06	0.00	19.54	0.02	19.49	0.02
293	1	19.65	0.00	19.90	0.00	19.65	0.02	19.57	0.02
294	1	20.04	0.01	19.87	0.01	19.83	0.06	20.20	0.06
295N	1	19.65	0.00	19.82	0.01	19.81	0.03	19.93	0.03
296	1	17.68	0.00	17.47	0.00	17.14	0.00	16.91	0.00

Table 5—Continued

ID	Mag type <sup>a</sup>	3.6 $\mu\text{m}$	$\pm$	4.5 $\mu\text{m}$	$\pm$	5.8 $\mu\text{m}$	$\pm$	8.0 $\mu\text{m}$	$\pm$
297	1	18.81	0.00	19.12	0.00	19.46	0.02	19.90	0.03
298	1	19.58	0.00	19.55	0.00	19.61	0.02	19.57	0.02
299	1	20.31	0.01	19.92	0.00	19.70	0.02	19.98	0.03
300	4	19.35	0.01	19.54	0.01	19.03	0.06	18.91	0.07
301	1	20.76	0.02	20.51	0.02	20.41	0.13	20.67	0.20
302	1	20.24	0.01	19.92	0.00	19.79	0.03	19.77	0.03
303	3	18.43	0.00	18.93	0.00	19.15	0.02	19.83	0.05
304	1	20.45	0.01	20.32	0.01	20.58	0.09	20.85	0.15
305	1	19.91	0.00	19.82	0.00	19.93	0.03	19.88	0.03
306	1	20.61	0.02	20.43	0.01	20.56	0.10	20.76	0.10
307	2	19.57	0.00	19.37	0.00	19.35	0.02	19.41	0.02
308	1	20.60	0.01	20.25	0.01	19.93	0.03	20.00	0.03
309	1	21.05	0.01	20.78	0.01	20.41	0.05	20.56	0.05
310	1	18.79	0.00	19.01	0.00	19.06	0.03	19.19	0.03
311	1	20.55	0.01	20.25	0.01	20.17	0.03	20.47	0.05
312	3	18.05	0.00	17.96	0.00	17.80	0.01	17.27	0.00
313	4	18.15	0.01	18.15	0.01	18.49	0.03	17.22	0.01
314	1	19.42	0.00	19.31	0.00	19.59	0.02	19.57	0.02
315	1	20.68	0.01	20.40	0.01	20.20	0.03	20.42	0.04
316	3	19.66	0.01	20.01	0.01	19.71	0.04	19.71	0.04
317	1	19.96	0.00	20.27	0.01	20.56	0.05	20.94	0.07
318	1	19.06	0.00	19.26	0.00	19.25	0.02	18.48	0.01
319	1	23.06	0.07	22.46	0.05	22.16	0.21	21.34	0.11
320	1	19.89	0.01	20.10	0.01	20.10	0.10	19.98	0.07
321	3	19.36	0.01	19.69	0.01	19.47	0.04	19.67	0.04
322	4	19.24	0.01	19.62	0.02	19.91	0.06	18.38	0.02
323	1	20.03	0.01	20.06	0.01	0.00	0.00	20.32	0.07
324	1	19.19	0.00	19.19	0.00	19.41	0.02	19.70	0.03
325	1	19.41	0.00	19.80	0.00	19.61	0.02	19.86	0.03
326	1	19.95	0.01	19.71	0.01	19.65	0.03	20.10	0.06
327	1	20.85	0.01	20.72	0.01	20.96	0.11	21.58	0.15
328	1	20.00	0.01	19.84	0.01	19.84	0.06	20.35	0.09
329	1	19.28	0.00	19.30	0.00	19.58	0.02	19.58	0.02

Table 5—Continued

ID	Mag type <sup>a</sup>	3.6 $\mu\text{m}$	$\pm$	4.5 $\mu\text{m}$	$\pm$	5.8 $\mu\text{m}$	$\pm$	8.0 $\mu\text{m}$	$\pm$
330	1	18.93	0.00	19.32	0.00	19.40	0.02	19.71	0.02
331	1	17.52	0.00	17.29	0.00	16.86	0.00	16.60	0.00
332	1	19.44	0.00	19.28	0.00	19.11	0.01	18.71	0.01
333	1	19.57	0.00	19.77	0.00	19.86	0.03	19.23	0.02
334	1	19.94	0.01	19.80	0.01	19.96	0.07	19.90	0.08
335	2	18.55	0.00	18.88	0.00	18.68	0.01	18.80	0.01
336	1	19.89	0.00	20.21	0.01	19.83	0.03	19.95	0.03
337	1	21.99	0.03	21.60	0.02	21.14	0.09	20.99	0.08
338	1	21.94	0.04	21.50	0.04	21.10	0.13	20.88	0.14
339	1	19.04	0.00	19.40	0.00	19.23	0.01	19.38	0.02
340	1	19.37	0.00	19.62	0.01	19.44	0.04	19.58	0.05
341	1	19.33	0.00	19.74	0.00	19.55	0.02	19.73	0.02
342	1	19.11	0.00	18.83	0.00	18.82	0.01	18.85	0.01
343	4	17.31	0.00	17.43	0.01	17.73	0.02	15.68	0.01
344	4	18.77	0.01	18.85	0.01	19.13	0.05	18.17	0.03
345	1	22.49	0.05	22.04	0.06	21.48	0.19	21.27	0.21
346	1	19.09	0.00	19.50	0.00	19.55	0.02	19.81	0.03
347	1	19.79	0.00	19.73	0.00	19.89	0.03	18.76	0.01
348	1	19.79	0.00	19.93	0.00	20.00	0.03	20.01	0.03
349	4	16.97	0.01	17.20	0.01	17.96	0.03	18.42	0.04
350	1	19.15	0.00	19.22	0.00	19.58	0.02	19.41	0.02
351	1	19.12	0.00	19.34	0.00	19.67	0.02	19.72	0.02
352	1	19.30	0.00	19.07	0.00	19.07	0.01	19.43	0.02
353	2	18.37	0.00	18.57	0.00	18.73	0.01	18.19	0.01
354	2	19.48	0.00	19.76	0.01	0.00	0.00	19.74	0.03
355	1	19.97	0.00	20.32	0.01	20.10	0.03	20.33	0.04
356	3	19.47	0.01	19.73	0.01	19.91	0.04	19.79	0.04
357	4	19.84	0.02	20.15	0.03	20.08	0.07	20.23	0.11
358W	1	20.33	0.01	20.01	0.01	19.91	0.03	20.06	0.03
359	1	22.29	0.05	21.92	0.05	21.42	0.15	20.70	0.08
360	1	20.86	0.01	21.06	0.01	21.43	0.11	21.83	0.17
361	1	19.16	0.00	19.08	0.00	19.24	0.02	19.67	0.02
362	1	19.72	0.00	19.55	0.00	19.76	0.02	19.81	0.03

Table 5—Continued

ID	Mag type <sup>a</sup>	3.6 $\mu\text{m}$	$\pm$	4.5 $\mu\text{m}$	$\pm$	5.8 $\mu\text{m}$	$\pm$	8.0 $\mu\text{m}$	$\pm$
363	1	18.53	0.00	18.76	0.00	19.01	0.01	18.91	0.01
364	1	19.83	0.01	19.69	0.00	19.69	0.03	19.40	0.02
365	1	20.04	0.01	19.87	0.01	19.51	0.04	19.09	0.03
366	1	18.39	0.00	18.89	0.00	18.74	0.01	19.09	0.01
367	1	21.73	0.02	21.40	0.02	21.13	0.09	21.17	0.09
368	1	18.72	0.00	19.23	0.00	19.37	0.02	20.03	0.03
369	1	17.15	0.00	17.64	0.00	18.00	0.00	18.54	0.01
370E	1	18.51	0.00	19.03	0.00	19.21	0.02	19.72	0.02
370W	1	19.51	0.00	19.83	0.00	19.99	0.03	20.16	0.03
371	4	18.42	0.01	18.83	0.01	18.82	0.06	19.01	0.06
372	1	18.98	0.00	19.27	0.00	19.19	0.01	19.34	0.02
373	3	18.07	0.00	18.56	0.00	18.70	0.01	19.26	0.02
374	3	18.52	0.00	18.86	0.00	18.90	0.02	18.74	0.02
375	1	18.49	0.00	18.42	0.00	18.78	0.01	17.02	0.00
376	1	19.69	0.01	19.83	0.01	19.61	0.06	19.62	0.04
377	1	19.84	0.00	19.69	0.00	19.46	0.07	19.60	0.05
378	1	18.92	0.00	19.26	0.00	19.21	0.02	17.02	0.00
379	1	20.53	0.01	20.85	0.01	21.33	0.11	21.84	0.15
380	1	19.70	0.00	19.29	0.00	19.07	0.02	18.65	0.01
381	1	19.27	0.00	19.63	0.00	19.41	0.02	19.48	0.02
382	1	21.64	0.02	21.39	0.02	21.11	0.08	20.60	0.05
383	4	17.83	0.01	17.96	0.01	18.34	0.04	17.81	0.02
384	3	18.87	0.00	19.04	0.00	19.15	0.02	18.43	0.01
385	1	19.11	0.00	19.08	0.00	19.23	0.02	17.88	0.00
386	1	20.17	0.01	19.70	0.00	19.29	0.02	18.85	0.01
387	1	21.40	0.02	21.00	0.02	20.61	0.06	20.60	0.06
388	1	19.86	0.00	19.70	0.00	19.90	0.03	19.93	0.03
389	3	19.28	0.00	19.36	0.01	19.70	0.04	18.45	0.01
390	1	20.24	0.00	19.97	0.00	19.79	0.02	20.19	0.03
391	1	19.91	0.00	19.74	0.00	19.89	0.03	19.87	0.03
392	1	17.72	0.00	18.17	0.00	18.49	0.02	19.11	0.03
393	1	18.76	0.00	19.04	0.00	19.33	0.02	19.45	0.02
394	1	21.45	0.02	21.17	0.02	20.76	0.07	21.04	0.08

Table 5—Continued

ID	Mag type <sup>a</sup>	3.6 $\mu\text{m}$	$\pm$	4.5 $\mu\text{m}$	$\pm$	5.8 $\mu\text{m}$	$\pm$	8.0 $\mu\text{m}$	$\pm$
395	1	19.31	0.00	19.13	0.00	19.19	0.01	18.95	0.01
396	1	19.12	0.00	19.47	0.00	19.43	0.02	19.20	0.02
397	1	20.16	0.01	20.11	0.01	20.22	0.04	20.53	0.05
398	1	19.48	0.00	19.85	0.00	19.63	0.02	19.90	0.03
399	4	17.88	0.01	18.10	0.01	18.34	0.03	17.95	0.04
400	1	18.88	0.00	19.02	0.00	19.44	0.02	19.62	0.02
401	3	18.08	0.00	18.45	0.00	18.39	0.01	18.61	0.01
402	1	21.86	0.03	21.56	0.03	21.11	0.12	20.45	0.06
403	1	19.56	0.00	19.71	0.00	20.09	0.04	0.00	0.00
404	1	19.53	0.00	19.19	0.00	18.94	0.01	18.87	0.01
405	4	18.35	0.01	18.42	0.01	18.65	0.04	17.43	0.02
406	1	20.79	0.01	20.63	0.01	20.76	0.06	20.81	0.07
407	1	19.78	0.00	19.72	0.00	19.94	0.03	19.97	0.03
408	1	19.45	0.00	19.74	0.00	19.72	0.02	19.55	0.02
409	1	20.24	0.02	19.98	0.01	19.57	0.04	20.01	0.05
410	1	20.20	0.01	19.93	0.01	19.84	0.03	19.75	0.03
411	1	21.19	0.01	20.78	0.01	20.35	0.05	20.17	0.04
412	4	16.67	0.01	16.94	0.01	17.51	0.03	16.86	0.02
413	1	19.33	0.00	19.40	0.00	18.60	0.01	17.51	0.00
414	2	20.71	0.02	20.44	0.02	19.94	0.08	19.03	0.02
415	2	18.92	0.00	19.27	0.00	19.28	0.02	19.40	0.02
416	1	19.95	0.00	20.17	0.01	20.27	0.04	19.90	0.03
417	1	21.83	0.02	21.22	0.02	20.41	0.04	19.51	0.02
418S	3	18.85	0.00	19.20	0.01	19.18	0.02	19.34	0.03
419	1	19.47	0.01	19.79	0.01	20.12	0.07	20.51	0.08
420N	1	22.03	0.03	21.90	0.03	21.91	0.18	21.64	0.14
421	1	23.18	0.06	22.69	0.05	22.11	0.19	21.30	0.09
422	1	19.61	0.00	19.67	0.00	20.00	0.03	20.23	0.04
423	1	20.13	0.00	20.00	0.01	20.25	0.04	20.74	0.06
424	1	19.61	0.00	19.14	0.00	18.68	0.01	18.38	0.01
425	4	19.10	0.01	19.11	0.01	19.61	0.06	17.94	0.02
426	1	19.54	0.00	19.47	0.00	19.79	0.03	19.73	0.02
427	1	20.41	0.01	20.77	0.01	20.55	0.05	20.78	0.06

Table 5—Continued

ID	Mag type <sup>a</sup>	3.6 $\mu\text{m}$	$\pm$	4.5 $\mu\text{m}$	$\pm$	5.8 $\mu\text{m}$	$\pm$	8.0 $\mu\text{m}$	$\pm$
428	1	19.86	0.00	20.28	0.01	20.56	0.05	21.01	0.08
429	1	19.94	0.00	19.83	0.00	20.04	0.03	19.86	0.02
430	1	20.32	0.01	20.19	0.01	20.40	0.04	20.42	0.05
431	1	20.36	0.01	20.14	0.01	20.32	0.04	20.21	0.04
432	4	18.33	0.01	18.73	0.01	18.68	0.04	18.81	0.06
433	1	18.39	0.00	18.35	0.00	18.73	0.01	17.04	0.00
435	1	19.58	0.00	19.54	0.00	19.33	0.02	19.26	0.02
436	1	19.20	0.00	19.55	0.00	19.58	0.02	19.52	0.02
437	4	16.42	0.00	16.78	0.01	16.97	0.01	15.50	0.00
438	3	17.98	0.00	17.33	0.00	16.62	0.00	16.07	0.00
439	1	20.50	0.01	20.61	0.01	20.66	0.08	19.99	0.05
440	1	19.83	0.00	19.70	0.00	19.97	0.03	19.96	0.03
441	1	20.92	0.01	20.77	0.01	20.81	0.07	21.24	0.09
442	1	20.74	0.01	20.35	0.01	20.16	0.04	19.46	0.02
443	1	20.05	0.01	19.98	0.01	20.35	0.09	20.16	0.07
444	1	19.10	0.00	19.49	0.00	19.59	0.02	19.63	0.03
445	1	20.82	0.01	20.56	0.01	20.30	0.04	20.67	0.06
446	1	21.14	0.01	20.83	0.01	20.38	0.04	20.53	0.05
447	1	19.61	0.00	19.92	0.00	19.75	0.03	19.40	0.02
448	1	20.46	0.01	20.12	0.01	19.70	0.02	19.81	0.02
449	1	20.42	0.01	20.24	0.01	20.29	0.04	20.64	0.06
450	1	21.68	0.03	21.41	0.04	20.86	0.11	21.27	0.19
451	1	21.27	0.03	21.01	0.05	20.66	0.13	20.35	0.15
452	1	19.17	0.00	19.01	0.00	19.26	0.02	17.73	0.00
453	1	18.68	0.00	18.75	0.00	18.45	0.01	17.89	0.00
454	1	21.05	0.01	20.65	0.01	20.42	0.05	19.88	0.03
455	1	22.74	0.05	22.45	0.05	22.80	0.43	21.78	0.16
456	4	18.15	0.01	18.32	0.01	18.73	0.04	18.14	0.03
457	1	22.30	0.05	21.99	0.04	21.49	0.13	21.38	0.12
458	4	17.96	0.01	18.21	0.01	18.58	0.06	17.17	0.01
459	1	18.97	0.00	19.18	0.00	19.27	0.01	18.94	0.01
460	1	19.63	0.00	19.63	0.00	19.83	0.03	19.85	0.03
461	2	18.22	0.00	18.66	0.00	18.75	0.01	19.18	0.02

Table 5—Continued

ID	Mag type <sup>a</sup>	3.6 $\mu\text{m}$	$\pm$	4.5 $\mu\text{m}$	$\pm$	5.8 $\mu\text{m}$	$\pm$	8.0 $\mu\text{m}$	$\pm$
462	1	21.96	0.03	21.69	0.04	21.31	0.14	21.36	0.17
463	1	20.54	0.01	20.36	0.01	20.27	0.04	20.53	0.07
464	1	20.90	0.01	20.49	0.01	20.00	0.03	20.01	0.03
465	4	17.98	0.01	18.13	0.01	18.40	0.04	16.32	0.01
466	1	20.82	0.01	20.59	0.01	20.18	0.04	20.08	0.04
467	1	22.04	0.03	21.74	0.03	21.33	0.11	20.95	0.08
468	1	19.84	0.00	20.08	0.01	20.07	0.04	20.02	0.03
469	1	19.05	0.00	19.66	0.01	19.40	0.03	19.66	0.06
470	1	20.54	0.01	20.62	0.01	20.80	0.07	20.58	0.05
471	1	19.94	0.00	19.69	0.00	19.51	0.02	19.65	0.02
472	3	18.79	0.00	19.25	0.01	19.54	0.05	20.27	0.09
473	1	17.90	0.00	18.04	0.00	18.11	0.01	15.80	0.00
474	1	18.98	0.00	19.15	0.00	19.51	0.03	19.51	0.03
475	1	19.13	0.00	19.13	0.00	19.29	0.02	18.10	0.01
476	1	19.24	0.00	19.61	0.00	19.55	0.02	19.80	0.03
477	1	22.13	0.04	21.65	0.03	21.16	0.12	21.04	0.11
478	1	20.59	0.01	20.53	0.01	20.58	0.07	20.65	0.07
479	1	20.98	0.02	20.65	0.02	20.70	0.12	21.12	0.17
480	1	17.16	0.00	16.61	0.00	15.92	0.00	15.41	0.00
481	1	20.20	0.01	19.93	0.01	19.64	0.07	19.22	0.04
482	1	20.43	0.01	20.33	0.01	20.56	0.07	20.72	0.08
483	3	19.33	0.01	19.14	0.01	19.31	0.03	19.42	0.04
484	1	18.95	0.01	18.89	0.01	18.92	0.04	17.57	0.01
485	1	22.40	0.04	21.65	0.02	20.73	0.07	19.95	0.04
486	1	18.98	0.00	18.56	0.00	18.32	0.01	17.78	0.01
487	1	19.27	0.00	19.75	0.01	19.93	0.07	20.55	0.17
489	1	18.87	0.00	19.28	0.00	19.32	0.02	19.26	0.02
490	1	19.51	0.00	19.31	0.00	19.24	0.02	19.69	0.03
491	1	19.46	0.01	19.74	0.01	19.84	0.06	19.76	0.03
492	1	19.62	0.01	19.84	0.01	19.93	0.06	19.98	0.04
493	1	22.10	0.04	21.96	0.04	22.17	0.28	21.26	0.13
494	1	22.88	0.07	22.46	0.05	...	...	22.24	0.25
495	1	17.48	0.00	17.62	0.00	17.24	0.00	17.22	0.00

Table 5—Continued

ID	Mag type <sup>a</sup>	3.6 $\mu\text{m}$	$\pm$	4.5 $\mu\text{m}$	$\pm$	5.8 $\mu\text{m}$	$\pm$	8.0 $\mu\text{m}$	$\pm$
496	1	20.32	0.01	20.21	0.01	20.37	0.10	20.40	0.10
497	1	21.35	0.02	20.99	0.02	20.62	0.08	20.05	0.05
498	1	21.44	0.02	21.22	0.02	20.66	0.08	19.60	0.03
499	3	18.29	0.00	18.47	0.00	18.65	0.02	16.46	0.00
500	1	21.34	0.02	21.04	0.02	20.76	0.08	20.77	0.09
501	1	19.35	0.00	19.70	0.01	19.96	0.06	20.24	0.07
502	1	20.12	0.01	20.39	0.01	20.72	0.12	20.74	0.09
503	4	18.68	0.02	18.92	0.02	18.76	0.06	18.58	0.08
504	1	18.19	0.00	18.34	0.00	18.49	0.01	16.54	0.00
505	2	18.69	0.00	18.84	0.00	19.14	0.02	18.57	0.01
506	1	17.91	0.00	18.21	0.00	18.14	0.01	16.01	0.00
507	1	18.45	0.00	18.66	0.00	19.04	0.02	19.34	0.03
508	1	20.17	0.01	20.26	0.01	20.05	0.05	19.98	0.05
509	1	19.10	0.00	19.22	0.00	19.50	0.03	19.37	0.03
510	1	18.35	0.00	18.25	0.00	18.49	0.01	17.08	0.00
511	1	20.32	0.01	20.06	0.01	20.00	0.08	20.26	0.09

Note. — Data in AB magnitudes. Uncertainty is statistical only and is based on fluctuations in the nearby sky. It is shown as 0.00 when less than 0.005 mag, but see text for discussion of systematic errors.

<sup>a</sup>Magnitude type: 1–3 = aperture magnitudes in 1''53, 2''14, or 3''06 radii respectively, 4 = magnitude in Kron aperture as measured by SExtractor